INFORMATION TO USERS

This material was produced from a microfilm copy of the original document. While the most advanced technological means to photograph and reproduce this document have been used, the quality is heavily dependent upon the quality of the original submitted.

The following explanation of techniques is provided to help you understand markings or patterns which may appear on this reproduction.

1. The sign or "target" for pages apparently lacking from the document photographed is "Missing Page(s)". If it was possible to obtain the missing page(s) or section, they are spliced into the film along with adjacent pages. This may have necessitated cutting thru an image and duplicating adjacent pages to insure you complete continuity.

2. When an image on the film is obliterated with a large round black mark, it is an indication that the photographer suspected that the copy may have moved during exposure and thus cause a blurred image. You will find a good image of the page in the adjacent frame.

3. When a map, drawing or chart, etc., was part of the material being photographed the photographer followed a definite method in "sectioning" the material. It is customary to begin photoing at the upper left hand corner of a large sheet and to continue photoing from left to right in equal sections with a small overlap. If necessary, sectioning is continued again — beginning below the first row and continuing on until complete.

4. The majority of users indicate that the textual content is of greatest value, however, a somewhat higher quality reproduction could be made from "photographs" if essential to the understanding of the dissertation. Silver prints of "photographs" may be ordered at additional charge by writing the Order Department, giving the catalog number, title, author and specific pages you wish reproduced.

5. PLEASE NOTE: Some pages may have indistinct print. Filmed as received.

University Microfilms International
300 North Zeeb Road
Ann Arbor, Michigan 48106 USA
St. John's Road, Tyler's Green
High Wycombe, Bucks, England HP10 8HR

THE UNIVERSITY OF OKLAHOMA

GRADUATE COLLEGE

THE MOLECULAR ORBITAL AND STRUCTURAL INVESTIGATIONS OF 3,4 Di-T-BUTYLCYCLOBUTANEDIONE & RELATED COMPOUNDS: The Effect of Alkyl Substitution on the n-π^* Absorption Spectra of α-Diketones

A DISSERTATION

SUBMITTED TO THE GRADUATE FACULTY

in partial fulfillment of the requirements for the

degree of

DOCTOR OF PHILOSOPHY

BY

JOHN K. COLEMAN

Norman, Oklahoma

1976

THE MOLECULAR ORBITAL AND STRUCTURAL INVESTIGATIONS

OF 3,4 Di-T-BUTYLCYCLOBUTANEDIONE & RELATED COMPOUNDS:

The Effect of Alkyl Substitution on the

n-π^* Absorption Spectra of α-Diketones

APPROVED BY

Stanley C. Nicky

Thomas Flatt

Bernard A. Hutton

Eddie Carol Smith

DISSERTATION COMMITTEE

ACKNOWLEDGEMENTS

The author wishes to express his appreciation to all who have contributed to this work. Special thanks go to the research advisors, Dr. S. C. Neely and Dr. D. van der Helm, for their valuable guidance and many helpful suggestions. Expressions of gratitude are extended to Dr. Steve Ealick and Dr. Robert Fink for their special friendship and assistance.

The computer time provided by the Oklahoma University Computing Center is also gratefully acknowledged.

SPECIAL ACKNOWLEDGEMENT

TO MY PARENTS, MR. & MRS. M. L. COLEMAN & MY WIFE, JOYCE

This Dissertation is respectfully dedicated to those above. Without their faith and encouragement, it would not have been completed. I thank my parents especially for being themselves. Their life has been life for me.

This Presentation is their Presentation.

TABLE OF CONTENTS

LIST OF TABLES

LIST OF ILLUSTRATIONS

CHAPTER I

Introduction

The ultraviolet spectra of Trans 3,4 Di-t-butylcyclobutanedione (DTCD) reported by deGroot, Oudman, and Wynberg[1], presents an unusual exception to the spectral trend of saturated unsubstituted α-diketones. It is established that the long-wavelength n-π* absorption band for this class of compound appears at approximately 482mμ or less[2]. The n-π* transition for DTCD is 536mμ (ε∿64) which is well above the suggested maximum for saturated unsubstituted dicarbonyls. This interesting phenomenon, leads to questions concerning the nature of the compound and is the topic of this presentation.

The primary factor determining the presence of a band in the absorption spectrum of an organic compound in solution is the occurrence of a so-called chromophoric group (e.g. dicarbonyl) within the molecule. If such a group is present, the appearance of the corresponding absorption band can be ex-

pected.

The precise location and intensity of the absorption band are not wholly predictable because of the effect of several factors such as the nature of the solvent, and, more particularly, the molecular environment of the chromophoric group[3]. The effect of a solvent on a chromophore in an absorption spectrum is more routinely detected and controlled, whereas the effect of the molecular environment is generally more complex[4]. The composition as well as the configuration of the molecular environment contribute to variations in the absorption band. Change of the intramolecular environment often has a marked effect upon the absorption band even when the chromophore itself remains apparently unchanged. These changes are not easily predictable from fundamental structural parameters but considerable knowledge of an empirical and theoretical nature is accumulating.

There are many environmental factors already known to significantly effect the n-π^* absorption band of the di-carbonyl chromophore (see chapter 3). Attention has been placed on the torsion angle between the adjacent carbonyls and on unsaturated or heteratom substituents of the compound. Previous studies[6] have indicated that for unsubstituted diketones, variations in the torsion angle would cause an n-π^* absorption of no greater than 482 mμ[8]. Since DTCD does not contain unsaturated or heteratom substituents, and since the corresponding 1,2 cyclobutanedione has its assigned n-π^* transition occurring in the expected range (λ= 487 mμ), attention must be given to the sigma network of the DTCD compound in analyzing this unusual absorption spectrum.

There has been no systematic investigation of the effect of alkyl substituents on the long wavelength spectra of dicarbonyls. This could be due to several empirical hurdles. One serious drawback could be solvent

effects. The n-π* absorption band usually shows distinct solvent dependence. In order for the spectra of different substances to be compared meaningfully, absorption characteristics must be determined in a common solvent, or the observed values must be corrected to a given solvent. The mass of data presently available has not been very amenable to classification. A wide variety of solvents have been used to determine λ_{max} in long wavelength spectra.

A more significant and inherently difficult problem in interpreting the absorption spectra for acyclic dicarbonyls is the necessity of distinguishing the influence of the torsion angle from that of the alkyl substituent. However, for some small cyclic α-diketones, the effect of the carbonyl angle is minimized. The carbonyls are not as free to rotate as in the acyclic systems. In the case of cyclobutanedione systems, this is especially true. These should be excellent models for study. But here again, there are not enough sequential compounds in existence to afford extensive comparable empirical data. The instability and difficult syntheses of such compounds further limit the feasibility of such an investigation.

Although the effect of an alkyl group substituent on an n-π* absorption band of a dicarbonyl has not been systematically studied, the effect of alkyl groups in the absorption spectra of other chromophoric groups is well documented. It is of interest to note some of these earlier empirical and theoretical investigations.

a. Empirical studies of the effects of alkyl substituents in absorption spectra

Dimroth and Troutmann directed attention to the fact that the light absorption due to the diene chromophore is influenced by the nature of the molecule in which it occurs.[7] Since then studies of the influence of various substituents on chromophoric groups via absorption spectra have become abundant in the literature. Khun and Grundmann [8] reported that a methyl group on a polyene chain causes displacement of the absorption maximum of the polyene to a longer wavelength. The displacement is about 1/4 of that found for one ethylene linkage. For a butadiene, the ethylene linkage displacement is 210 A^{o}, while a methyl shift is 50 A^{o}.

Booker, Evans & Gillam[3] sought to collect and classify both new and previously published absorption-spectra data for conjugated dienes. Various substituents were studied and found to produce characteristic displacements of the absorption maximum. They observed that when alkyl groups (normally regarded as non-absorbing) are substituted, a big change in the location of the absorption maximum may occur. Replacement of one hydrogen atom by a single alkyl or substituted alkyl group resulted in a bathochromic displacement of the absorption band. When butadiene was the parent compound the inclusion of one methyl group displaced the absorption maximum to longer wavelengths by 30 and 65 A^{o}, respectively for the two different compounds, piperylene and isoprene. Displacements of 90 and 100 A^{o} were reported for the two dimethyl substituted butadienes, $\beta\gamma$-dimethylbutadiene and 2,4 hexadiene.

Booker and coworkers[3] were able to group the compounds studied as: acyclic dienes having one, two or no cyclic substituents; semicyclic dienes

and mono-, di-, and polycyclic dienes. In the latter case, the arrangement of the conjugated system in one or in two rings, respectively, produced a marked difference in the location of the absorption maximum. When the substituent of the butadiene was a single cyclohexyl group, as in allylidenecyclohexane, there was a larger displacement than that with either one or two methyl groups. The displacement of the maximum from that of butadiene was found to be 190 A^{o}. When two substituents of the butadiene were cyclohexyl groups, there was a further displacement of about 90 A^{o} for the second cyclohexyl group. The presence or absence of a ring in a normal diene has no intrinsic effect on the position of λ_{max}, except in-so-far as the structure is such that the ring exerts a normal substitution or positional effect. Since the compounds that were studied were non-polar, the effect of different solvents were negligible; however, the intensities of the spectra did vary with solvent change.

It was R. B. Woodward[9] who first studied and suggested that the nature of the substitution of the chromophoric group in compounds can be predicted from the location of the main absorption band. Woodward's work focused on the short-wavelength absorption spectra of αβ-unsaturated ketones. When ethylenic and carbonyl groups are conjugated in the same molecule, the effect is apparently to displace both bands toward longer wavelengths (see chapter 3); hence, the characteristic absorption spectrum of an αβ-unsaturated ketone with its intense k-band and its low intensity r-band due to the carbonyl group.

It was shown from the study of the αβ -unsaturated ketones[9] in the short wavelength spectra that the presence of methyl groups is significant, and that these and similar saturated radicals exert an environmental effect on the absorption due to the conjugated system. The effect is again almost

invariably bathochromic. Substitution of an alkyl group in the α or β position caused a shift of approximately 15 mμ toward the red. The determination of λ_{max} reveals unequivocally the extent of substitution of the C-C double bond in an αβ-unsaturated ketone. The wavelength , λ_{max}, may be correlated with the extent of substitution of the C-C double bond in the αβ-unsaturated carbonyl system, and consequently the determination of this physical property throws considerable light upon the structure of the compound under examination. Woodward[9] went even further to predict the substituents from the location of the main absorption k-band, and included the following formulation for αβ-unsaturated ketone systems:

WOODWARD'S PREDICTION OF THE LOCATION OF ALKYL SUBSTITUENTS FROM THE LOCATION OF THE ABSORPTION K-BAND.

Alkyl-substituents	Absorption k-band (A^o)
mono-substitution (α or β)	2250± 50
di- (αβ or ββ)	2390
tri- (αββ)	2540

In addition, Woodward observed that the substitution, atleast in the α -position, of a bromine atom or an acetoxy group has much the same effect as the substitution of an alkyl group.

Evans & Gillam[3,4,10,11] established a four part series, collecting experimental data on the absorption spectra of compounds containing specific chromophore groups, with the object of discovering the effect of various

well -defined molecular environments upon absorption spectra. They extended their work to many more αβ-unsaturated carbonyls and verified Woodward's main thesis. They also found that substitution on the β-carbon produced a larger bathochromic effect than that on the α-carbon, and that unsaturated αβ-aldehydes had a λ_{max} approximately 50 A^{o} lower than the corresponding ketones. It was also felt by Evans and Gillam that the correlation shown to exist between molecular structure in these compounds and the location of the short-wavelength absorption band should also affect the location of the long-wavelength r-band due to the carbonyl group. Examination of the data however, revealed no apparent correlation. They also studied the short wavelength spectra for dienones and semi-carbazone chromophores. In all known cases for the dienones, the absorption band lies between 2690 and 3170 A^{o}, depending on the number and position of the alkyl substituents. Each successive alkyl substituent on this chromophore displaces the absorption band by approximately 100 A^{o} towards longer wavelengths. In this particular series however, the difference of aldehydes and ketones disappeared. Just as in the case of the αβ unsaturated carbonyl, the substituent furtherest removed exerted the greatest bathochromic effect. The (δ) substituted compounds provided the longer wavelength absorption k-band.

Evans & Gillam did not, however, observe a substituent effect in the semi-carbazone chromophore. It was summarized that the effect of going from a typical unsaturated ketone to its semicarbazone derivative generally netted the following spectral observation: 1) The displacement of the absorption maximum to longer wavelengths, 2) the disappearance of the band due to the carbonyl group, and 3) a distinct increase in intensity of the absorption. For some 33 compounds, it was observed that although

the semicarbazone generally had higher maximum absorption bands than their carbonyl counterparts, the substitutent effect observed in the unsaturated aldehyde and ketone did not occur for the semi-carbazone. The corresponding absorption maximum appeared to level at a constant value of 2670± 75 A^{o} for most compounds studied.

These empirical studies do not directly relate the effects of alkyl substituents in the r-band absorption spectra, however they do reveal an apparent bathochromic shift observed for alkyl substituents in the k-band absorption spectra; an effect that can be altered according to the position of the substituents.

No consistent alkyl substituent effect was observed in the n-π^* absorption spectra in the studies of Evans and Gillam. This could be due to the strong sensitivity of the r-band spectra to the various solvents used. It could also be due to the influence of the unsaturated bond in the systems studied. Furthermore, the k-band is quite prominent in these spectra and may reasonably overshadow or otherwise affect the r-band spectra as in the case of ascorbic acid , where the r-band disappears (see chapter 3). However, in a dicarbonyl compound the n-π^* intensity will be less affected. Accordingly, the cyclic dicarbonyl chromophore should present a better system for detecting the effect of an alkyl substituent on the location of the r-band.

This speculation is further supported by the apparent bathochromic shift observed in monocarbonyl systems where the dicarbonyl "rotation effect" is eliminated. Alkyl substitution at the α-position for both the propanone and butanone chromophore systems show a definite shift toward the red in the n-π^* absorption spectra, as summarized in Table 2. The displacement of the n-π^* absorption band per methyl group for the two systems ranges

Table 1

n-π* Bands in Cyclopropanones and Cyclobutanones (cyclohexane solution)

COMPOUND	λ_{max} (mμ)	$\Delta\lambda_{max}$
	310*	-
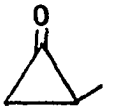	330*	20
	340*	30
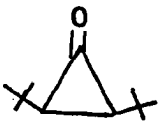	354+	44
	279**	-
	290**	11
	294**	15

+Reference 12 (isooctane solution)
*Reference 13
**Reference 14

from 7-20 mμ with an average value of 12 mμ. This is comparable to the value of 15 mμ per methyl substituent observed in the k-bands discussed earlier[9]. The apparent di-t-butyl displacement in the propanone compound (44 mμ) does indeed compare favorably with the speculative di-t-butyl displacement in the DTCD compound (49 mμ).

It would be feasible to speculate that a bathochromic shift effect should occur in the n-π* absorption region due to α or β alkyl substituents on a dicarbonyl chromophore. It can further be expected that this effect would be distinct if the strong influence of the dicarbonyl torsion angle is stabilized, as in the case of a rigid cyclobutanedione ring. A relatively large absorption displacement could be anticipated if the maximum displacement due to the dicarbonyl chromophore occurs (i.e. planar or near planar configuration) and a substantial displacement due to alkyl substitution also arises (i.e. poly alkyl substitution).

DTCD is one of only two reported saturated unsubstituted (without heteratom substituent) α-diketones to show this unusually long wavelength n-π* transition. The other such compound, Spiro(adamentane-2,1'-cyclobutane-2',3'-dione), also reported by Wynberg & Coworkers[15], has an n-π* transition occurring at 516 mμ (ε∿44.5). From a purely speculative view point -and assuming that the two butane rings in question to be in a near planar configuration (for maximum absorption)-, the poly alkyl substitution at the α-positions of both species, could be expected to be a major contributor to the adnormal displacement of the respective n-π* absorption bands. However, in the absence of any direct empirical comparisons this assumption remains speculative at best.

b. Theoretical studies of the effects of sigma bond networks on absorption spectra

As in the case with empirical studies, there is also little theoretical work relating the effect of alkyl substitutents in the n-π^* absorption spectra. In fact, most of the reported theoretical investigation involving organic compounds have probed isolated π systems[16]. With the recent advances in all-valence electron methods (see chapter 2) however, there have been significant studies indicating the importance of including sigma bonds in MO calculations involving spectral interpretation.

Hoffmann, Heilbronner and Gleiter calculated the interactions between nonconjugated ethylene groups in molecules.[17] It was noted that not only the direct overlap between the π systems but also the interaction through the intervening sigma bonds is necessary for spectral interpretations.

R. Hoffmann used perturbation theory to treat interactions of localized orbitals and groups of orbitals with each other, both directly (through space) and indirectly (through other bonds in the molecule).[69] Studying the N lone pairs and carbon radical lobes (via extended Huckel MO calculations), he observed splitting patterns in pyrazine, p-benzyne and diazabicyclooctane that were completely opposite to expectations. The antisymmetric combination of the nonbonding MO was below that of the symmetric combination. He concluded that this phenomenon was due to through-bond coupling (inclusion of the sigma bond network) rather than to direct interaction between the two orbitals. This large splitting and ordering have been fully confirmed in recent photoelectron work.[70,71]

Hoffmann, Imamura and Hehre used a variety of molecular orbital methods to deduce significant and specific interactions among radical lobes

in the same molecule separated by a number of intervening sigma (σ) bonds.[72] These are explored in detail for benzynes and didehydroconjugated molecules. They verified that the splitting order of the radical lobes depended on the likelihood of through-space or through bond interaction of the respective molecule.

Another investigation demonstrating the importance of the sigma network in the interpretation of an n-π^* absorption spectrum of a dicarbonyl chromophore was performed by Neely, Fink, van der Helm and Bloomfield.[18] In this work, theoretical calculations, using various MO methods, were made on the α-diketones illustrated in figure 1: tricyclo $(4.4.2.0)^{1,6}$ dodeca-3,8-diene-11,12-dione (2DB) and its tetrahydro derivative (ODB).

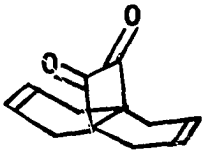

2DB

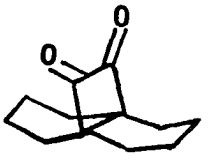

ODB

Figure 1: tricyclo$(4.4.2.0)^{1,6}$dodeca-3,8-diene-11,12-dione (2DB) and its tetrahydro derivative (ODB).

The abbreviated names (in parenthesis) of the species indicate the number of C-C double bonds contained in each compound. Theoretical results obtained by considering the π- interactions alone were compared with those in which the sigma (σ) electronic structure was also included. The significant conclusion of the investigation was that the qualitative spectral trend could be accounted for only when all valence electrons were included

in the calculations.

It is interesting to note that the λ_{max} of the 2DB species (537 mμ) is almost identical to that of DTCD (536 mμ). The nonconjugated diene network of the cyclobutanedione (2DB) appears to have virtually the same influence on the α-diketone chromophore as does the di-t-butyl network of DTCD. This observation was fundamental in leading to the investigation reported here.

It might appear logical to seek a theoretical approach to investigate the effects of alkyl substituents in the dicarbonyl n-π* absorption spectra in view of the apparent difficulties encountered with an empirical study. A theoretical study, as opposed to an empirical one, will allow for a more detailed and discrete analysis of the problem. However, a theoretical analysis involving a molecular system as large as DTCD must be approximate at best. Accordingly, any such approach must be undertaken cautiously.

DTCD appears to be an excellent model for expanding this type of theoretical study. Previous investigations have demonstrated the importance of a sigma or saturated network in π -system interactions. The DTCD system offers the opportunity to study the perturbation of a sigma or saturated network on the α dicarbonyl π and σ systems. Such an investigation, although only qualitative, should nevertheless offer valuable insight in the interpretation of n-π* absorption spectra and the intramolecular interactions giving rise to variations.

This study employes a theoretical treatment directed towards gaining an explanation of the "unusual" n-π* solution spectrum of DTCD. α -alkyl substitution to the diketone system is considered specifically since it is

the t-butyl addition to the 1,2 cyclobutanedione structure that is the apparent cause of the adnormally large λ_{max}. It is understood that the intramolecular environment of a chromophore, in both its constituency as well as its conformation, may have a significant and unique influence in the absorption spectrum. Accordingly, various alkyl substituents (including the t-butyl group) as well as various orientations of each substituent are considered specifically to determine their respective influences on the electronic states of the 1,2 cyclobutanedione system. The final results establish a trend for alkyl substitution effects on the n-π^* spectrum of α-substituted diketones. The most favorable model for DTCD, in terms of molecular stability and in terms of relative conformational effects on the n-π^* absorption spectrum, is speculated. This theoretical model is then compared with a model obtained via an x-ray molecular structure determination of DTCD.

CHAPTER II

MO Calculations for Saturated Systems

In 1955, Sandorfy applied Huckel-type approximations to saturated hydrocarbons and for the first time included the hydrogens[16]. He concluded that MO methods of the LCAO-type (linear combination of atomic orbitals) would be capable of giving as good charge distributions for such molecules as for conjugated systems. This historically significant paper made way for the development of Sigma Molecular Orbital Theory: the theoretical treatment of sigma as well as pi electrons of molecular species.

There was a time when non-empirical calculations were carried out on the smallest of molecules, and semi-empirical ones on the pi electrons of conjugated systems alone. Recently, semi-empirical molecular orbital methods have been extended to include all electrons, sigma and pi, and to apply to saturated as well as conjugated systems. Purely non-empirical MO calculations, although still in general far from the desired Hartree-Fock MO result, are being made on sizable organic molecules[16,20].

Basically, the sigma-MO concepts are developed from the pi-electron MO methods.[16,19] A theoretical description of the electronic structure and the bonding in such molecules can be obtained by expanding the MO basis set to include the valence-shell AO's of all atoms in the mole-

cule. Thus the 1s AO of hydrogen and the 2s and three 2p AO's of any atoms from the second row of the periodic table would contribute as basis functions and be treated explicitly in these methods. The extended basis set allow mixing of sigma and pi orbitals in non-planar unsaturated molecules where these interactions are not symmetry forbidden and is thereby capable of showing the role of sigma bonds in the interactions between nonconjugated, unsaturated groups in such molecules as well. The set of MO's obtained allows not only the calculation of pi-pi* electronic transition energies as in the pi-electron methods, but also those involving any combination of orbitals, e.g. sigma-pi* ($\sigma - \pi^*$), sigma-sigma*($\sigma - \sigma^*$), as well as the presently desired n-pi* ($n - \pi^*$).

Clearly, for predictions of chemical phenomena, sigma electrons are essential. Inclusion of sigma electrons in conjugated systems shows that although some qualitive conclusions based on pi electrons alone, remain valid, in general the picture changes. Sigma and pi networks are not as clearly separable as once thought[16]. This is important since almost all molecules involve sigma electrons. As in the pi-electron methods, the sigma-MO theory has also evolved over various stages of approximation. The Huckel Method, which does not include electron-electron interactions, has been extended in a number of ways as has the self-consistent field methods, which included electron-electron repulsion in an approximate way.

Several formulations from within the SCF framework have been introduced for calculating self-consistent molecular orbitals for all-valence electrons in molecules. One of the more widely used SCF

methods is based on the CNDO-type (complete neglect of differential overlap) approximation in which the overlap distribution, $\phi_u(1)\phi_v(1)$, of any two atomic orbitals ϕ_u and ϕ_v is neglected in all electron repulsion integrals. By choosing some parameters in a semi-empirical manner to fit atomic data and others to fit more precise calculations on diatomics, it was found possible to obtain wavefunctions and energies which predicted geometries, bending force constants, rotational barriers, etc. in fair agreement with experiment, atleast for small polyatomic molecules. Modifications (e.g. CNDO/2 Method) as well as additions to the basic SCF all-valence-electron methods are quite abundant in the literature [28-32].

In the Huckel-type theories, the total energy is assumed to be a sum of one-electron orbital energies, and only the one-electron Hamiltonian matrix is diagonalized to obtain these [33-36]. The H_{rs}, one-, and two- center Hamiltonian matrix elements are obtained either from atomic properties or are related to overlap integrals S_{rs} in a number of ways. Further, the LCAO may be that of the regular atomic orbitals (AO's) such as the 2s's and 2p's and the hydrogen 1s's or of hybridized valence atomic orbitals (LCVO).

Fukui and Co-workers, in their pioneering applications, used primarily an LCVO-method. They obtained charge distributions and sigma dipole moments for a large number of saturated and unsaturated molecules, and they studied chemical reactivities and phenomena such as the break-up of hydrocarbons under electron impact. These applications, as well as references to the literature up to 1965, have been surveyed by Fukui [37].

In 1963, R. Hoffmann provided a strong impetus to the treatment of

sigma systems, with his Extended Huckel Theory (EHMO) [19]. Hoffmann used a Huckel method with all the one-electron matrix elements H_{rs} and all the overlaps S_{rs} included. The method was applied with the same parametrization to a large class of saturated and unsaturated hydrocarbons. Hoffmann concluded that with such a method the geometries of molecules could be predicted. Barriers to internal rotation, ring conformations, and geometrical isomerism are among the topics treated. Consistent sigma and pi charge distributions and overlap populations are obtained for aromatics and their relative roles are rationalized. For alkanes and alkenes charge distributions are also presented. Failures of the EHMO method included overemphasis on steric factors, leading to some incorrect isomerization energies and the failure to predict strain energies. As previously mentioned, the Huckel-type methods do not include electron-electron interactions or the adjustments of the parameters that would result from these. Such changes in the parameters are particularly important in ionic species and with heteratoms, where straight extended Huckel calculations run into more difficulty. As in the pi-electron theory, one way to go beyond the Huckel methods while retaining their basic simplicity and lack of difficult integrals has been to introduce iteractions to the parameters dependent on charge distribution. Such iterated extended Huckel methods (EIHC) have been the main proponents of Cusche and McGlynn [22].

Another interesting method which differs from the Huckel approach and which also gives remarkable success in the predictions of geometries, is the subminimal ab initio method of Frost [39]. In the method of Frost, the full exact Hamiltonian and all the matrix elements that it

gives rise to are used, but, in turn, the orbitals themselves are chosen in the simplest possible manner.

It is apparent that for a proper theoretical probe of the diketone, DTCD, that an all-valence-shell MO method be employed. The Extended Huckel Molecular Orbital Theory (EHMO) is the sigma-MO method chosen for this investigation; mainly because of its previous success in qualitatively treating values of the n-π^* spectra [18] as well as its success in predicting molecular stability and molecular conformations [19,26]. The EHMO is quite useful in qualitative analysis and is especially good for rationalizing and correlating experimental results for s class of related compounds [22]. The method generally leads to good approximations of equilibrium conformation, and the method is superior, in this respect, to CNDO-type methods [26]. Although its calculated transition energies are generally smaller than the observed transition energies, qualitative trends in these values can still be reasonably well correlated for a series of similar compounds [18-21]. It is easy to criticize the Huckel-type methods. The litany of theoretical deficiences is indeed large. However, these deficiences are partially compensated by the simplicity of the computational scheme which is frankly empirical, easy to use, and which works quite well. One must assume that the parametrization process subsumes many deficiencies and corrects for them in a wholly empirical way [22].

The Huckel-Type Calculation

The Extended Huckel MO Theory, as introduced by Hoffmann is derived from the most widely used of all quantum-chemical computational schemes, the Huckel MO method (HMO) [19,34]. The basic HMO is based on a series of assumptions, of which many are arbitrary. It is patterned on quantum mechanics, but it is hardly more than a useful empirical scheme which rationalizes much chemical experience. Basically MO's are formed and are given as linear combinations of atomic orbitals (LCAO), usually one AO from each of the various atomic centers encompassed by the MO.

The wave function, ϕ_i, is taken to be a molecular orbital which in turn is constructed by the LCAO procedure from a set of atomic orbitals, χ_i, centered on the atoms of the molecule.

$$\phi_i = \sum_{j=1}^{n} C_{ij}\chi_j \qquad (1)$$

n is the number of AO's

The expression for the energy, E, of that particular MO is

$$E = \frac{\int \phi_i^* H \phi_i \, d\tau}{\int \phi_i^* \phi_i \, d\tau} \qquad (2)$$

Differentiation of the energy with respect to each of the coefficients, C_{ij}, and application of the variational theorem yields n simultaneous equations,

$$\sum_{j=1}^{n} C_{ij} \left(\int \chi_i^* H \chi_j \, d\tau - \varepsilon \int \chi_i^* \chi_j \, d\tau \right) = 0 \qquad (3)$$

Since the energy of the independent particles can be written $E_{total} = \Sigma_i N_i \varepsilon_i$, where N_i is the occupation number of molecular orbital i, which has energy ε_i, minimization of each of the orbital energies will cause E_{total} to be a minimum.

Equation 3 becomes:

$$\sum_{j=1}^{n} C_{ij}(H_{ij} - \varepsilon S_{ij}) = 0 \qquad (4)$$

for i = 1,n

where,

$$S_{ij} = \int \chi_i^* \chi_j d\tau \qquad (5)$$

$$H_{ij} = \int \chi_i^* H \chi_j d\tau \qquad (6)$$

S_{ij} is the overlap integral between the two AO's

H_{ij} is called a coulomb integral when i=j and represents the energy of an electron in AO χ_i. When $i \neq j$, H_{ij} is called a resonance integral. Equation (4) provides a set of secular equations which may be conveniently written as the secular determinant given in equation (7). Being a determinant of order n, it has n roots, ε_i; where i=1,n. Solutions to the secular equations can be obtained by diagonalizing the determinant.

$$|H_{ij} - \varepsilon S_{ij}| = 0 \qquad (7)$$

Each of these roots, in turn, when used in eq. (4) yield a set of n coefficients C_{ij} that make up a molecular orbital. Since the right-hand side of eq.(4) is identically zero, one can only find the ratios of (n-1) of the C_{ij} to a particular coefficient. Normalization of the MO's then enables one to assign actual values. The molecular orbitals are doubly occupied, starting with the orbital of lowest energy and proceed-

ing upward in energy. If the highest-occupied MO is a member of a degenerate group, then the particles are assigned to the degenerate orbitals with spin parallel, leading to the state of maximum multiplicity in accordance with Hund's rule.

The Hamiltonian (H) is treated as an effective one-electron Hamiltonian. The integral H_{ij} in eq. (6) are thus empirical parameters and the MO energies are obtained in terms of these parameters. The HMO approximation, applied to hydrocarbons, sets all coulomb integrals equal to a common value, α. Resonance integrals between AO's centered on nuclei which are bonded to each other are all assigned a common value β. H_{ij}'s between all other AO pairs are taken as zero. All overlap integrals are taken as zero when $i \neq j$ and set equal to one when $i=j$, thereby assuming an orthonormal set of basis functions.

The scope of application of the Huckel Theory, of course was widely broadened with the development of the Extended Huckel approach. Both theories (HMO & EHMO) ignore inner-shell electrons on the atoms; however, the EHMO uses all the valence electrons, while the HMO generally employs only the pi electrons of the molecule.

The EHMO also differs from the HMO Theory in the extent to which approximations are used in developing the H and S matrices in the Secular Equation and in the atomic orbitals admissible to the basis set. In the EHMO theory s, p, d, and f-type basis functions are employed, together with a full overlap matrix and a systematic set of rules for the selection of coublomb integrals, in constructing the secular equation. It is no longer necessary to invoke a sigma-pi separation because one uses a definite coulomb integral for each type of orbital

on each atom. The coulomb integrals are taken from the valence-state ionization potentials of Pritchard and Skinner[40]. The method approximates the H_{ij} resonance integrals by one of three formulas, all involving a direct proportion to the corresponding overlap integral.

1. Proportionality to overlap

$$H_{ij} = -KS_{ij}$$

2. Wolfsberg-Helmholtz arithmetic mean formula

$$H_{ij} = KS_{ij}(H_{ii} \pm H_{jj})$$

3. Geometric mean formula

$$H_{ij} = -KS_{ij}(H_{ii} \cdot H_{jj})^{1/2}$$

K is usually assigned a value of 1.7 to 2.0. Since a full overlap matrix is employed, the method is sensitive to the choice of atomic orbitals.

The actual Extended Huckel calculations described above are carried out using Hoffmann's routine[41]. Slater Atomic orbitals are used as basis functions with Slater exponents of 1.3000, 1.625, 2.275 for hydrogen 1s, carbon (2s & 2p), and oxygen (2s & 2p) respectively. Coulomb integrals, H_{ii}, for the various basis functions were taken as the valence state ionization potentials. The diagonal matrix elements are taken to be the negative of the valence state ionization potentials: -13.6 eV for hydrogen, -21.4 eV for carbon 2s, -11.4 eV for carbon 2p, -35.3 eV for oxygen 2s, -17.8 eV for oxygen 2p. Resonance integrals, H_{ij}, are calculated as the geometric mean (formula 3 above), with $K = 1.75$. The resulting MO's reveal not only the pi-electron structure, but also the sigma orbitals and any nonbonding orbitals. Electronic

transition energies are taken as the difference in orbital energies between the leaving and accepting MO's thereby neglecting any electron rearrangement upon transition.

CHAPTER III

The Carbonyl and Dicarbonyl Chromophore

A theoretical study of the n-π^* absorption spectra of Di-t-butyl-cyclobutanedione (DTCD) requires an analysis of the atomic and molecular composition of the dicarbonyl chromophore.

A typical carbonyl bond, e.g. formaldehyde, is formed by the combination of carbon and oxygen atomic orbitals [42]. These orbitals can be divided into those which are antisymmetric with respect to reflection in the xz plane, where $2p_{y_c}$ and $2p_{y_o}$ will form the π MO's and those which are symmetric, where the 1s, and 2s, $2p_x$, and $2p_z$ atomic orbitals will form the sigma (σ) MO's. The carbon 2s, $2p_x$, $2p_z$ orbitals can be formed into three trigonal hybrids, similar to those of ethylene; two of these will form sigma (σ) bonds with the hydrogens, and the third will go to make the C-O sigma bond.

The state of hybridization of the oxygen atom is significantly different from that of the carbon atom [4]. The oxygen 2s orbital is much more stable than its 2p orbitals. The excitation $(2s^2 2p^2)^3p \rightarrow (2s2p^3)^3p$ of carbon requires 9.34 eV, while the corresponding oxygen transition $(2s^2 2p^4)^3p \rightarrow (2s2p^5)^3p$ requires 15.66 eV. This means that to some extent the oxygen 2s orbital, having a much lower energy than either the carbon 2s or 2p orbital, or the oxygen 2p orbitals, does not take part in the bonding. In other words, it is nonbonding in the same sense as are

the 1s orbitals. The C-O sigma bond is then formed by a carbon sp^2 hybrid and $2p_{x_o}$. This extreme situation does not really arise in practice: some of the $2s_o$ orbital is used to form the C-O sigma bond, and some of the $2p_{x_o}$ is mixed with the $2s_o$ to form a hybrid nonbonding orbital. But the important fact is that the electrons in this particular nonbonding orbital are quite tightly bound because the orbital is largely $2s_o$.

There is one oxygen orbital which has not been used so far, $2p_{z_o}$. This can be considered to be nonbonding, since the only other orbital which might combine with it, $2p_{z_c}$ is already used in forming C-H bonds (or C-C bonds as the case may be) . The π orbitals are therefore antisymmetric to reflection in the plane (xz) of the paper; the σ and n orbitals are symmetric.

In general, nonbonding lone-pair electrons are the least strongly bound in a molecule [4], and in the bonding levels π-electrons have higher energies than corresponding σ-electrons, while in the antibonding levels that order is reversed, as shown below.

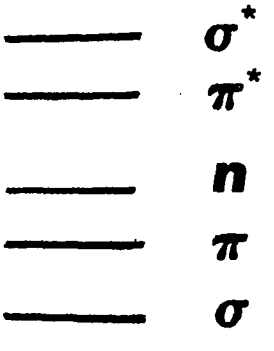

Figure 2

The bonding and antibonding order in a simple carbonyl.

Thus in a simple molecule an n-π^* transition generally should require a smaller energy, ΔE, than a π-π^* excitation, while a σ-σ^* transition should require a relatively large ΔE. In general, simple carbonyl compounds give four main regions of absorption below the Rydberg bands in the far ultraviolet region. A very weak absorption ($\varepsilon_{max} \simeq 10^{-4}$) near 4000 A^o and a weak band ($\varepsilon_{max} \simeq 10$) near 2900 A^o are due, respectively, to the (triplet and the singlet) transitions of an oxygen 2p lone-pair electron to the carbonyl antibonding π-orbital (n-π^*). A n-σ^* band of moderately-strong intensity lies near 1800 A^o, and an intense π-π^* absorption at a shorter wavelength. The excitation of an oxygen $2p_z$ lone-pair electron is forbidden to the carbonyl π_y^* orbital, but it is partly allowed to the carbonyl σ_x^* orbital. The permitted atomic orbital components are $2p_z(O) - 2p_x$, 2s (C).

It is, of course, the weak absorption and long wavelength absorption bands that are of particular interest. More specifically, the lowest singlet-singlet transition has been characterized as the transition corresponding to the excitation of a nearly nonbonding oxygen electron to an antibonding π molecular orbital (n-π^*)[43]. There is definite physical evidence of this interpretation and there are analogous transitions (involving the nonbonding electrons) in compounds containing nitrogen and sulfur as well [44].

These low transition bands are characterized by distinct physical properties: In vapor spectrum these n-π^* transition bands have "atomic-like" sharpness while in the solution spectra the bands are very blurred. Usually only slight vibrational structure remains, even in hydrocarbon solvents. This of course is striking in view of the sharpness

of the vapor absorption lines. Probably it is a characteristic of the nonbonding orbitals which leads to an unusual perturbation in solutions.

There is a large blue-shift for the n-π* transition on going from a non-polar to a polar solvent. It was pointed out by Kasha [43] that this appears to be a general property of n-π* bands. The reason for the strong solvent effect is certainly tied up with the large change in the electron distribution on excitation. The blue shift is particularly noticeable on going from a hydrocarbon to a hydroxylic solvent, and it is fairly certain that this is due to the formation of hydrogen bonds rather than to a general dielectric effect of the solvent[40]. In the ground state the nonbonding lone-pair of electrons are particularly suitable for forming a hydrogen bond, but this capacity is largely lost when one of these electrons is promoted to the π system. It has been pointed out by McConnell[46] and Pimental[47] that the Franck-Condon principle plays an important part in the n-π* solvent effect. Since the solvent molecules cannot re-orient during the excitation process, the maximum of the absorption band is determined by the particular solvent configuration which is favored by the ground state. On the other hand, the maximum of the emission band is determined by the solvent configuration which gives the greatest stability to the excited state[46,47].

In acidic solvents the n-π* transition is shifted so much that it "disappears". Addition of a proton to the nonbonding pair of the heteroatom greatly increases the binding energy of the "lone-pair". This behavior offers the clearest proof of the excitation of nonbonding electrons in such molecules, and remains the sole universal indication of a transition involving lone pair electrons.

It must be pointed out that the position and intensity of a "typical" carbonyl n-π* absorption band can be significantly altered by both conjugated and formally non-conjugated substituents[44]. For example, progressive substitution by methyl in formaldehyde doubles, and then quadruples, the extinction coefficient of the n-π* transition. In addition alkyl groups or monatomic substituents with lone-pair electrons replacing the aldehydic hydrogen atom will shift the carbonyl n-π* absorption to a shorter wavelength. However, in compounds such as $MeCOCH_2Br$, where the effect of the alkyl group or monatomic substituent travels through a (CH_2) linkage from the α position a bathochromic shift is observed[45]. This is observed for the substituted formaldehydes listed in Table 2 below. Methyl substitution on formaldehyde causes a blue n-π* shift, while the $-CH_2Br$ substitution on MeCOBr results in a red n-π* shift.

Table 2.

Compound	n-π* transition
H_2C-O	3100 A^o ($\varepsilon \simeq 5$)
Me-CHO	2935 A^o ($\varepsilon \simeq 12$)
Me_2-CO	2750 A^o ($\varepsilon \simeq 22$)
MeCOBr	2500 A^o ($\varepsilon \simeq 21$)
$MeCOCH_2Br$	3105 A^o ($\varepsilon \simeq 21$)

n-π* transitions for some substituted formaldehydes.

If the carbonyl group is part of a conjugated system the n-π* absorption band is invariably shifted to a longer wavelength[44], and can be intensified greatly relative to the corresponding value of the saturated species. This intensification has been attributed, by Cookson and

Wariyar[48], to the mixing of the n-π* and π-π* transitions for non-coplanar ethylene and carbonyl double bonds. The long wavelength shift is due to the interaction of the conjugated system. The conjugation of a carbonyl with a vinyl group gives four π-electron energy levels, figure 3 , of which the highest occupied and the lowest unoccupied have higher and lower energies respectively than the corresponding orbitals of the carbonyl group. The bonding and antibonding MO's (π_C and π_C^*) of a carbonyl are about 2.1 and 0.5 eV, lower than the respective MO's (π_E and π_E^*) of an ethylene group[50]. The lone-pair and sigma orbitals of the carbonyl to a good approximation are generally unchanged, so that the n-π* and, more particularly, the π-π* carbonyl absorption shift to longer wavelengths in the α,β-unsaturated derivatives while the n-σ* band retains practically the same energy.

The energy of an n-π* transition may also be slightly altered by the presence of a non-conjugated double bond. Labhart and Wagniere showed that a small red shift should be obtained for this band when overlap between the two π systems exists[50], although a notable exception to this has been shown by Snyder and Franzus[51]. α,β-unsaturated ketones, in many cases, have shown n-π* intensities 10 to 100 times the value of the corresponding saturated species, a situation also due to the non-coplanarity of the π systems[48].

For α-diketones, the n-π* absorption intensity is less affected by a mutual perturbation of two carbonyl groups than by the interaction of a vinyl and carbonyl group. An α-diketone with a range of angles of twist about the inter-carbonyl bond has uniformly weaker n-π* bands than a non-planar α,β-unsaturated ketone[4]. The π-π* bands lie near 1750 A^o

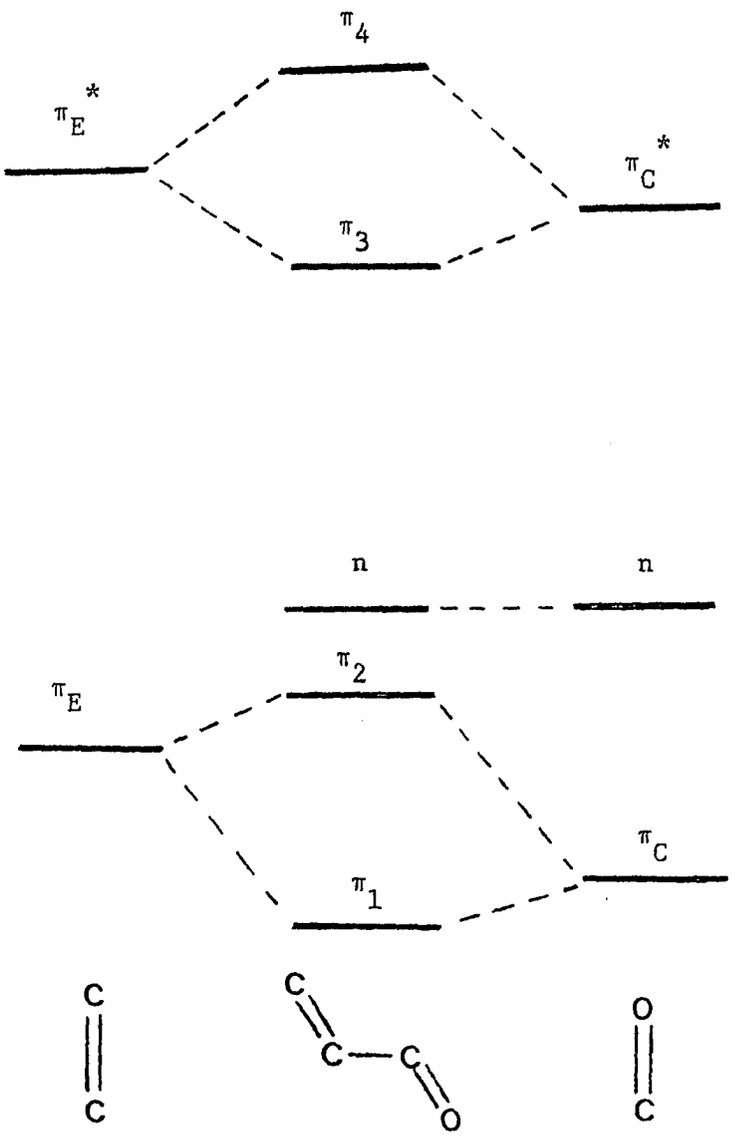

Figure 3. Interactions of π MO's in α,β-unsaturated ketones depicting a red shift of the n-π* transition.

in the α-diketones, compared with 2300 A^{o} in the α,β-unsaturated ketones, so that the former are the further separated in energy from the n-π* bands and there is a smaller mixing of the transitions[52]. The mixing of the carbonyl π-π* and n-π* transitions is not negligible however, as is evidenced through the spectra of β-diketones. An orthogonal β-diketone as opposed to a coplanar species allows more transitional mixing and gives the larger ε_{max}[44].

Whenever nonbonding orbital interactions were considered in the past, those interactions were judged small[57]. This is now not in accord with either theoretical or experimental results. Lone-pairs, double bond and other isolated subunits of a molecule interact significantly with other such units by direct through-space and indirect through-bond mechanisms. Both through-space and through-bond interactions are discussed here in detail.

In the simple dicarbonyls there are two lone-pair molecular n orbitals and two antibonding π* molecular orbitals; each pair being formed by the symmetric and the antisymmetric combination of the respective orbitals of the separate carbonyl groups. Figure 4 shows a typical (camphorquinone) dicarbonyl energy diagram of the n and π network energies resulting from through-space interactions, as a function of twists around the intercarbonyl C-C bond. The symmetric orbital(n_S or π_S) has the lower energy for all angles of twist about the intercarbonyl bond except at 90° (where the two levels of each type are degenerate). The maximum energy separation between the two lone-pair orbitals is obtained in the cis configuration of the α-diketone group, where the oxygen 2p lone-pair orbitals have maximum overlap, but the energy differ-

Figure 4

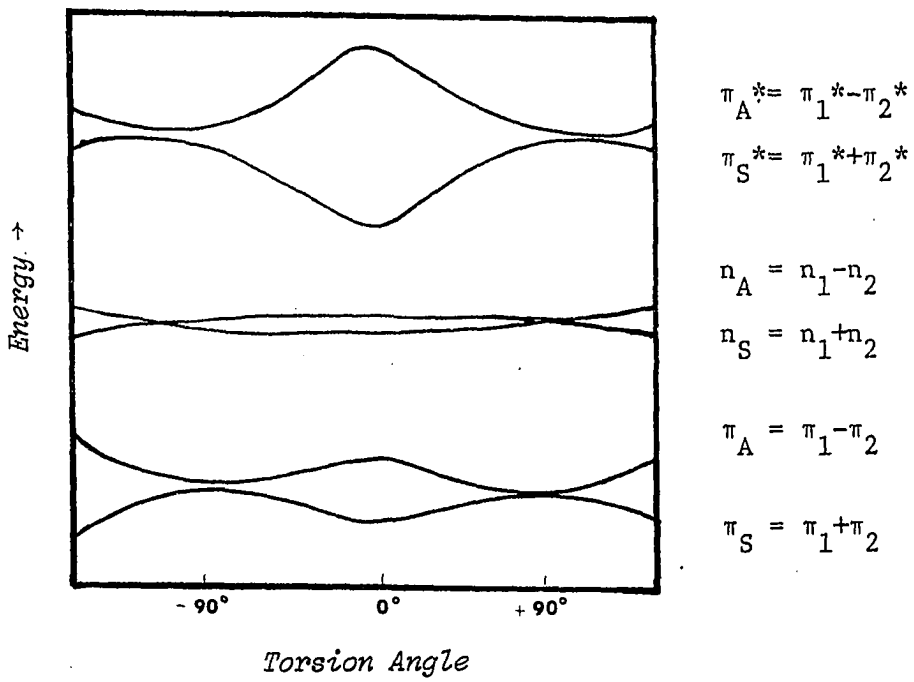

Figure 4: Typical dicarbonyl energy diagram of the n and π network energies resulting from through-space interaction as a function of twists around the intercarbonyl C-C bond.

ence between the π^*-orbitals is a maximum for both the cis and the trans configurations. The lower and upper π^* orbitals have an antinode and a node, respectively, in the intercarbonyl region.

Of the four possible n-π^* transitions in α-diketones, only those between the two symmetric (n_S-π_S^*) or the two antisymmetric orbital (n_A-π_A^*), are allowed by molecular symmetry, though they are all atomically forbidden, as in monocarbonyl compounds.

It is pointed out here that the ordering of the dicarbonyl MO's may be altered when through-bond interactions of the two lone-pair (n) orbitals increase. The symmetric lone-pair MO is raised above that of the antisymmetric MO in some cases.[18,69-72]

Swenson and Hoffmann[57] via EHT and CNDO/2 calculations, first prophesied that interaction between the nonbonding orbitals, n_1 and n_2, of two carbonyl groups in a dicarbonyl compound would lead to molecular orbitals with clearly split orbital energies. This should be true even when n_1 and n_2 are widely separately in space. It was shown that the interaction mechanism is mainly of the "through-bond" type. That is, the linear combinations

$$S, \quad n_S = (n_1+n_2)/(2)^{1/2}$$

$$A, \quad n_A = (n_1-n_2)/(2)^{1/2}$$

(which differ little in energy as a result of "through-space" interaction), can mix strongly with other σ-orbitals of appropriate symmetry.

One important aspect of the through-bond interaction relative to the through-space interaction is the anomaly of the antisymmetric, A, nonbonding (n_A) level appearing at lower energy than the symmetric, S, nonbonding (n_S) level. This is rationalized via of the through-bond coupling (interaction). The splitting of the two n orbitals is a result of their interaction with some other orbitals.

Consider the case of two lone pairs separated by three intervening sigma bonds. For brevity consider only the 2-3 σ-bond orbitals. The interaction diagram of the $S(n_1+n_2)$ and $A(n_1-n_2)$ combinations of the lone pairs are shown in figure 5. The levels are classified with respect to the yz mirror plane which passes through the 2-3 bond. With respect to this plane the 2-3 σ orbital is S and the 2-3 σ* level is A. The four orbitals are allowed to interact. The standard restriction is that only orbitals of like symmetry interact with each

Figure 5

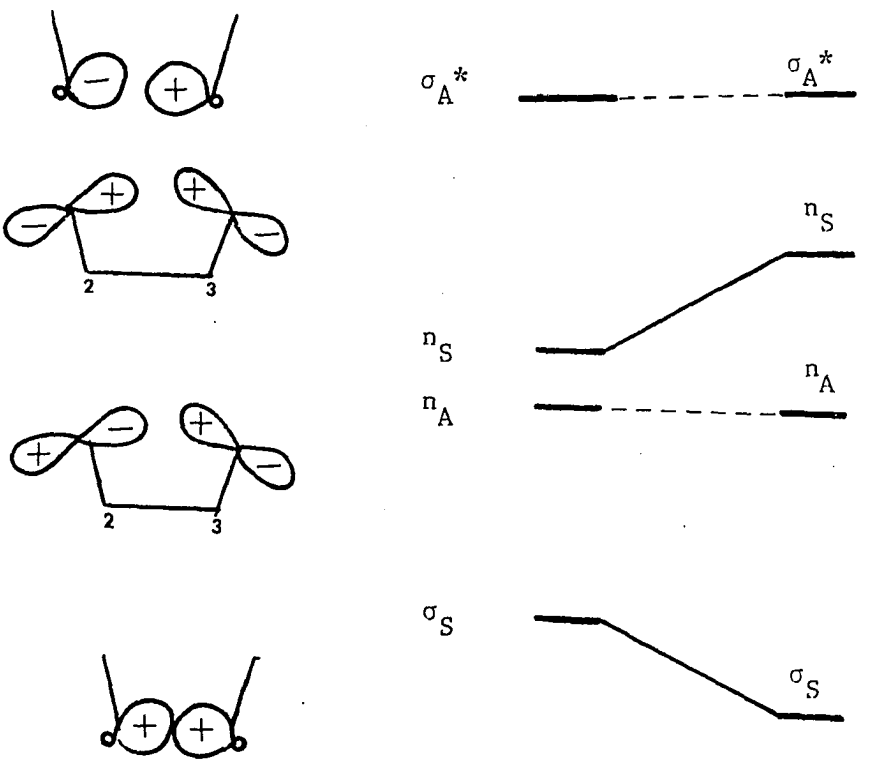

Figure 5. Schematic orbital diagram of "through-bond" coupling over the three sigma bonds of cis glyoxal. Interaction between the linear combination n_S and and σ_S is shown.

other. Thus n_1+n_2, S symmetry, mixes with σ and as a result of the interaction moves to higher energy. Because the oxygen nonbonding orbitals are at lower energy, any interaction of the S or A nonbonding orbital with the C-C σ* is unimportant. However, the interaction of the S and A nonbonding orbital with C-C σ is prevalent. The symmetric (S) nonbonding combination is clearly destabilized by this interaction. The 1-2 and 3-4 σ bond yield an S and A pair of σ orbitals and an S and A pair of σ* orbitals. In the first approximation the effect on n_1+n_2 of having one S level below it and one above it will cancel out[69]. However increasing the σ-bond frame (such as with substituents) may cause an increase of A and S σ orbitals and thus further interactions of the S and A nonbonding pairs. However, the direction of the interaction is unambiguous; n_1-n_2 emerges at lower energy than n_1+n_2. The magnitude of the shifts is a function of the overlap of $n_1 \pm n_2$ with the σ molecular orbitals. The large magnitude of such interactions has been confirmed[70,66] and more recently, the energy ordering has been proven[49].

Leonard & Mader have examined the spectra of cyclic diketones of the type below, with n = 1,2,3,4 and 14.

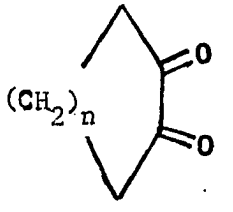

For the small rings the carbonyl groups are almost coplanar and have the cis configuration,and for large n they are again coplanar with the trans configuration. For intermediate ring sizes, however, the carbonyl groups are no longer coplanar. The spectrum depends on the π-electron interaction of the two groups, which in turn depends on the angle (the torsion angle) between the planes of the two carbonyl groups. Two bands with intensities comparable to that of the n-π* absorption of monocarbonyl compounds are observed in the spectra. See Table 3. The band at longer wavelengths due to the n_S-π_S* transition, varies with the angle of twist about the intercarbonyl bond over a range of 1290 A°, but the band at shorter wavelengths, due to the n_A-π_A transition, lies close to the position of the monocarbonyl absorption, the range of displacement being only 200 A°. [6,7,44]

The studies by Leonard and Mader[5], along with others[53,54] have established the n_S-π_S absorption maximum to be no greater than 482 mμ

Table 3

The dependence of the carbonyl absorption band on the geometry of some cyclic α,β-diketones. λ_1 is due to the $n_S-\pi_S^*$ transition. λ_2 is due to the $n_A-\pi_A^*$ transition.

n	Torsion Angle	λ_1 (A°)	λ_2 (A°)
1	0-10°	4660	2800
2	0-60°	3800	2975
3	90-110°	3370	2990
4	100-140°	3430	2955
14	100-180°	3840	2865

for unsubstituted α-dicarbonyls which are not further conjugated with other π bonds in the molecule (A conjugation of this sort may lower the lowest antibonding MO, compared to that of an isolated diketone, and impart a greater red shift to the n-π* abosrption maximum[50]. The 482 mμ maximum for the saturated species of course is based primarily on the extent of the influence of the torsion angle in the long wavelength spectra.

However, with the unusual absorption spectra of 3,4 di-t-butyl-cyclobutanedione (536 mμ) reported[1], attention must be placed on the possibility of other significant bathochromic influences in the n-π* spectra. The DTCD diketone contains no unsaturated or heteratom substituent since the 3,4-disubstituted group is an alkyl species. There has been no significant study on the effect of alkyl groups in the n-π* absorption spectra, although it is established that alkyl substituents in the α or β position of other chromophoric groups could have a significant bathochromic influence in the absorption spectra (See Chapter I).

This chapter has dealt with the influence of molecular structure of simple saturated and unsaturated carbonyl and dicarbonyls. From most previous theoretical and empirical analysis of the carbonyl spectra, satisfactory interpretation has mainly revolved around energy variations of the π MO's. However, the n-π* transition of the carbonyl system, especially the α-diketone system can have significant dependence on the interaction of the nonbonding MO.[69-72]

It is apparent that a valid theoretical interpretation of the spectral features of these systems should require an assessment of the nonbonding molecular orbitals as well as the π and σ MO's. Therefore an assessment of the extent to which the molecular orbitals in a diketone can interact will entail a study of the various effects of molecular substituents and molecular conformations on the energy of the respective MO's. Calculations presented in chapter IV will show the importance of these effects on n-π* transition energies in 3,4 substituted cyclobutanediones.

Chapter IV

Calculations and Results

As mentioned in the preceeding chapter, this study will employ the Extended Huckel Molecular Oribtal Method in an attempt to gain a better insight of the unusual n-π^* solution spectra of 3,4 di-t-butylcyclobutanedione (DTCD). Attention will be focused on alkyl substitution to the diketone system since it is the t-butyl addition to the basic 1,2 cyclobutanedione structure that is the apparent influence for the abnormally long wavelength absorption spectra of DTCD. Since the alkyl group can obviously have many possible conformations in solution, it will be necessary not only to study the effects of the substituent on the electronic network of the diketone system but to consider the effects of various prospective molecular conformations as well.

The method of study is to examine the electronic states of several selected alkyl-substituted models and to basically focus on the intramolecular interactions of each. The EHMO method can satisfactorily show the changes in the nonbonding as well as the sigma (σ) and pi (π) orbitals in these models. The electronic interactions can occur not only through spatial overlap but also through the sigma bonds of the molecule which are appropriately included in the EHMO method. The likely importance of this inclusion can be detected by examining the contribution of the σ bond network to the molecular orbitals of the respective models. The

total interaction is reflected in the resulting EHMO's and each model will be presented in terms of these as well as the total ground state energy.

The relative effects of the various substituents will be correlated inorder to provide adequate interpretation to the solution absorption spectra of DTCD. Since the n-π^* transition of each species is of particular interest, the n and π^* MO's will be examined specifically. The most favorable conformations for DTCD in solution in terms of both molecular stability and maximum shift of the n-π^* peak are considered.

Selected models include different 1,2 cyclobutanedione structures having various alkyl substituents (with varying conformations) in the 3,4 position of the butane ring. The alkyl substituents used are methyl, ethyl and t-butyl groups. The study includes the mono- and di-substituted models but tri- and tetra- substituted models are also considered for some cases. Primary attention is placed on the trans isomer; however, cis isomers are studied when sterically allowed. Various degrees of rotation of the respective substituents are included. In addition to these models, glyoxal models are also investigated. The results of the EHMO calculations are presented in four separate sections:

(1) Glyoxal Interactions
(2) Methyl Interactions
(3) Ethyl Interactions
(4) T-butyl Interactions

The initial coordinates for the models investigated were obtained,

where appropriate, from the crystal structure of tricyclo (4.4.2.0)[16] dodeca-3,8-diene-11,12-dione (2DB)[19]. Other needed coordinate portions were calculated using C-C bond distances and C-H bond distances of 1.54 A^{o} and 1.10 A^{o} respectively. All C-C-C, C-C-H and H-C-H bond angles, not including butane ring angles, were assumed to be tetrahedral. The atomic coordinates and the corresponding EHMO results are presented for each system studied.

(1) Glyoxal Interactions

The cis-glyoxal (gly-120) model, where C-C-H equals 120^{o}, figure 6, is investigated. The gly-120 model has C_{2v} point-group symmetry and all atoms of the molecule are coplanar in the xz plane.

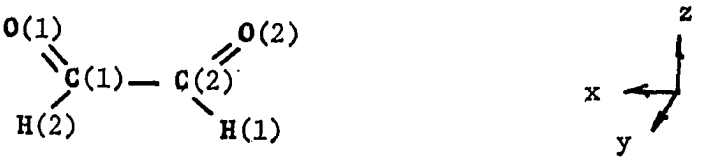

Figure 6. gly-120 model; C-C-H = 120^{o}

Table 4b shows the atomic coordinates used in the gly-120 calculations. This common atom-numbering scheme for the identification of atomic coordinates will be used for subsequent coordinate tables. Table 4a shows the EHMO energies and corresponding atomic coefficients for the gly-120 model. The identification and labeling of these is also typical of subsequent such tables in this study. The EHMO's are identified as σ, π or n. An asterisk superscript dentoes antibonding. Absence of the asterisk denotes bonding. The subscript (S or A) denotes the symmetric or antisymmetric symmetry of that MO with respect to the mirror plane (yz) that bisects the C-C bond of the dicarbonyl. Point-group symmetries are shown in parenthesis. The MO coefficients are identified by the atom symbol, number, and atomic orbital respectively. The s,x,y and z stand for the 2s, $2p_x$, $2p_y$ and $2p_z$ AO's respectively. The 1s AO is used for hydrogen in all cases but is not specified. The coefficients of the respective atomic orbitals can be studied to determine the electronic distribution in a particular MO. Only the coefficients with a value greater than 0.1 will be considered significant contributors.

Table 4a

(Model I)

Selected EHMO's for Glyoxal (gly-120) + C_{2v} symmetry (C-C-H=120°)

MO(sym.)	$\pi_S^*(B_2)$	$n_S(A_1)$	$n_A(B_1)$	$\sigma_S(A_1)$	$\pi_A(A_2)$	$\sigma_A(B_1)$
Energy (eV)	-11.277	-13.910	-15.703	-17.456	-18.123	-18.147
C_{ij}'s						
H(2)	0.0	-0.324	-0.395	0.131	0.0	0.084
O(1,s)	0.0	0.006	0.037	0.043	0.0	0.027
C(1,s)	0.0	0.103	-0.153	0.100	0.0	-0.018
O(1,x)	0.0	-0.313	-0.020	-0.354	0.0	-0.600
C(1,x)	0.0	0.355	-0.009	0.179	0.0	-0.054
O(1,y)	0.334	0.0	0.0	0.0	0.662	0.0
C(1,y)	-0.642	0.0	0.0	0.0	0.150	0.0
O(1,z)	0.0	-0.240	-0.451	0.464	0.0	-0.253
C(1,z)	0.0	0.226	0.269	-0.153	0.0	-0.134

+Symmetry related values are not shown.
This is typical for all tables

Table 4b

Atomic Coordinates for gly-120 (A°)

(Model I)

	x	y	z
O(1)	-1.624	0.0	2.368
O(2)	1.624	0.0	2.368
C(1)	-0.775	0.0	1.533
C(2)	0.775	0.0	1.533
H(1)	1.325	0.0	0.580
H(2)	-1.325	0.0	0.580

The n and π^* MO's of interest are the highest occupied (HOMO) and lowest empty molecular orbitals (LEMO), respectively. This is the case for all diketone models studied here. The HOMO is always identified as the symmetric combination of two lone-pair orbitals from the oxygen atoms, delocalized somewhat over neighboring atoms. The coefficients of the AO's of the HOMO, n_S, are such that the resulting contributing orbitals are nearly perpendicular to the carbonyl bonds and coplanar with the diketone. This MO is symmetric to reflection in the plane (xz) of the paper. In each case there are significant contributions from the $2p_x$ and $2p_z$ AO's of both the carbonyl carbon and carbonyl oxygen. Contributions, although usually small, also arise from several other basis functions. In the case of glyoxal, the hydrogen 1s AO has substantial contribution. Overall, the HOMO is interpreted to be a molecular orbital arising from the interaction of two lone- pair 2p AO's of the oxygens through the C-C bond of the carbonyl carbons. The HOMO no longer has the appearance of an isolated nonbonding atomic orbital, since it is clearly delocalized. All-valence-shell as well as *ab initio* calculations of other molecular systems have also shown the liberal delocalization of lone-pair orbitals.[55,56,57]

The LEMO, π_S^*, is centered on the diketone. This MO has its major contribution obtained from the $2p_y$ AO's of the two carbonyl carbons with significant contribution from the $2p_y$ AO's of the carbonyl oxygen. This MO is of an antibonding nature and is antisymmetric to reflection in the plane of paper (xz).

The symmetry-allowed n-π^* transition from the HOMO (n_S) to the LEMO (π_S^*) is the n-π^* transition of particular interest.

From chapter III it was established that for the electronic network of a simple dicarbonyl there are generally two nonbonding MO's (n_S & n_A) and there are four π MO's: two bonding (π_S & π_A) and two antibonding MO's (π_S^* & π_A^*). For an EHMO system, where the sigma bonds are included, sigma MO's also appear.

The HOMO and LEMO of each diketone system are much closer in energy to the lower occupied MO's than to higher unoccupied MO's. It is interesting to note that the orbitals closest in energy to the n and π^* MO's with the proper symmetry for mixing are the lower, occupied σ orbitals. Any interaction between either an isolated n or an isolated π^* orbital with these MO's would result in the destabilization of either orbital, since when two isolated states are allowed to interact, the level of higher energy is destabilized.

The cis-glyoxal system with sp^2 hybridized angles similar to those of the cyclobutanedione structure is also investigated. This investigation clearly reveals the sensitivity of the MO's to conformational changes. Table 5a presents the EHMO results for cis-glyoxal, where angle C_1-C_2-H_1 equals 90° (gly-90). See Figure 7 . Table 5b shows the coordinates used . From these results, the importance of the sigma network to the intramolecular interactions of the glyoxal system is forthcoming.

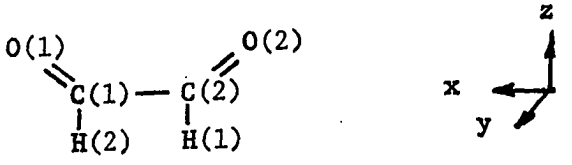

Figure 7. gly-90 model; C-C-H = 90°

Table 5 a

(Model II)

Selected EHMO's for Glyoxal (gly-90)

C_{2v} symmetry

(C-C-H=90°)

MO(sym.)	$\pi_S^*(B_2)$	$n_S(A_1)$	$n_A(B_1)$	$\sigma_S(A_1)$	$\sigma_A(B_1)$	$\pi_A(A_2)$
Energy (eV)	-11.277	-13.406	-15.298	-17.807	-18.078	-18.123
H(2)	0.0	-0.282	0.423	-0.165	0.049	0.0
O(1,s)	0.0	-0.019	-0.027	-0.060	0.019	0.0
C(1,s)	0.0	0.126	0.195	-0.048	-0.007	0.0
O(1,x)	0.0	-0.325	-0.016	0.309	-0.578	0.0
C(1,x)	0.0	0.413	-0.002	-0.146	-0.064	0.0
O(1,y)	0.334	0.0	0.0	0.0	0.0	0.662
C(1,y)	-0.642	0.0	0.0	0.0	0.0	0.151
O(1,z)	0.0	-0.176	0.378	-0.500	-0.323	0.0
C(1,z)	0.0	0.246	-0.304	0.121	-0.128	0.0

TEE = -473.009 eV

Table 5b

Atomic Coordinates (A°) for gly-90

(Model II)

	x	y	z
O(1)	-1.624	0.0	2.368
O(2)	1.624	0.0	2.368
C(1)	-0.775	0.0	1.533
C(2)	0.775	0.0	1.533
H(1)	0.785	0.0	0.432
H(2)	-0.785	0.0	0.432

The n-π^* transition of the glyoxal is significantly altered, in changing the hybridized angles to that of gly-90. The n-π^* transition is shifted from 2.633 eV to 2.129 eV. This red shift is caused totally by the greater destabilization of the HOMO (n), relative to the LEMO (π_S^*), as depicted in figure 8 .

The "strained" 90^o hybridized angle of gly-90 alone should be expected to cause destabilization of the molecule, since a sp^2 hybridized angle is generally 120^o. [42] This is reflected in the total energy of gly-90 (-473.019 eV) relative to gly-120 (-474.277 eV). Destabilization is observed throughout the bonding MO's. The MO's most affected are the HOMO and σ_S MO. The HOMO is destabilized by approximately 0.5 eV; the σ_S MO is stabilized by approximately 0.4 eV.

The manipulation of the C_1-C_2-H_1 bond angle, which is part of the carbon sp^2 hybridized network, should indeed affect the sigma MO's as well as the nonbonding MO. The carbon sp^2 hybrid system (which includes carbon $2p_x$ and $2p_z$) as well as the hydrogen 1s orbital contribute significantly to the sigma bonds as well as to the nonbonding hybrid. The C-H, C-C, and C-O sigma bonds are all formed from the carbon sp^2 hybrid network. The variation of the C-C-H angle can basically be described through the change of the sigma and nonbonding network portions of the glyoxal model. From figure 6, it can be seen that the π MO's of the two systems (gly-90 & gly-120) are identical in energy. That is, the change in the hybridized angle causes no change in the pi network energies of the glyoxal system.

The destabilization of the n MO is apparently caused by sigma network interactions. One interesting observation is that the glyoxal

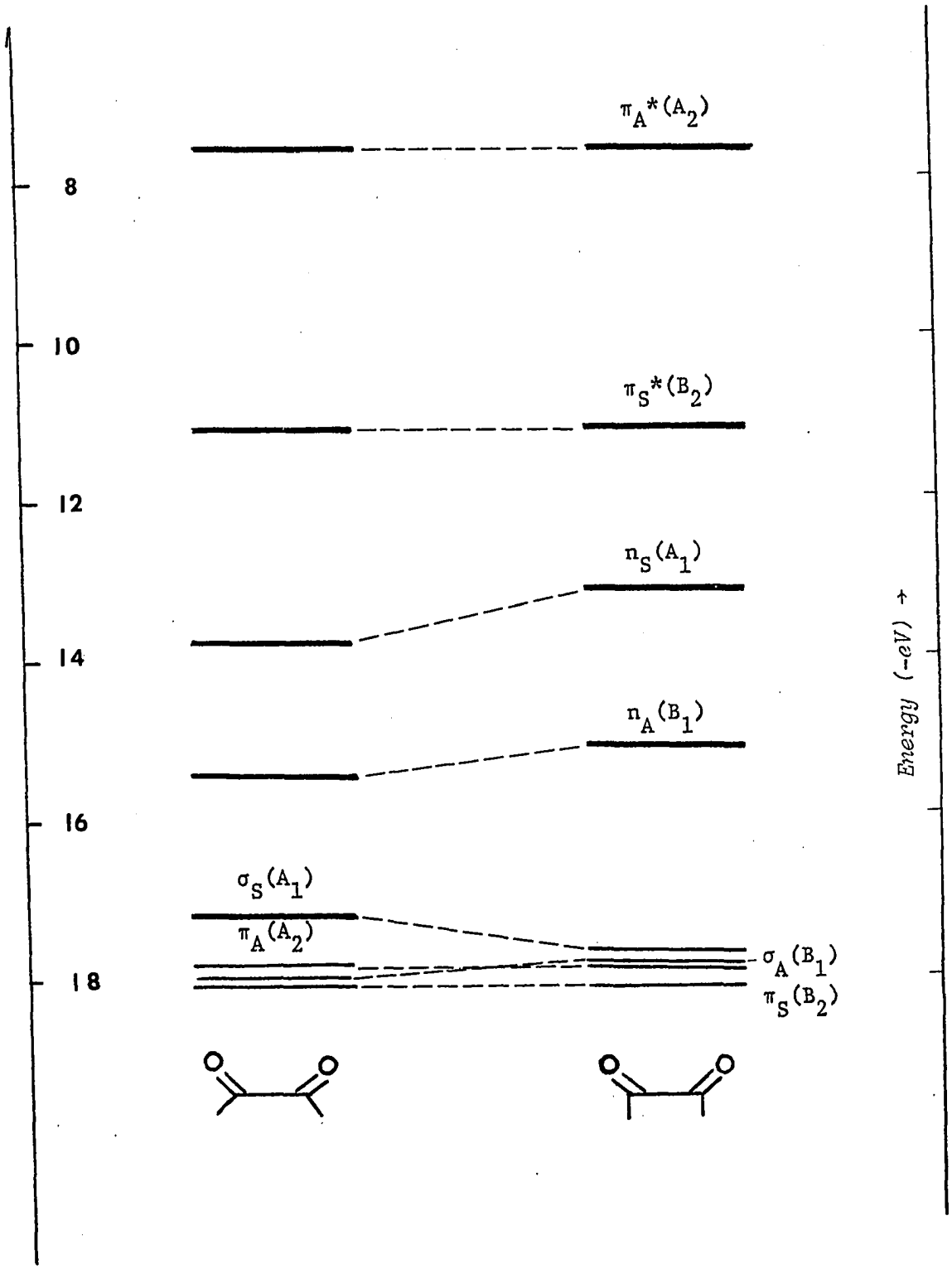

Figure 8. The energy level diagram depicting the gly-120 → gly-90 interactions.

sp^2 orbitals in gly-90 reveal greater contribution from the carbonyl carbons (C_1 & C_2) to the nonbonding hybrid than in the gly-120 system. This increases the opportunity for interaction of the nonbonding MO with substituents on the carbonyl carbon.

The gly-90 has two sigma MO's (σ_S & σ_A) between the HOMO and highest energy π bonding MO (π_A). The gly-120 has only one such MO (σ_S) in the parallel case. This increases the opportunity for interactions involving the sigma network with the n or π^* MO's.

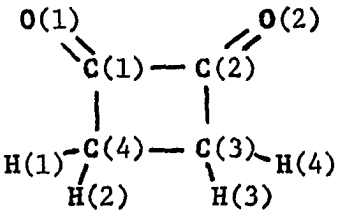

Figure 9. CBD Model & numbering scheme

The next system investigated in 1,2 cyclobutanedione (CBD). In essence, this is a glyoxal with an ethane substituent (C_3 & C_4) that defines a butane ring with the glyoxal system, figure 9 above. The coordinates were obtained from the 2DB crystal structure[54], and are listed in Table 6b. The diketone and butane ring portions are coplanar (xz). The EHMO results are presented in Table 6a.

A destabilization (relative to the gly-120 or gly-90 systems) for the n and π^* MO's of CBD is observed. The energy of the nonbonding MO

Table 6_a

(MOdel III)

Selected EHMO's for CBD

(C_{2v} symmetry)

MO(sym.)	$\pi_S^*(B_2)$	$n_S(A_1)$	$n_A(B_1)$	$\sigma_S(A_1)$	$\sigma_A(A_2)$
Energy(eV)	-10.907	-12.857	-13.724	-14.089	-14.891
C_{ij}'s					
H(1)	-0.134	-0.081	0.147	-0.143	-0.335
H(2)	0.134	-0.081	0.147	-0.143	0.335
O(2,s)	0.000	0.020	0.035	0.028	0.000
C(2,s)	0.000	-0.091	-0.205	-0.084	0.000
C(3,s)	0.000	0.0666	-0.043	0.082	0.000
O(2,x)	0.000	0.284	0.005	0.059	0.000
C(2,x)	0.000	-0.389	0.031	-0.056	0.000
C(3,x)	0.000	0.034	-0.010	0.536	0.000
O(2,y)	-0.319	0.000	0.000	0.000	0.074
C(2,y)	0.638	0.000	0.000	0.000	-0.064
C(3,y)	-0.055	0.000	0.000	0.000	-0.381
O(2,z)	0.000	0.178	-0.266	-0.101	0.000
C(2,z)	0.000	-0.278	0.313	0.060	0.000
C(3,z)	0.000	0.298	-0.440	-0.126	0.000

TEE = -649.764 eV

Table 6b

Atomic Coordinates (A^o) for CBD

(Model III)

	x	y	z
O(1)	-1.624	0.0	2.368
O(2)	-1.624	0.0	2.368
C(1)	0.775	0.0	1.533
C(2)	-0.775	0.0	1.533
C(3)	-0.786	0.0	0.0
C(4)	0.786	0.0	0.0
H(1)	-1.298	0.883	-0.408
H(2)	-1.298	-0.883	-0.408
H(3)	1.298	-0.883	-0.408
H(4)	1.298	0.883	-0.408

is increased by 1.05 eV and the π^* energy is increased 0.37 eV relative to the gly-120 system. The same MO's are increased by 0.55 eV and 0.37 eV respectively, relative to the gly-90 system. In both comparisons a significant interaction is implied for the n and π^* MO's of CBD with the predominant interaction involving the nonbonding MO. The over-all relative effect is a red shift in the n-π^* transition for the CBD system.

The energy of the π bonding MO's (π_A & π_S) does not change significantly on going from the glyoxal systems to that of CBD (i.e. an energy change of less than 0.015 eV). The destabilization of the n and π^* MO's is apparently caused by interactions of the sigma bonding system. See figure 10. Close scrutiny of the MO's support this assertion. There are 5 sigma (σ) MO's between the HOMO and the highest energy π bonding MO, π_A. The highest of these, σ_S, is within 1.5 eV. of the HOMO. For the previous models studied, no σ MO fell within this 1.5 eV range. The sigma-interactions in the CBD system are enhanced accordingly.

The contribution to the HOMO (n_S) from the Carbon $2p_x$ and $2p_z$ of C_1 & C_2 is increased in the CBD system relative to glyoxal. The increase is largest in the $2p_z$ direction. This gives the n MO more of a component in the z direction, and increases the chance for overlap of the nonbonding MO with carbonyl substituents, especially in the C_3 & C_4 positions. Furthermore, the CBD nonbonding delocalization is significantly extended to the two carbon substituents (C_3 & C_4). The significant contribution comes primarily from the carbon $2p_z$ atomic orbitals ($C_{3,z}$ & $C_{4,z}$). This observation further implicates through-bond interaction of the nonbonding and sigma networks. The nonbonding-sigma MO

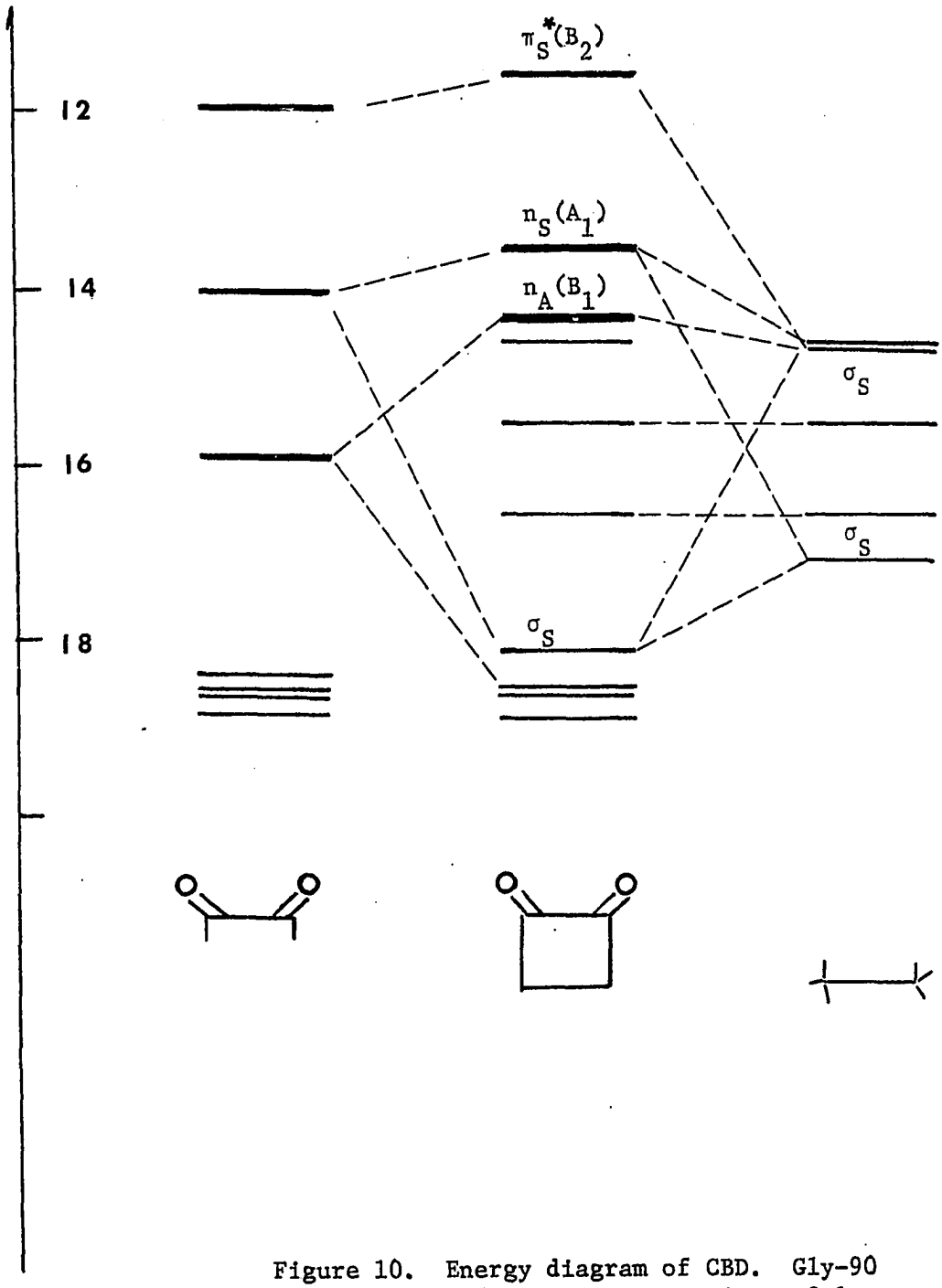

Figure 10. Energy diagram of CBD. Gly-90 and ethane interaction. Only selected MO's are labeled.

interactions result in the increased delocalization of the hybrid-nonbonding MO throughout the CBD σ system.

The destabilization of the π* MO is also due to its interaction with the σ bond network. This is further realized from the delocalization of the π* system with the CBD system. For the glycxal system, the only contribution to the π* MO was from the carbonyl carbon and carbonyl oxygen, and exclusively from the $2p_y$ atomic orbitals. For CBD, however, significant contribution to the π* MO is observed for the atomic 1s orbitals of the four hydrogen substituents (H_1, H_2, H_3 & H_4). The destabilization of the π* MO is probably due to interactions of the dicarbonyl π system with the hydrogen orbitals such as those shown in figure 11. The bulk of the π* MO is located on the carbonyl carbon, which may facilitate the interaction.

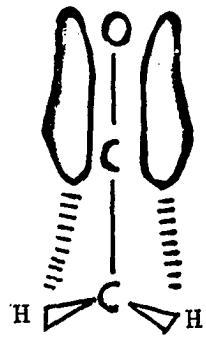

Figure 11. Depiction of probable interaction of CBD π system with hydrogen orbitals. (yz projection)

While the ethane substituent (C_3 & C_4) in a bonding relation to the glyoxal, increases the delocalization of the system's MO's, it will be of considerable interest to observe the interaction of a methane group and a diketone system in a through-space capacity (i.e. at a distance too large for intramolecular bonding but in close proximity for significant interaction). This is especially interesting since in the case of a system such as DTCD orientation of the tertiary butyl groups may allow for significant methyl through-space interactions between methyl groups and the diketone network.

The intermolecular interaction of the glyoxal systems (both gly-120 & gly-90) with methane molecules is studied. The purpose of this calculation is to consider the influence of through-space interactions on the n and π^* MO's. The distance of the methane molecule from the glyoxal is chosen to be approximately 1 1/2 C-C bond distances. It is situated much the same as a methyl on the DTCD t-butyl group, figure 12. (The t-butyl orientation presenting the shortest methyl distance to the glyoxal is used, assuming normal tetrahedral angles). This, of course , would allow for maximum interaction. Interactions are studied using one and two methane groups respectively. The two methane groups are situated in a trans position to the glyoxal. Table 7a shows the EHMO results for the gly-90 molecule interacting with the two isolated methanes and table 7b presents the corresponding coordinates. Table 8 summarizes the results for the interactions. For other results, see Appendix Guide, Page 156. For both the gly-90 and gly-120 a blue shift of the n-π^* transition occurs for this type of interaction. The n-π^* ΔE increases from 2.13 eV for gly-90 to 2.24 eV

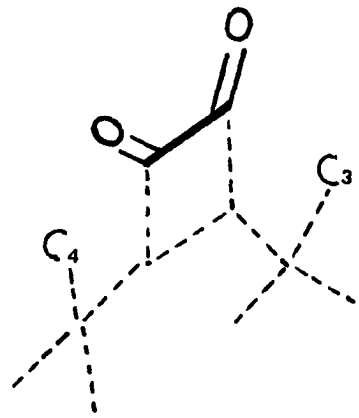

Figure 12a

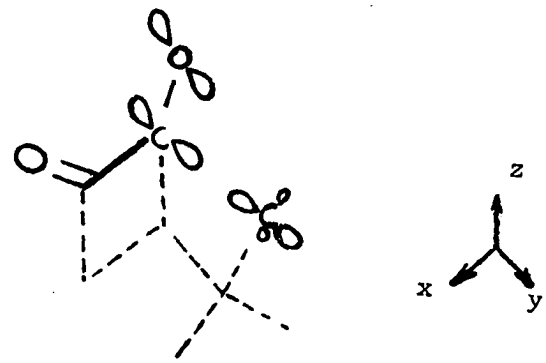

Figure 12b

Figure 12: a) illustrates the relative position of the methanes (C_3 & C_4) to the glyoxal system. Dashed lines outline a t-butyl. b) shows atomic orbitals making major contribution to the LEMO of gly-90 and methane system.

Table 7a

Selected EHMO's for Glyoxal Interactions

Models: V & VII
C_2 Symmetry
Model V: Gly-120 with two methanes
Model VII: Gly-90 with two methanes

	Model V			Model VII		
MO(sym.)	π_S^*(B)	n_S(A)	n_A(B)	π_S^*(B)	n_S(A)	n_A(B)
Energy (eV)	-11.048	-13.697	-14.696	-11.052	-13.298	-14.607
C_{ij}'s						
H(2)	-0.028	0.320	-0.290	0.0310	-0.283	-0.338
H(3)	-0.036	0.029	-0.130	0.036	-0.019	-0.131
H(4)	-0.012	0.060	-0.177	0.011	-0.028	-0.144
H(5)	0.058	-0.026	0.153	-0.057	0.008	0.141
H(6)	0.039	-0.111	0.199	-0.038	0.072	0.171
O(1,s)	-0.004	-0.002	0.015	0.006	-0.020	0.008
C(1,s)	-0.011	-0.082	-0.122	0.012	0.118	-0.159
C(3,s)	0.029	-0.019	0.031	-0.029	0.012	0.031
O(1,x)	0.001	0.284	0.002	-0.002	-0.313	0.021
C(1,x)	0.011	-0.338	0.029	-0.008	0.404	0.028
C(3,x)	0.043	-0.045	0.131	-0.043	0.032	0.132
O(1,y)	0.311	0.031	-0.117	-0.311	-0.010	-0.108
C(1,y)	-0.647	-0.015	0.045	0.647	0.010	0.045
C(3,y)	-0.067	0.104	-0.276	0.066	-0.063	-0.243
O(1,z)	-0.008	0.230	-0.239	0.004	-0.173	-0.228
C(1,z)	0.022	-0.239	0.207	-0.020	0.252	0.247
C(3,z)	0.061	0.074	-0.005	-0.060	-0.066	0.003

TEE = -756.505 eV

Table 7b

Atomic Coordinates (A^{o}) for Models V & VII

	Model V			Model VII		
	x	y	z	x	y	z
O(1)	-1.624	0.0	2.368	-1.624	0.0	2.368
O(2)	1.624	0.0	2.368	1.624	0.0	2.368
C(1)	-0.775	0.0	1.533	-0.775	0.0	1.533
C(2)	0.775	0.0	1.533	0.775	0.0	1.533
C(3)	-2.014	2.135	0.600	-2.014	2.135	0.600
C(4)	2.014	-2.135	0.600	2.014	-2.135	0.600
H(1)	1.325	0.0	0.580	0.786	0.0	0.433
H(2)	-1.325	0.0	0.580	-0.786	0.0	0.433
H(3)	-3.108	2.228	0.537	-3.108	2.228	0.537
H(4)	-1.548	3.129	0.526	-1.548	3.128	0.526
H(5)	-1.737	1.656	1.551	-1.737	1.656	1.551
H(6)	-1.659	1.509	-0.232	-1.659	1.509	-0.232
H(7)	3.108	-2.228	0.537	3.108	-2.228	0.537
H(8)	1.737	-1.656	1.551	1.737	-1.656	1.551
H(9)	1.548	-3.128	0.526	1.548	-3.128	0.526
H(10)	1.659	-1.509	-0.232	1.659	-1.509	-0.232

Table 8

SUMMARY OF GLYOXAL–METHANE
INTERMOLECULAR INTERACTIONS

(EHMO energy values for the four through-space glyoxal-methane interactions)

Glyoxal Model	Compound No.	No. of Methanes	LEMO(eV)	HOMO(eV)	TEE(eV)	$n-\pi^*$ ΔE
gly-120	I	0	-11.278	-13.910	-474.277	2.632
gly-90	II	0	-11.278	-13.406	-473.009	2.128
gly-120	IV	1	-11.167	-13.788	-615.394	2.621
gly-90	VI	1	-11.170	-13.348	-614.273	2.178
gly-120	V	2	-11.049	-13.697	-756.505	2.648
gly-90	VII	2	-11.052	-13.298	-755.535	2.246

when through-space interaction with the methane groups are included. Although the n & π* MO's are both destabilized, the blue shift is caused basically by the destabilization of the π* (LEMO). The increase of energy of the LEMO (0.226 eV) is more than twice that of the nonbonding MO (0.108 eV). The reason for this can be seen in figure 10b, which shows the hybridized atomic orbitals making contribution to the LEMO. The major contributors are the $2p_y$ atomic orbitals of the carbonyl carbon and oxygen. Some contributions from the $2p_y$ and $2p_z$ ao's of the "extended" methan carbons are also observed. The position of the methane group relative to the glyoxal allows for a greater interaction with the π* MO than with the nonbonding MO (n). The π* MO, which is located predominantly on the carbonyl carbon and points along the y axis, is more accessable for interaction. The n MO on the other hand is in the xz plane which minimizes its chance for interaction.

This effect is in agreement with another theoretical study involving EHMO calculations of glyoxal-ethane and glyoxal-ethylene intermolecular interactions[55]. In that study, both the ethane and ethylene species caused destabilization of the n & π* MO's. In both cases, however, the greatest destabilization was in the LEMO and a blue shifted n-π* transition was predicted. Application of HMO and SCF MO methods also predicted a blue shift in the n-π* transition due to the diketone-ethylene interaction[55].

Through-space interactions for CBD with one and with two isolated methane groups is also investigated. The positioning of the methane (s) relative to the diketone portion of CBD is the same as that used for the gly-90 - methane interactions, figure 13. The methane groups are located

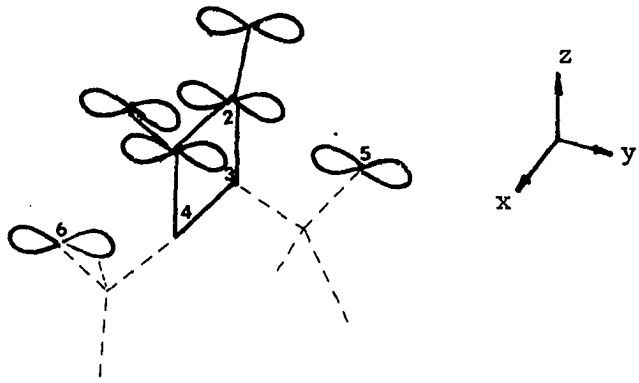

Figure 13 depicts the atomic orbitals making major contribution to the LEMO of the CBD-2 methane interaction. The methane groups (C_5 & C_6) are trans to the CBD model. The dashed lines reveal their position relative to a t-butyl group.

Table 10

Selected EHMO energy values for CBD-methane through-space interactions.

No. of Methanes	Compound No.	LEMO (eV)	HOMO (eV)	TEE(eV)	$n-\pi^*$ ΔE
0	III	-10.907	-12.857	-649.764	1.950
1	VIII	-10.873	-12.849	-789.622	1.976
2	IX	-10.840	-12.839	-929.475	1.999

to correspond to the appropriate parts of the t-butyl network of DTCD. The CBD and two-methane system typifies the results. Figure 13 illustrates the CBD interactions with the two methanes by depicting the atomic orbitals making major contributions to the LEMO. Table 9 shows the EHMO results for the CBD and two-methane system and the corresponding atomic coordinates.

The CBD-methane interactions show much the same effects on the n and π^* MO's as the previously studied through-space interactions of the glyoxal-methane systems. The n and π^* MO's are again both destabilized with the π^* MO being the most affected. The HOMO increases in energy by approximately 0.02 eV while the LEMO increases by approximately 0.07 eV, relative to the isolated CBD.

While the through-space interaction of CBD (in terms of n & π^* energies) is somewhat less than that of the glyoxal system, the qualitative effects are identical. As in the parallel case for the gly-90 - methane system, the position of the methan group to CBD allows for more interaction of the π^* MO than for the n MO. As expected, the n-π^* blue shift due to the CBD-methane interactions is due primarily to the effect on the LEMO. Table 10 shows the LEMO and HOMO results for the two calculations. Table 37, appendix lists the EHMO results for the one methane interactions. The corresponding atomic coordinates are in table 54.

Table 9a

Selected EHMO's for CBD Interaction

Model IX: CBD & two methanes

C_2 symmetry

MO(sym.)	π_S^*(B)	n_S(A)	σ_S(A)	n_A(B)
Energy (eV)	-10.840	-12.839	-13.204	-13.640
C_{ij}'s				
H(2)	0.127	0.090	-0.067	-0.166
H(3)	-0.127	0.041	0.302	-0.103
H(5)	-0.026	-0.014	0.172	0.013
H(6)	0.046	-0.022	-0.003	0.079
H(7)	-0.005	0.036	-0.168	-0.045
H(8)	-0.019	0.019	-0.135	-0.056
O(2,s)	0.001	-0.021	-0.006	-0.031
C(2,s)	0.003	0.081	0.072	0.202
C(3,s)	0.006	-0.066	-0.014	0.057
C(5,s)	-0.013	0.008	-0.056	-0.015
O(2,x)	0.001	-0.275	-0.076	-0.007
C(2,x)	-0.003	0.382	0.077	-0.036
C(3,x)	-0.005	0.014	-0.373	0.000
C(5,x)	-0.070	-0.070	0.003	-0.071
O(2,y)	-0.314	-0.004	-0.001	0.015
C(2,y)	0.640	-0.001	0.036	-0.006
C(3,y)	-0.041	-0.033	0.251	0.048
C(5,y)	0.015	-0.052	0.204	0.077
O(2,z)	0.002	-0.179	0.015	0.252
C(2,z)	-0.008	0.283	-0.018	-0.311
C(3,z)	0.007	-0.305	0.027	0.427
C(5,z)	-0.018	0.010	0.051	-0.041

Table 9b

Atomic Coordinates (A^{o}) for Model IX

Model IX: CBD & two methanes

	x	y	z
O(1)	1.624	0.0	2.368
O(2)	-1.624	0.0	2.368
C(1)	0.775	0.0	1.533
C(2)	-0.775	0.0	1.533
C(3)	-0.786	0.0	0.0
C(4)	0.786	0.0	0.0
C(5)	-2.014	2.135	0.600
C(6)	2.014	-2.135	0.600
H(1)	1.298	0.883	-0.408
H(2)	-1.298	-0.883	-0.408
H(3)	-1.298	0.883	-0.408
H(4)	1.298	-0.883	-0.408
H(5)	-2.369	2.759	1.433
H(6)	-2.288	2.605	-0.355
H(7)	-2.475	1.139	0.666
H(8)	-0.920	2.036	0.656
H(9)	2.369	-2.760	1.432
H(10)	2.288	-2.606	-0.355
H(11)	2.475	-1.138	0.666
H(12)	0.920	-2.036	0.656

(2) Methyl Interactions

This particular phase of the investigation will focus on the intramolecular interactions of the 1,2 cyclobutanedione (CBD) model, with methyl substituents in the 3,4 position of the butane ring. Arbitrary rotations of the methyl substituents are made in order to observe the effects of various molecular conformations of the methyl group on the molecular orbital energies of the CBD system. The positive direction of rotation is clockwise when viewed down the axis of rotation toward the substrate. The eclipsed conformation of the substituent is referenced as the zero degree angle of rotation, while its staggered conformation is considered a 60 degree rotation. Since each methyl (or alkyl) substituent can have three points of reference, the point representing the smallest positive angle of rotation is used. For instance, the staggered conformation of the methyl group in figure 14a can have a 60°, 180° or a 300° angle of rotation when referring to H_1, H_2 or H_3 respectively. Atoms C(2), C(3), and C(5) define the zero plane of reference. H_1, rotated 60°, has the smallest positive angle of rotation and is therefore used to designate this conformation. H_2 and H_3 exhibit rotation angles of 180° and 300° respectively. Similarly, the eclipsed conformation will be designated as 0°, figure 14b.

Mono, di, tri and tetra substituted models are studied in order to determine the effect of poly substitution of the methyl group. The results of the various models investigated are categorized according to the number of methyl substituents and will be reported under the following headings:

(a) mono-substitution

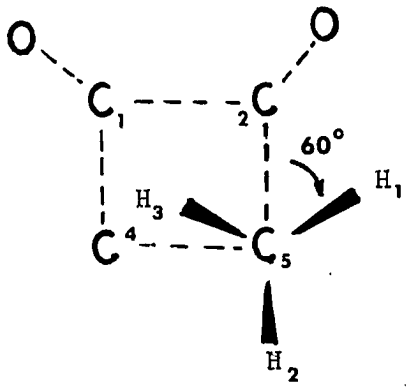

M_2

Figure 14a

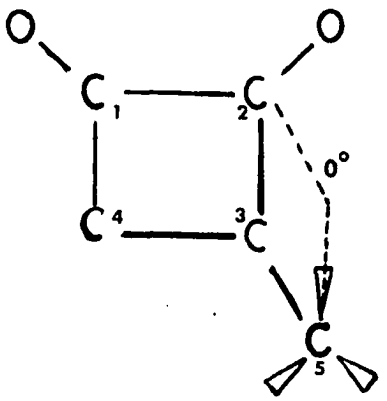

M_1

Figure 14b

Figure 14: a) view along C_5-C_3 bond of the staggered configuration of a methyl group on C_3 of CBD. C_3 is eclipsed by C_5.
b) 0^o (eclipsed) conformation of methyl substituent .

(b) di-substitution

(c) tri-substitution
&
tetra-substitution

(a) monosubstitution

For the mono substituted systems, the methyl substituent was in either an eclipsed (0^{o}) or staggered (60^{o}) conformation. The two different models thus derived will be respectively referred to as M_1 and M_2 and are seen in figure 14. The EHMO results and corresponding atomic coordinates are in tables 11a & 11b.

The molecular orbital network of both models reveals a destabilization of their respective n and π^* MO's relative to the CBD system. By the same comparison, the n MO for M_1 increases in energy approximately 0.11 eV, while the π^* MO increases 0.05 eV. The same two MO's for model M_2 increas 0.11 eV and 0.04 eV respectively. The n MO is obviously the MO most affected, having an increase in energy of over twice that of the π^* MO in both cases. Again the predicted red shift of the n-π^* transition of both systems is due largely to interactions of the nonbonding MO hybrid. The π bonding MO's of M_1 and M_2 are practically identical to those of the CBD system, therefore the methyl orbitals have mixed significantly in the n MO but negligibly in the π-bonding MO's. The nonbonding MO interactions are enhanced by the presence of seven sigma MO's that lie between the HOMO and the π-bonding MO's for M_1 as well as for M_2. σ_S lies within 1.5 eV of the n_S MO.

The HOMO for M_1 and M_2 reveals an increase in delocalization of that MO relative to the CBD system. The delocalization is extended through

Table 11a

Selected EHMO's for Models X & XI

Model X: Mono-substituted Methyl-CBD (eclipsed)

Model XI: Mono-substituted Methyl-CBD (staggered)

C_1 Symmetry

	Model X TEE = -755.576 eV			Model XI TEE = -755.681 eV		
MO(sym.)	$\pi_S^*(A)$	$n_S(A)$	$n_A(A)$	$\pi_S^*(A)$	$n_S(A)$	$n_A(A)$
Energy (eV)	-10.856	-12.743	-13.477	-10.868	12.751	-13.483
C_{ij}'s						
H(1)	-0.130	0.108	0.121	-0.129	0.074	-0.069
H(2)	-0.130	0.049	-0.145	0.129	0.046	-0.157
H(3)	0.130	0.049	-0.145	-0.130	0.102	0.106
H(4)	0.022	0.079	0.032	-0.036	-0.132	-0.144
H(5)	-0.015	-0.085	-0.156	-0.001	0.027	0.032
H(6)	-0.030	-0.076	-0.040	0.015	0.021	-0.055
O(1,s)	-0.001	-0.025	-0.034	-0.001	-0.025	-0.034
O(2,s)	0.000	-0.015	0.027	-0.000	-0.014	0.029
C(1,s)	0.007	0.118	0.174	0.006	0.117	0.173
C(2,s)	-0.006	0.048	-0.184	-0.004	0.050	-0.189
C(3,s)	0.005	-0.057	-0.010	0.005	-0.057	-0.007
C(4,s)	0.002	-0.057	0.025	-0.001	-0.058	0.030
C(5,s)	0.042	0.026	0.045	0.041	0.027	0.044
O(1,x)	0.005	0.268	-0.055	0.004	0.269	-0.056
O(2,x)	-0.006	-0.269	0.061	-0.004	-0.270	0.062
C(1,x)	-0.007	-0.364	0.106	-0.006	-0.366	0.107
C(2,x)	0.011	0.380	-0.046	0.008	0.381	-0.047
C(3,x)	-0.009	-0.057	-0.173	-0.013	-0.058	-0.153
C(4,x)	-0.003	0.042	0.137	0.003	0.039	0.112
C(5,x)	0.050	0.055	0.163	0.072	0.053	0.144
O(1,y)	0.321	-0.011	-0.005	0.321	-0.008	-0.005
O(2,y)	0.310	-0.027	-0.058	0.312	-0.023	-0.037
C(1,y)	-0.646	0.017	0.008	-0.645	0.013	0.008
C(2,y)	-0.626	0.039	0.047	-0.628	0.034	0.050
C(3,y)	0.076	0.037	0.106	0.078	0.042	0.120
C(4,y)	0.053	-0.005	-0.032	0.052	-0.010	-0.037
C(5,y)	-0.117	-0.089	-0.152	0.117	-0.097	-0.172
O(1,z)	0.001	-0.132	0.285	0.001	-0.134	0.283
O(2,z)	-0.009	-0.206	-0.156	0.006	-0.206	-0.165
C(1,z)	-0.001	0.219	-0.342	0.001	0.221	-0.342
C(2,z)	0.019	0.327	0.204	0.014	0.326	0.210
C(3,z)	0.028	-0.373	-0.316	-0.022	-0.368	-0.211
C(4,z)	0.001	-0.219	0.477	0.003	-0.221	0.475
C(5,z)	0.089	0.127	0.158	0.069	0.122	0.162

Table 11b

Atomic Coordinates (A^{o}) for Models X & XI

Mono-substituted methyl-CBD

	Model X			Model XI		
	x	y	z	x	y	z
O(1)	1.624	0.0	2.368	1.624	0.0	2.368
O(2)	-1.624	0.0	2.368	-1.624	0.0	2.368
C(1)	0.775	0.0	1.533	0.775	0.0	1.533
C(2)	-0.775	0.0	1.533	-0.775	0.0	1.533
C(3)	-0.786	0.0	0.0	-0.786	0.0	0.0
C(4)	0.786	0.0	0.0	0.786	0.0	0.0
C(5)	-1.497	1.259	-0.578	-1.497	1.259	-0.578
H(1)	-1.285	-0.891	-0.409	1.285	-0.891	-0.409
H(2)	1.285	-0.891	-0.409	1.285	0.891	-0.409
H(3)	1.285	0.891	-0.409	-1.285	-0.891	-0.409
H(4)	-1.845	1.887	0.254	-1.476	1.208	-1.677
H(5)	-2.354	0.937	-1.189	-0.968	2.159	-0.234
H(6)	-0.783	1.819	-1.200	-2.538	1.276	-0.223

the σ network of M_1 and M_2. The predominant contribution comes from $2p_x$ and $2p_y$ of the carbonyl carbon and oxygen, while significant contribution comes from the $2p_z$ atomic orbitals of carbons 3, 4 and 5 respectively. The presence of the methyl substituent apparently causes further interaction of the sigma-nonbonding MO's and consequently increased delocalization.

Whereas the eclipsed and staggered orientation of the methyl group cause similar n-π* shifts of the diketone species, the staggered conformation is predicted to be the most stable from the Extended Huckel total electronic energies (TEE). M_1 has a total electronic energy of -755.576 eV while M_2 has a value of -755.681 eV.

(b) di-substitution

For the di-substituted systems both cis and trans isomers are investigated. Several degrees of rotation of the methyl groups are studied. The rotation angles selected are: 0°, 30°, 60° and 90°. Five different configuration of the di-substituted models are considered. They are labeled: D_1, D_2, D_3, D_4 and D_5. The configurations are categorized by the rotation angle of one methyl group while C_s or C_2 symmetry is maintained. For the D_5 configuration, however, the "second" methyl group is rotated 60° out of symmetry. Table 12 summarizes the total energies & n-π* transitions of the 10 calculations.

The trans isomer is the most stable for each configuration (D_1,D_2,etc.)

Table 12: Selected EHMO results for Cis and Trans 3,4 dimethyl - CBD. Various methyl rotation angles are studied.

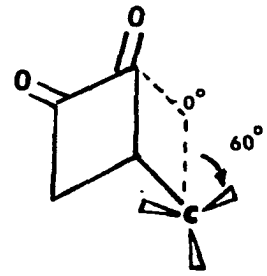

Config-uration	Methyl rotation	Cis isomer Model NO.	TEE(eV)	n-π* ΔE(eV)	Point group	Trans isomer Model No.	TEE(eV)	n-π* ΔE(eV)	Point group
D_1	0°	XII	-861.12	1.884	C_s	XIII	-861.38	1.865	C_2
D_2	30°	XIV	-861.16	1.869	C_s	XV	-861.40	1.859	C_2
D_3	60°	XVI	-861.48	1.871	C_s	XVII	-861.73	1.855	C_2
D_4	90°	XVIII	-861.38	1.893	C_s	XIX	-861.52	1.869	C_2
D_5+	90°	XX	-861.38	1.877	C_1	XXI	-861.46	1.862	C_1

+ For the D_5 configuration one methyl group is rotated 60° out of symmetry.

studied, and the configuration having the lowest total electronic energy (LTEE) for both the cis and trans isomer is the D_3 model (60^o rotation). The EHMO calculations of the D_3 model typify the results for all configurations surveyed and will be the case-in-point for this section. EHMO results and corresponding atomic coordinates for the D_3 configuration for both the cis and trans isomers are listed in tables 13 and 14. For other results, see Appendix Guide, Page 156.

In comparison to the CBD system, the π^* MO of the cis-D_3 model has a 0.08 eV increase in energy; its n MO energy is increased 0.16. The same MO's of the trans-D_3 model increase 0.08 eV and 0.18 eV, respectively. The enrgies of the π^* and n MO's are increased for all 10 di-substituted models, relative to CBD, and the increase is approximately 2 to 1 in favor of the nonbonding MO. The energy values of the n and π^* MO's vary slightly for each model. The n-π^* transitions of the trans configurations fluctuate within 0.01 eV, while the cis configurations exhibit a 0.03 eV range. This larger variation for the cis isomer is probably due to some through-space interactions of the adjacent methyl groups. For the trans isomer, this effect is less important. However, over-all, di-substitution creates a bathochromic shift of the n-π^* transition, in relation to the CBD system as well as to the mono-substituted systems. This observed destabilization of the n and π^* MO's of the di-substituted system relative to the CBD system is evidence of the effect of substituent interaction on these MO's.

The π bonding MO's of the di-substituted system are practically identical in energy to those of the CBD system (i.e. an energy change

Table 13

Selected EHMO's for CBD with cis di-Methyl Substitution (60° rotation)

Model XVI

C_s Symmetry

TEE = -861.480 eV

MO(sym)	π^*_S(A'')	n_S(A')	n_A(A'')	σ_S(A')	σ_A(A'')
Energy (eV)	-10.828	-12.699	-13.216	-13.517	-13.903
C_{ij}'s					
H(1)	-0.126	0.090	0.067	0.123	0.309
H(6)	-0.034	-0.104	-0.170	0.032	-0.062
H(7)	0.015	0.023	0.001	-0.201	0.049
H(8)	-0.001	0.021	0.020	0.036	0.199
O(1,s)	-0.001	-0.019	0.031	-0.023	0.009
C(1,s)	0.002	0.079	-0.183	0.073	-0.064
C(4,s)	0.004	-0.052	-0.008	-0.057	-0.051
C(6,s)	0.040	0.018	0.046	0.023	-0.032
O(1,x)	0.007	0.268	-0.001	0.040	0.000
C(1,x)	-0.013	-0.374	-0.033	-0.035	-0.012
C(5,x)	0.015	0.038	0.034	0.510	-0.026
C(6,x)	-0.071	-0.030	-0.110	-0.185	0.079
O(1,y)	0.314	-0.022	-0.028	-0.017	0.055
C(1,y)	-0.634	0.034	0.038	0.027	-0.066
C(4,y)	0.075	0.021	0.124	0.058	-0.342
C(6,y)	-0.112	-0.065	-0.170	-0.117	0.314
O(1,z)	-0.004	-0.173	-0.214	0.084	-0.088
C(1,z)	0.011	0.281	0.280	-0.061	0.102
C(4,z)	-0.017	-0.304	-0.406	0.104	-0.105
C(6,z)	0.065	0.089	0.181	0.008	-0.003

TABLE 14

Selected EHMO's for CBD with trans di-methyl Substitution (60° rotation)

Model XVII (C_2 Symmetry)

TEE = -861.576 eV

MO(sym)	π^*(B)	n_S(A)	n_A(B)	σ_S(A)	σ_S(B)
Energy (eV)	-10.826	-12.681	-13.292	-13.369	-14.110
C_{ij}'s					
H(1)	0.126	0.067	0.146	-0.002	-0.325
H(6)	-0.036	-0.107	0.171	0.030	-0.027
H(7)	0.016	0.016	-0.016	-0.206	0.062
H(8)	-0.001	0.018	-0.044	0.003	-0.183
O(1,s)	-0.001	-0.020	0.032	-0.018	0.015
C(1,s)	0.009	0.079	-0.194	0.056	-0.053
C(4,s)	-0.005	-0.051	-0.019	-0.036	0.077
C(6,s)	-0.040	0.025	0.031	0.046	0.034
O(1,x)	-0.000	0.266	-0.002	0.010	-0.073
C(1,x)	0.002	0.372	-0.035	0.000	0.072
C(4,x)	-0.009	0.053	0.028	0.456	-0.219
C(6,x)	0.070	-0.050	-0.072	-0.223	-0.013
O(1,y)	-0.314	-0.012	-0.034	-0.026	-0.059
C(1,y)	0.634	0.018	0.047	0.038	0.065
C(4,y)	-0.076	0.046	0.047	0.173	0.327
C(6,y)	0.007	-0.170	-0.230	0.087	-0.021
O(1,z)	0.007	-0.170	-0.230	0.087	-0.021
C(1,z)	-0.014	0.278	0.297	-0.074	-0.002
C(4,z)	0.024	-0.301	-0.422	0.104	-0.053
C(6,z)	-0.067	0.103	0.159	0.041	0.076

TABLE 15

Atomic Coordinates for Models XVI & XVII

	XVI			XVII		
	x	y	z	x	y	z
O(1)	1.624	0.0	2.367	1.624	0.0	2.367
O(2)	-1.624	0.0	2.367	-1.624	0.0	2.367
C(1)	0.775	0.0	1.532	0.775	0.0	1.532
C(2)	-0.775	0.0	1.532	-0.775	0.0	1.532
C(3)	-0.785	0.0	0.0	-0.785	0.0	0.0
C(4)	0.785	0.0	0.0	0.785	0.0	0.0
C(5)	-1.511	1.250	-0.578	-1.511	-1.250	-0.578
C(6)	1.511	1.250	-0.578	1.511	1.250	-0.578
			Hydrogens			
H(1)	1.298	-0.883	-0.408	1.298	-0.883	-0.408
H(2)	-1.298	-0.883	-0.408	-1.298	0.883	-0.408
H(3)	-1.490	1.200	-1.676	1.490	1.200	-1.676
H(4)	-2.552	1.256	-0.223	2.552	1.256	-0.223
H(5)	-0.992	2.156	-0.233	0.992	2.156	-0.233
H(6)	1.490	1.200	=1.676	-1.490	-1.200	-1.676
H(7)	2.552	1.256	-0.223	-2.552	-1.256	-0.223
H(8)	0.992	2.156	-0.233	-0.992	-2.156	-0.233

less than 0.01 eV). However, the σ MO network of the same system is again altered significantly. Nine sigma MO's now occur between the HOMO (n) and the highest π bonding MO (π_A), compared to five such MO's in the case of CBD. Two sigma MO's are within 1.5 eV of the HOMO compared to one and none, respectively, in the cases of CBD and glyoxal. Destabilization in the LEMO and more significantly the HOMO networks is due to their interactions with the sigma molecular orbitals.

Analysis of the nonbonding MO for the di-substituted models reveals a delocalization of this MO throughout the entire model. Significant contributions occur for all oxygen and carbon atoms. For the carbonyl carbon and oxygen, the $2p_x$ and $2p_z$ atomic orbitals are the biggest contributors. For carbons 3, 4, 5 and 6 the $2p_z$ atomic orbital is the sole contributor, with a coefficient value greater than 0.1.

(c) tri- and tetra-substitution

A trend for the effect of methyl substitution on CBD has now been established from the study of mono- and di-substituted models. The effect of methyl substitution as viewed for the tri- and tetra-substituted models only tends to confirm such a trend.

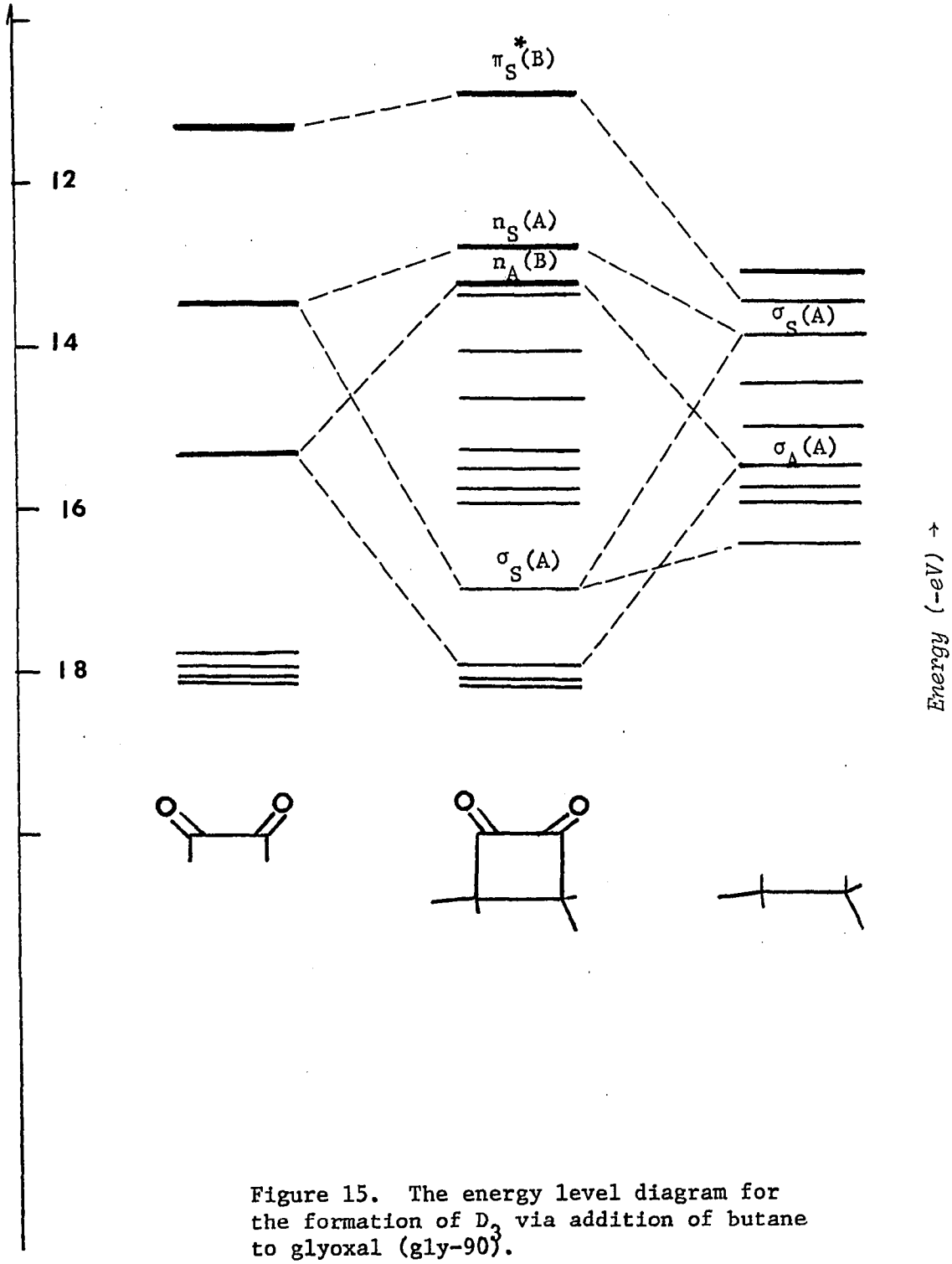

Figure 15. The energy level diagram for the formation of D_3 via addition of butane to glyoxal (gly-90).

For the tri- and tetra-substituted models, only the eclipsed (0^{o}) conformation of the methyl group is used. The two species will be referred to as T_1 and T_2, respectively. EHMO results for the two systems are in table 16 and 17 together with the corresponding atomic coordinates.

For both systems, T_1 and T_2, destabilization of the n and π^* MO's is again observed (relative to the CBD system). The effect is larger for the tetra-substituted model (T_2). However, in each case the HOMO (n_S) has the greatest increase in energy. Its increase is again almost twice that of theπ^* for both T_1 and T_2. T_1 reveals a 0.27 eV and 0.14 eV energy increase of its n and π^* MO's respectively. T_2 reveals a corresponding 0.31 eV and 0.18 eV increase. The over-all effect, however, is a red shifted n-π^* transition for both species with both having values significantly lower than the di-substituted systems.

Interaction of the additional methyl substituents with the n and π^* MO's in the T_1 and T_2 systems is observed. This is evident since the energies of n and π^* for the T_1 and T_2 systems are again higher than the energies of the corresponding MO's of CBD.

The σ MO network of T_1 and T_2 reveals the most pronounced interaction since it is significantly altered from that of the corresponding CBD system. This is in complete contrast to the corresponding π-bonding networks which are practically identical for all three systems (CBD, T_1 and T_2). The energy values for the three corresponding π systems are the same within 0.01 eV. Both the T_1 and T_2 models have an increased number of σ MO's in between the HOMO (n_S) and highest π-bonding MO (π_A). Where there are only five such MO's for the corresponding case of the CBD system, the T_1 and T_2 systems number 11 and 13 respec-

Table 16a

Selected EHMO's for CBD with tri-methyl Substitution (60° rotation)

Models XXII

(C_1 Symmetry)

TEE = -966.712 eV

MO(sym)	π^*_S(A)	n_S(A)	n_A(A)	σ_S(A)
Energy (eV)	-10.766	-12.589	-13.055	-13.500
C_{ij}'s				
H(1)	0.027	-0.067	-0.123	-0.099
H(2)	-0.012	0.083	0.056	0.028
H(3)	0.006	-0.083	-0.053	0.113
H(4)	-0.021	0.040	-0.082	0.147
H(5)	0.015	-0.048	0.119	0.079
H(6)	0.027	-0.030	0.119	-0.089
H(7)	0.014	0.079	0.113	0.131
H(8)	-0.008	-0.080	-0.085	0.115
H(9)	-0.030	-0.077	-0.045	-0.077
H(10)	0.122	0.059	-0.100	0.012
O(1,s)	0.000	-0.026	-0.022	0.024
O(2,s)	0.001	-0.014	0.034	0.013
C(1,s)	0.005	0.116	0.150	-0.090
C(2,s)	-0.006	0.030	-0.205	-0.027
C(3,s)	-0.001	-0.045	0.009	0.031
C(4,s)	-0.003	-0.044	0.031	0.041
C(5,s)	0.040	0.034	0.011	-0.055
C(6,s)	-0.042	0.031	0.039	-0.005
C(7,s)	-0.043	0.017	-0.039	-0.028
O(1,x)	-0.004	0.252	-0.064	-0.007
O(2,x)	0.003	-0.253	0.065	0.006
C(1,x)	0.008	-0.348	0.120	-0.008
C(2,x)	-0.004	0.368	-0.049	-0.002
C(3,x)	-0.001	-0.071	0.015	0.472
C(4,x)	-0.010	0.047	-0.084	-0.467
C(5,x)	0.047	0.048	0.013	-0.212
C(6,x)	-0.054	0.048	0.038	-0.085
C(7,x)	0.053	-0.042	0.087	0.164
O(1,y)	0.316	0.010	-0.037	-0.012
O(2,y)	0.306	0.001	0.011	0.022
C(1,y)	-0.643	-0.015	0.051	0.020
C(2,y)	-0.624	-0.002	-0.017	-0.033
C(3,y)	0.097	0.012	-0.112	-0.144
C(4,y)	0.073	-0.014	0.109	0.135
C(5,y)	-0.113	-0.106	0.018	0.213
C(6,y)	-0.106	0.080	0.184	-0.015
C(7,y)	-0.105	0.037	-0.188	-0.176

TABLE 16b

Atomic Coordinates for Model XXII

	x	y	z
O(1)	1.624	0.0	2.367
O(2)	-1.624	0.0	2.367
C(1)	0.775	0.0	1.532
C(2)	-0.775	0.0	1.532
C(3)	-0.785	0.0	0.0
C(4)	0.785	0.0	0.0
C(5)	-1.497	1.258	-0.578
C(6)	-1.497	-1.258	-0.578
C(7)	1.497	-1.258	-0.578
		Hydrogens	
H(1)	1.285	0.890	-0.408
H(2)	-0.782	-1.819	-1.199
H(3)	-1.845	-1.887	0.254
H(4)	-2.353	-0.936	-1.188
H(5)	1.845	-1.887	0.254
H(6)	2.353	-0.936	-1.188
H(7)	0.783	-1.819	-1.199
H(8)	-1.845	1.887	0.254
H(9)	-2.353	0.936	-1.188
H(10)	-0.783	1.819	-1.199

Table 17

Selected EHMO's for CBD with Tetra-Methyl Substitution (60° rotation) (C_{2v} Symmetry)

Model XXIII TEE = -1072.044 eV

MO(sym)	$\pi^*_S(B_2)$	$n_S(A_1)$	$n_A(B_1)$	$\sigma_S(A_1)$
Energy (eV)	-10.728	-12.551	-12.864	-13.151
C_{ij}'s				
H(1)	-0.014	0.060	-0.095	-0.111
H(2)	0.008	-0.066	0.090	0.041
H(3)	0.027	-0.050	0.096	-0.100
H(4)	-0.027	-0.050	-0.096	-0.100
H(5)	0.014	0.060	0.095	-0.111
H(6)	-0.008	-0.066	-0.090	0.041
H(7)	0.014	0.060	-0.095	0.111
H(8)	-0.008	-0.066	0.090	-0.041
H(9)	-0.027	-0.050	0.096	0.100
H(10)	-0.014	0.060	0.095	0.111
H(11)	0.008	-0.066	-0.090	-0.041
H(12)	0.027	-0.050	-0.096	0.100
O(1,s)	-0.000	-0.021	-0.029	-0.000
O(2,s)	-0.000	-0.021	0.029	-0.000
C(1,s)	0.000	0.074	0.190	0.000
C(2,s)	0.000	0.074	-0.190	0.000
C(3,s)	-0.000	-0.044	-0.009	-0.000
C(4,s)	-0.000	-0.044	0.009	-0.000
C(5,s)	-0.041	0.027	-0.031	0.051
C(6,s)	-0.041	0.027	0.031	-0.051
C(7,s)	0.041	0.027	0.031	0.051
C(8,s)	0.041	0.027	-0.031	-0.051
O(1,x)	0.000	0.257	-0.001	0.000
O(2,x)	-0.000	-0.257	-0.001	-0.000
C(1,x)	-0.000	-0.365	0.040	-0.000
C(2,x)	0.000	0.365	0.040	0.000
C(3,x)	-0.000	-0.071	-0.043	-0.001
C(4,x)	0.000	0.071	-0.043	0.001
C(5,x)	0.052	-0.047	0.036	-0.074
C(6,x)	-0.052	0.047	0.036	-0.074
C(7,x)	0.052	0.047	0.036	0.074
C(8,x)	-0.052	-0.047	0.036	0.074

Table 17(cont.)

	$\pi_S^*(B_2)$	$n_S(A_1)$	$n_A(B_1)$	$\sigma_S(A_1)$
O(1,y)	-0.310	0.000	0.000	0.000
O(2,y)	-0.310	0.000	-0.000	0.056
C(1,y)	0.634	-0.000	-0.000	-0.000
C(2,y)	0.634	-0.000	0.000	-0.083
C(3,y)	-0.093	0.000	0.000	-0.369
C(4,y)	-0.093	-0.000	-0.000	0.369
C(5,y)	0.103	-0.069	0.116	-0.310
C(6,y)	0.103	-0.069	-0.116	0.310
C(7,y)	0.103	0.069	0.115	0.310
C(8,y)	0.103	0.069	-0.115	-0.310
O(1,z)	-0.000	-0.164	0.206	0.001
O(2,z)	0.000	-0.164	-0.206	0.090
C(1,z)	0.000	0.280	-0.294	-0.000
C(2,z)	0.000	0.280	0.294	0.000
C(3,z)	0.000	-0.309	-0.415	0.000
C(4,z)	-0.000	-0.310	0.415	0.000
C(5,z)	-0.076	0.085	-0.157	0.079
C(6,z)	-0.076	0.085	0.157	-0.079
C(7,z)	0.076	0.085	0.156	0.079
C(8,z)	0.076	0.085	-0.156	-0.079

tively. The tetra-substituted model has a σ MO energy state within 0.6 eV of its HOMO. This is compared to values of 0.7 eV, 1.2 eV and 4.4 eV for the cases of T_1, CBD, and glyoxal.

It is apparent that the poly substitution of the methyl groups decrease the n-π* transition energy of the CBD system, and there is a sequential decrease in that energy value for mono-, di-, tri- and tetra systems, figure 16.

The result of the nonbonding-sigma network interactions is again a more delocalized HOMO for the T_1 and T_2 models. Figure 17 a shows the tetra substituted model (T_2) and the hybrid AO's making major contributions to its HOMO. The π* MO also displays significant delocalization along the carbon substituents. Figure 17b shows the LEMO for the same model.

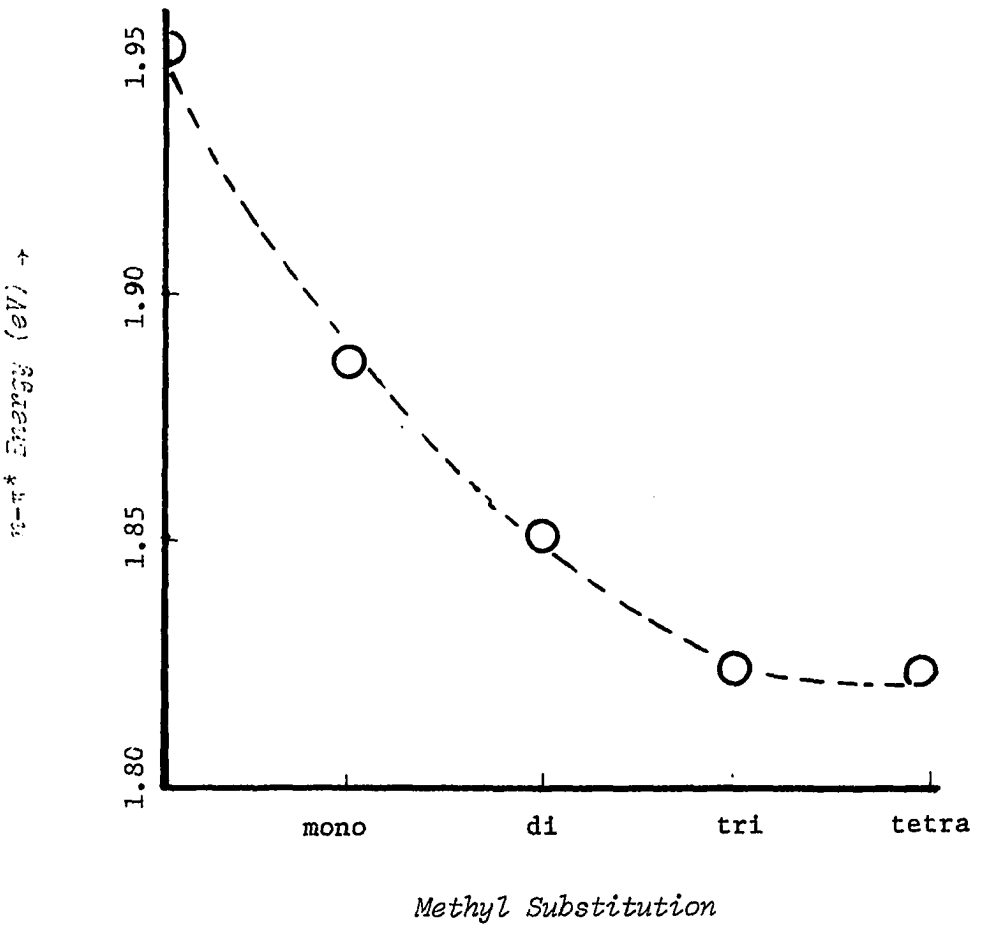

Figure 16. The n-π* transition energy for methyl-substituted CBD. The value corresponding to the most stable configuration of each is used.

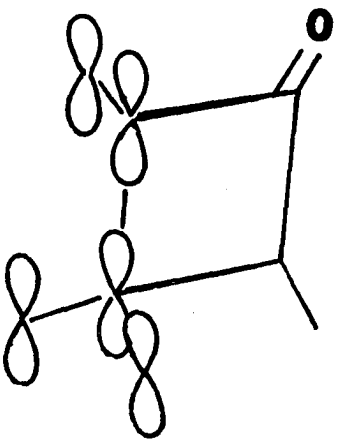

Figure 17a

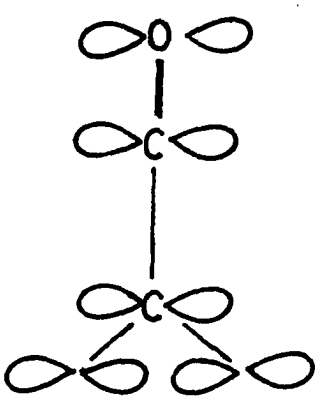

Figure 17b

Figure 17. a) AO's making major contribution to the HOMO of tetra-substituted methyl-CBD (T_2). Two-fold symmetry related values are not shown. (xz projection). b) The LEMO atomic orbitals of T_2 (yz projection).

(3) Ethyl Interactions

For the ethyl substituent, there can be an enormorous number of configurations. However, since the ultimate aim of this investigation is to gain insight into the electronic make-up of DTCD, the selected conformations of the ethyl substituent simulate some likely methyl orientations on a t-butyl group, figure 16. For all models studied, the position of the C_3-C_5 bond remains fixed, and C_6 is positioned to give a normal tetrahedral angle. The methyl hydrogens maintain an eclipse (0^o) conformation and the movement of the ethyl group around the C_3-C_5 axis defines the only path for rotation. Three such rotations are used for the ethyl substituents: 0^o, 120^o and 180^o. The zero degree rotation of this group occurs when C_2, C_3, C_5 and C_6 are coplanar.

Five species are investigated. Three monosubstituted models, having the three ethyl rotations (0^o, 120^o, 180^o) are labeled: E_1, E_2 & E_3 (figure 18). Two di-substituted models having 0^o & 180^o ethyl rotations are referred to as: E_4 and E_5. The C_2 point-group symmetry is preserved for the di-substituted cases, with only trans isomers being studied.

A summary of the EHMO energy values for all five calculations are in table 18. The ethyl-substituted models for all five configurations studied show a red-shifted n-π^* transition, relative to the CBD system. However, the n-π^* values prove to be quite sensitive to the angle of rotation of the methyl carbon around the C_3-C_5 axis. For the mono-substituted models there is a 0.11 eV fluctuation in this value; for the di-substituted models there is a 0.15 eV variation. For E_1, E_2 & E_3, the

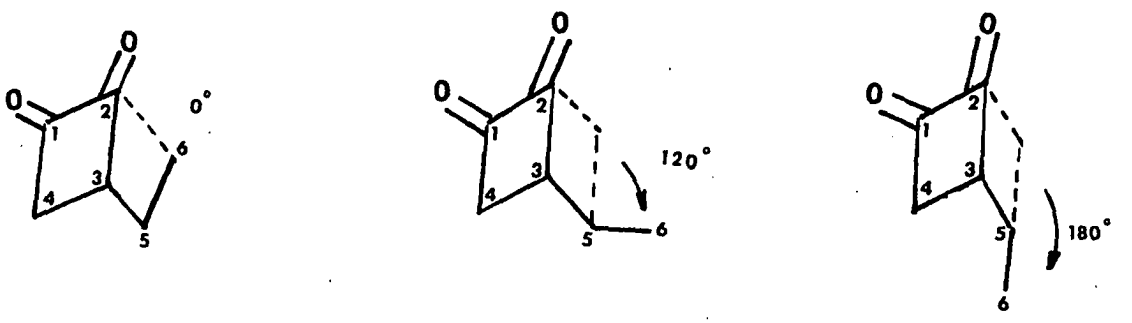

$E_1(E_4)$ E_2 $E_3(E_5)$

Figure 18: The rotated mono-substituted ethyl-CBD models are depicted. Rotations 0^o, 120^o & 180^o are labeled E_1, E_2 & E_3 respectively. E_4 & E_5 are indicated in parenthesis.

Table 18: Selected EHMO values for the ethyl and di-ethyl substituted models.

Model	No.	Rotation	LEMO(eV)	HOMO(eV)	TEE(eV)	$n-\pi^*$ ΔE(eV)
E_1	XXIV	0^o	-10.824	-12.712	-860.727	1.888
E_2	XXV	120^o	-10.830	-12.693	-861.221	1.863
E_3	XXVI	180^o	-10.857	-12.634	-861.418	1.778
E_4	XXVII	0^o	-10.739	-12.626	-1071.677	1.887
E_5	XXVIII	180^o	-10.808	-12.539	-1072.992	1.731

n-π* energy decreases consistently with increasing the angle of rotation (i.e. $E_1 > E_2 > E_3$). The maximum decrease occurs for the 180° rotation. The same trend is observed for the di-substituted models, E_4 & E_5. The 180° rotated di-substituted model, E_5 shows the smallest n-π* energy value for all five models.

The di-substituted models, E_4 & E_5 reflect the typical electronic make-up of the ethyl substituted systems. Thsese 0° and 180° rotated configurations will be the object of further analysis. EHMO results for the trans di-substituted models are in table 19 and 20. The corresponding atomic coordinates are included. For other selected data see appendix guide, page 156.

The energy of the n and π* MO's of E_4 have an increase of 0.23 eV and 0.16 eV respectively, compared with the CBD system. The energy values of the corresponding MO's of E_5 are increased 0.32 eV and 0.10 eV. The most affected molecular orbital is the n MO in both cases; however the relative affect for the two configurations are not really similar. The increase of the n MO energy for E_4 is approximately 1 1/2 times the increase of the corresponding π* MO energy. The increase of the n MO energy for E_5 is over three times the increase of its corresponding π* MO energy. The construction of models E_4 & E_5 from the CBD system produces significant destabilization of the respective n and π* molecular orbitals. This, of course, implies significant interactions of these MO's within the E_4 & E_5 systems.

The n MO of the E_5 system has a greater degree of interaction than the n MO of the E_4 system. This is implied from the relative degree of destabilization of the respective MO's (i.e. 0.32 eV to 0.23 eV). The

Table 19

Selected EHMO's for CBD with trans di-ethyl Substitution (C_2 Symmetry)

Models XXVII & XXVIII

	XXVII			XVIII		
	TEE = -1071.667 eV			Tee = -1072.992 eV		
MO(sym)	π_S^*(B)	n_S(A)	σ_S(A)	π_S^*(B)	n_S(A)	n_A(B)
Energy (eV)	-10.738	-12.626	-12.934	-10.808	-12.539	-12.971
C_{ij}'s						
H(1)	-0.123	-0.081	0.056	0.121	-0.059	-0.139
H(3)	-0.002	0.070	0.097	0.023	0.038	0.038
H(4)	-0.021	0.077	-0.059	-0.016	-0.052	-0.080
H(5)	-0.013	0.022	-0.115	-0.027	-0.050	-0.071
H(6)	0.021	0.026	0.081	0.001	-0.014	-0.039
H(7)	0.014	0.006	-0.072	-0.014	-0.013	-0.021
O(1,s)	-0.002	0.016	0.007	-0.001	0.019	-0.028
C(1,s)	-0.013	-0.072	-0.063	0.013	-0.068	0.175
C(4,s)	-0.004	0.045	0.017	-0.007	0.036	0.005
C(5,s)	0.041	-0.026	-0.032	0.037	-0.015	0.005
C(6,s)	0.023	-0.021	0.043	-0.012	0.033	-0.048
O(1,x)	-0.000	-0.260	-0.044	-0.001	-0.245	-0.000
C(1,x)	-0.006	0.363	0.042	0.003	0.348	0.036
C(4,x)	0.005	-0.018	-0.378	-0.012	-0.061	-0.039
C(5,x)	-0.048	0.018	0.235	0.073	-0.059	0.063
C(6,x)	-0.030	0.030	-0.121	-0.005	0.021	-0.030
O(1,y)	-0.304	-0.001	0.004	0.311	-0.019	-0.052
C(1,y)	0.637	0.013	0.031	-0.631	0.029	9.077
C(4,y)	-0.061	0.018	0.224	0.080	0.072	0.064
C(5,y)	0.112	-0.040	-0.264	-0.116	0.106	-0.097
C(6,y)	0.044	-0.054	0.168	0.005	-0.036	0.054
O(1,z)	-0.007	0.173	-0.038	0.010	0.160	0.196
C(1,z)	0.023	-0.281	0.034	-0.021	-0.270	-0.270
C(4,z)	-0.032	0.303	-0.051	0.033	0.296	0.380
C(5,z)	0.082	-0.137	0.001	0.079	-0.157	0.225
C(6,z)	0.058	0.091	-0.077	-0.048	0.150	-0.231

TABLE 20

Atomic Coordinates for Models XXVII & XXVIII

	XXVII			XXVIII		
	x	y	z	x	y	z
O(1)	1.624	0.0	2.367	1.624	0.0	2.367
O(2)	-1.624	0.0	2.367	-1.624	0.0	2.367
C(1)	0.775	0.0	1.532	0.775	0.0	1.532
C(2)	-0.775	0.0	1.532	-0.775	0.0	1.532
C(3)	-0.785	0.0	0.0	-0.785	0.0	0.0
C(4)	0.785	0.0	0.0	0.785	0.0	0.0
C(5)	-1.511	1.250	-0.578	-2.014	2.134	0.600
C(6)	-1.481	1.179	-2.133	2.014	-2.134	0.600
C(7)	1.511	-1.250	-0.578	-1.511	1.250	-0.578
C(8)	1.481	-1.179	-2.133	1.511	-1.250	-0.578
	Hydrogens			Hydrogens		
H(1)	1.298	0.883	-0.408	1.298	0.883	-0.408
H(2)	-1.298	-0.883	-0.408	-1.298	-0.883	-0.408
H(3)	0.954	-0.263	-2.440	2.364	-0.918	-1.188
H(4)	0.954	-2.063	-2.521	0.804	-1.819	-1.199
H(5)	2.514	-1.162	-2.511	3.108	-2.227	0.536
H(6)	0.992	-2.156	-0.233	1.736	-1.656	1.550
H(7)	2.552	-1.256	-0.223	1.548	-3.128	0.526
H(8)	-0.954	0.263	-2.440	-3.108	2.227	0.536
H(9)	-0.954	2.063	-2.521	-1.548	3.128	0.526
H(10)	-2.514	1.162	-2.511	-1.738	1.656	1.550
H(11)	-0.992	2.156	-0.233	-0.804	1.819	-1.199
H(12)	-2.552	1.256	-0.223	-2.364	0.918	-1.188

opposite effect is observed, however, in the comparison of the respective π^* MO's of the two systems. π^* of the E_5 system apparently undergoes less interaction than the π^* MO of E_4 (i.e. 0.1 eV to 0.16).

The increased interaction of the n MO of E_5 is evident from the increased delocalization of this MO relative to that of E_4. The atomic orbital contribution is extended to carbon ($C_{6,z}$), which is not the case for E_4. The σ system mixes best with the HOMO for the E_5 configuration .

The LEMO's of both E_4 and E_5 are practically identical, with the major contributions coming from the $2p_y$ atomic orbitals of the carbonyl carbon & oxygen and smaller contributions from the $2p_y$ atomic orbitals of atoms 3 & 4. Slight contributions from the $2p_y$ of carbon (6) is observed for E_4; this is not true for E_5. From the through-space interaction calculations of the glyoxal systems, it was observed that a methyl group, located in the identical position as C_6 of the E_4 configuration, can cause significant destabilization of the LEMO of a diketone system. This same destabilization is expected to occur for the E_4 system but not for the E_5. Through-space as well as through-bond interactions of the π^* of E_4 are significant.

(4) T-butyl Interactions

In the previous studies where the mono- and respective di-substituted models are investigated, the mono-substituted and di-substituted species reveal identical trends in their respective molecular interactions. For this reason, and not merely because the mono-substituted model demands fewer basis functions and therefore less computor time, the t-butyl mono-substituted model will be used for most analyses of the t-butyl interactions. However, when appropriate, the di-substituted model will be introduced.

The construction of the various models studied in this section is quite tedious. Since the location of the t-butyl group relative to the CBD network could be crucial as far as molecular stability, the most stable position of the vertex t-butyl carbon (C_5), approximated, using EHMO calculations on selected t-butyl mono-substituted models. The position of the vertex carbon is defined using a "vertical" angle (C_2-C_3-C_5) and a "horizontal" angle (C_4-C_3-C_5) along with the 1.54 A^o C_3-C_5 bond distance, . Using the crystal structure of 2DB as a reference, the vertical angles selected are: 107^o, 112^o & 117^o; and the horizontal angles are: 110^o, 120^o and 130^o.

Nine t-butyl mono-substituted models are constructed using each vertical angle with each horizontal angle for the vertex carbon. The eclipsed (0^o) conformation is used for all methyl hydrogens, and the t-butyl group maintains an eclipsed conformation relative to the butane ring with C_2-C_3-C_5-C_6 planar and defining the zero angle of rotation.

Table 21

Table 20: Selected EHMO values for mono-substituted t-butyl-CBD models. The horizontal angle (a) and vertical angle (b) of the vertex carbon (C_5) are varied.

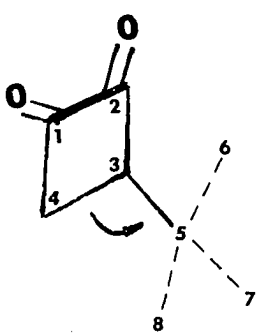

(a)

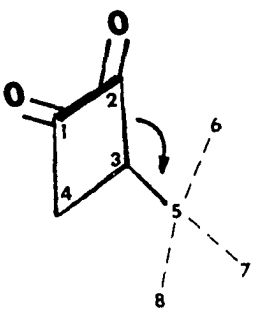

(b)

Model No.	Horizontal Angle (a)	Vertical Angle (b)	$n-\pi^*$ ΔE(eV)	TEE(eV)
XXIX	110°	107°	1.838	-1070.346
XXX	110°	112°	1.811	-1070.610
XXXI	110°	117°	1.789	-1070.665
XXXII	120°	107°	1.761	-1070.665
XXXIII	120°	112°	1.774	-1071.227
XXXIV	120°	117°	1.787	-1071.271
XXXV	130°	107°	1.675	-1070.243
XXXVI	130°	112°	1.731	-1070.969
XXXVII	130°	117°	1.774	-10.71.295

EHMO calculations are made using the coordinates of these respective models. The total electronic energies (TEE) as well as the n-π* energy values of each model are monitored closely. A summary of these results are in table 21. The EHMO coefficients and corresponding atomic coordinates are in appendix. See guide, page 156

Collectively, the configurations having the horizontal angle of 120^{o} presented the most stable species (LTEE). Among these three, the two most stable models are those with vertical angles of 112^{o} & 117^{o}. Of these two, the vertical angle of 112^{o} presents the smallest n-π* transition (i.e. greatest red shift). The 117^{o} angle presents the most stable species. Although the optimum vertical angle would probably be between the 112^{o} & 117^{o} (i.e. both the lower transition value and the lower TEE value are desired), the 120^{o} horizontal angle and the 112^{o} vertical angle are selected for further model construction.

An EHMO study in the variation of the vertex carbon position not only serves to approximate an optimum position of the t-butyl group, but simulates possible solution activity for the t-butyl species as well. The n-π* transition values (although with a 0.15 eV fluctuation) shows a red shift for all nine models relative to the CBD system.

Destabilization of both the n and π* MO's of each system is observed. This suggests interaction of these MO's within each system. Although the relative degree of interaction is obviously dependent on the conformation used, the relative trends of influences and effects are identical for all systems. The red shift of the n-π* transitions is due primarily to the destabilization of the nonbonding MO of each system. For instance, for the t-butyl system selected (XXXIII) for the model pattern,

TABLE 22

Selected EHMO's for CBD with Mono t-Butyl Substitution, (0° rotation), eclipsed hydrogens

Model XXXIII (C_1 Symmetry)

TEE = -1071.227 eV

MO(sym)	π^*_S(A)	n_S(A)	σ_S(A)	n_A(A)	σ_A(A)
Energy (eV)	-10.780	-12.554	-13.106	-13.235	-13.373
C_{ij}'s					
H(1)	-0.141	0.031	0.106	-0.140	0.070
H(2)	0.137	0.058	0.140	-0.030	-0.086
H(3)	0.122	0.123	0.009	0.074	0.208
H(4)	-0.019	-0.065	0.005	-0.100	0.028
H(5)	-0.012	-0.002	0.003	0.016	-0.197
H(6)	0.010	0.015	0.153	0.052	0.005
H(7)	-0.012	0.026	0.141	0.060	0.001
H(8)	0.016	-0.042	-0.011	-0.046	0.179
H(9)	-0.019	0.088	-0.050	0.111	-0.008
H(10)	-0.021	0.013	0.010	-0.027	-0.181
H(11)	-0.036	0.088	-0.029	0.051	0.028
H(12)	0.043	-0.047	-0.153	0.029	-0.019
O(1,s)	0.001	-0.027	-0.007	-0.023	-0.002
O(2,s)	0.003	-0.003	-0.025	0.030	-0.005
C(1,s)	-0.005	0.124	-0.006	0.111	0.002
C(2,s)	0.007	0.012	0.124	-0.150	-0.011
C(3,s)	-0.005	-0.027	0.004	0.025	-0.056
C(4,s)	-0.007	-0.041	-0.072	0.014	-0.000
C(5,s)	-0.038	0.017	0.001	0.008	-0.001
C(6,s)	-0.019	0.026	-0.070	0.013	0.058
C(7,s)	0.002	-0.045	-0.034	-0.047	-0.062
C(8,s)	0.021	-0.037	0.054	0.009	0.050
O(1,x)	-0.007	0.228	0.058	-0.117	-0.002
O(2,x)	0.007	-0.234	-0.054	0.115	0.001
C(1,x)	0.011	-0.314	-0.084	0.182	0.009
C(2,x)	-0.018	0.335	0.055	-0.142	0.001
C(3,x)	0.001	-0.086	-0.308	-0.212	0.053
C(4,x)	0.002	0.053	0.334	0.164	0.017
C(5,x)	-0.057	0.081	0.377	0.187	0.150
C(6,x)	0.025	0.027	-0.167	-0.013	0.045
C(7,x)	0.018	-0.128	-0.169	-0.171	-0.217
C(8,x)	0.043	0.030	-0.269	0.109	-0.208
O(1,y)	-0.320	-0.024	-0.011	0.004	0.003
O(2,y)	-0.295	-0.026	-0.007	0.001	0.040
C(1,y)	0.649	0.040	0.017	-0.004	-0.007
C(2,y)	0.617	0.069	0.012	0.039	-0.072

TABLE 22(continued)

Selected EHMO's for CBD with Mono t-Butyl Substitution, (0° rotation)

Model XXXIII (C_1 Symmetry)

TEE = -1071.227 eV

MO(sym)	π^*_S(A)	n_S(A)	σ_S(A)	n_A(A)	σ_A(A)
Energy (eV)	-10.780	-12.554	-13.106	-13.235	-13.373
C_{ij}'s					
C(3,y)	0.075	0.082	0.115	0.130	-0.287
C(4,y)	0.071	0.007	0.019	-0.057	0.071
C(5,y)	0.117	-0.092	-0.080	-0.115	0.494
C(6,y)	0.041	-0.059	0.176	0.005	-0.243
C(7,y)	0.015	0.006	-0.019	0.005	-0.163
C(8,y)	-0.046	0.094	-0.093	-0.032	-0.195
O(1,z)	0.002	-0.088	-0.047	0.263	0.010
O(2,z)	0.010	-0.209	0.098	-0.051	-0.003
C(1,z)	-0.005	0.161	0.097	-0.333	-0.008
C(2,z)	-0.027	0.335	-0.112	0.066	0.018
C(3,z)	0.044	-0.395	0.132	-0.136	0.027
C(4,z)	0.010	-0.147	-0.090	0.457	0.015
C(5,z)	-0.087	0.253	-0.198	0.231	0.090
C(6,z)	-0.061	-0.126	0.203	-0.084	-0.166
C(7,z)	0.007	-0.120	-0.031	-0.157	-0.143
C(8,z)	0.017	-0.104	0.172	-0.053	0.098

the n MO is destabilized 0.30 eV and the π* MO is destabilized 0.13 eV, relative to the CBD system. These relative amounts of destabilization of the respective MO's for this system are comparable to corresponding values of systems previously studied that revealed through-bond interactions. The EHMO results for XXXIII are listed in table 22.

There are 13 sigma MO's between the HOMO and highest bonding MO, with the proper symmetry, available for interaction with either the n or π* MO. Three such MO's are within 1.5 eV of the HOMO

Increased delocalization of the n and π* MO's relative to the CBD system, is observed. For the CBD system the n and π* are located predominantly along the di-carbonyl network, with delocalization within the butane ring. For the t-butyl substituted system, however, further delocalization of the n and π* MO's occurs . It is of interest to note that the increased delocalization of the two MO's is more pronounced along the side of the system (atoms 2, 3, and 5) in which the t-butyl is attached.

The n MO now has $2p_z$ atomic orbital contribution extended through the four-carbon t-butyl system. HOMO-sigma MO interaction is apparent. The π* MO has significant contributions extending to $C_{3,y}$ & $C_{5,y}$ and to the ring-hydrogen substituents. Slight contribution on $C_{5',y}$ atomic orbital is also observed. Some through-space as well as through-bond interactions may occur for π*.

The next selection of models have varied rotations of the t-butyl group about the C_3–C_5 axis. Table 23 summarizes these results.

Table 23

Selected EHMO values for mono-substituted t-butyl-CBD models. The rotation angle of the t-butyl is varied. Group I has staggered methyl hydrogens. Group II has eclipsed methyl hydrogens.

Group I (Staggered methyl hydrogens)

Model No.	t-butyl rotation	LEMO(eV)	HOMO(eV)	n-π* ΔE	TEE(eV)
XXXVIII	0°	-10.802	-12.580	1.778	-1072.533
XXXIX	30°	-10.832	-12.581	1.748	-1072.581
XL	50°	-10.856	-12.579	1.723	-1072.014
XLI	60°	-10.833	-12.591	1.758	-1072.921
XLII	70°	-10.837	-12.575	1.738	-1072.334
XLIII	80°	-10.821	-12.601	1.780	-1072.974
XLIV	90°	-10.814	-12.600	1.786	-1072.859
XLV	100°	-10.807	-12.594	1.787	-1072.748

(Group II, eclipsed methyl hydrogens)

XXXII	0°	-10.780	-12.554	1.774	-1071.227
XLVI	30°	-10.822	-12.556	1.734	-1071.195
XLVII	60°	-10.853	-12.581	1.728	-1072.252
XLVIII	90°	-10.790	-12.557	1.767	-1072.200

The EHMO coefficients and atomic coordinates are in the appendix. Eclipsed (0^{o}) as well as staggered (60^{o}) conformations are used for the methyl hydrogens. Rotations: 0^{o}, 30^{o}, 50^{o}, 60^{o}, 70^{o}, 80^{o}, 90^{o} and 100^{o} are selected for observing the systems with staggered methyl hydrogens (Group I). Rotations: 0^{o}, 30^{o}, 60^{o} and 90^{o} are selected for observing the systems with eclipsed hydrogen conformation (Group II). In all, twelve (12) models are investigated. These arbitrary rotations which also simulate some phase of solution activity also provide an opportunity to study the conformational effects on the n-π^{*} transition and total electronic energy of the t-butyl system.

The n-π^{*} transition values for the twelve systems fluctuated only 0.06 eV. Although categorically the observed red shift of each respective n-π^{*} energy is due to the predominant destabilization of the HOMO (n), the observed fluctuations of these values (due to rotations) is due to a different effect. The variations in these values is due apparently to the variation of the respective LEMO's.

Figure 19 shows the variations of the HOMO and LEMO of group I with respect to the angle of rotation. Figure 20_{a} shows the same variations for group II. Plots of the corresponding n-π^{*} transition values are also included in the figures.

It can be seen that the MO curve showing the largest deviation with respect to the various rotations is the LEMO for group I and group II. The HOMO curve for group I shows practically no fluctuation and the same curve for group II shows very little. The shape of the curve representing the n-π^{*} transitions parallels that of the LEMO curve in both cases. This indicates practically a direct correlation of the n-π^{*}

Figure 19

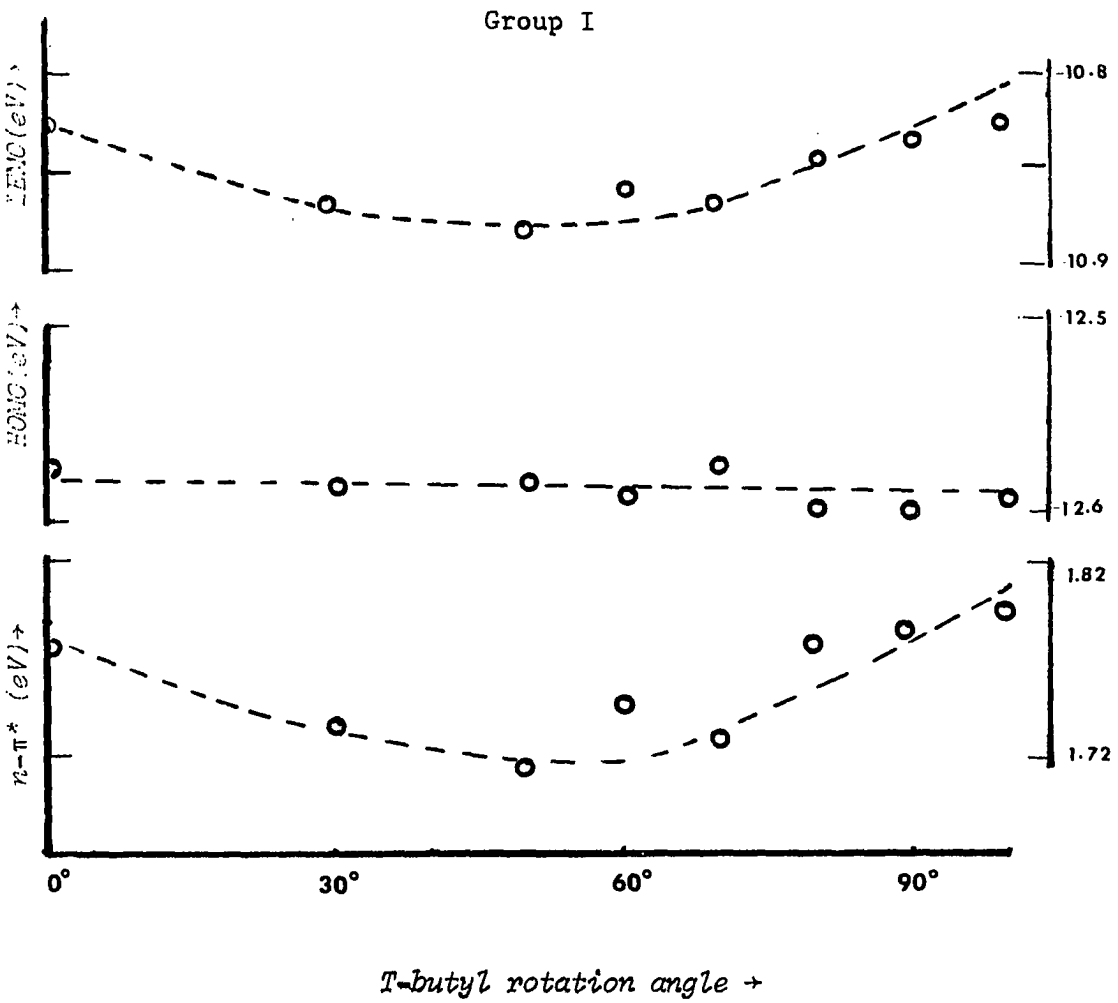

Figure 19. Variations of the HOMO, LEMO and n-π* energy values are plotted vs the t-butyl rotation angle for Group I. (The dashed lines indicate the general trends).

Figure 20a

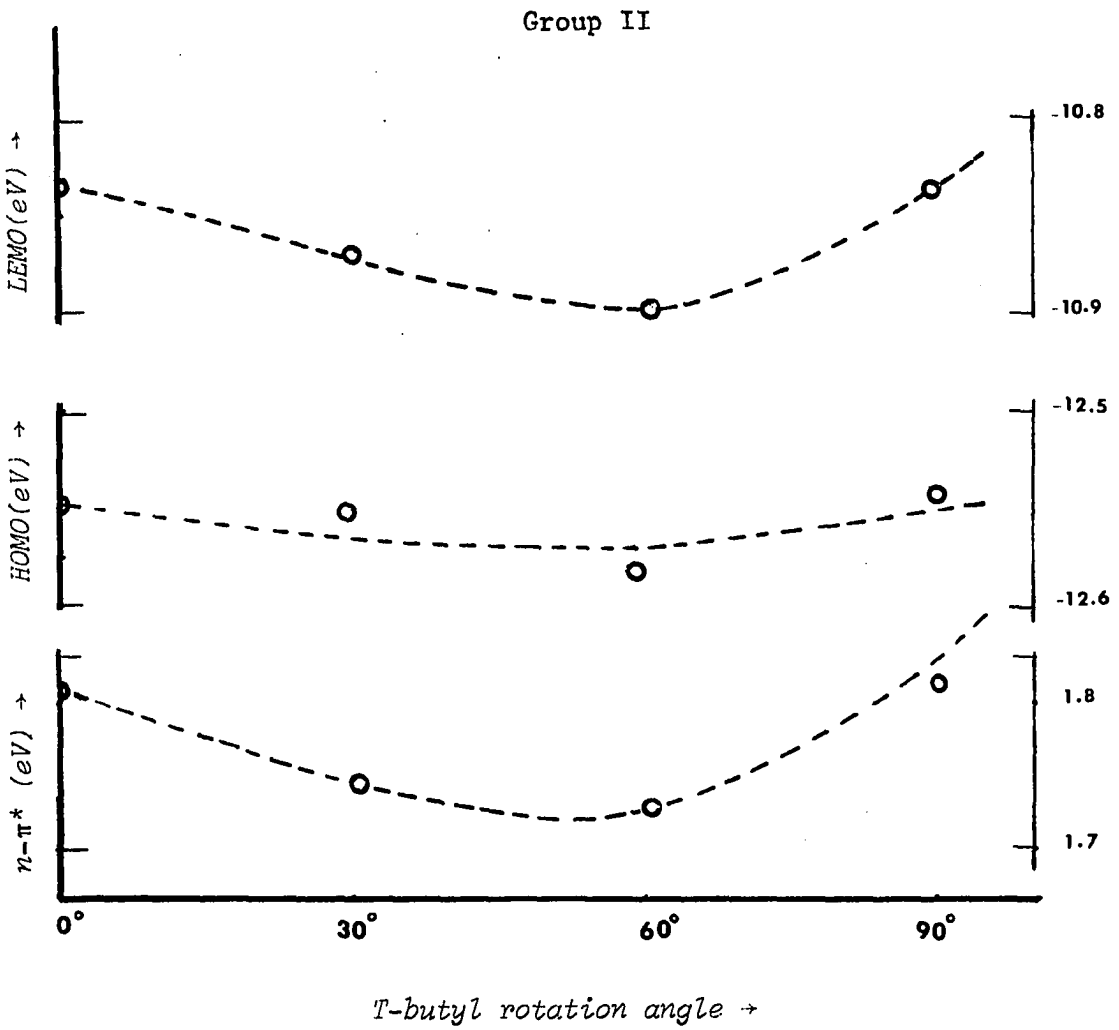

Figure 20 a Variations of the HOMO, LEMO and n-π* energy values are plotted vs the t-butyl rotation angle for Group II. (The dashed lines indicate the general trends.)

Figure 20 (b) & (c)

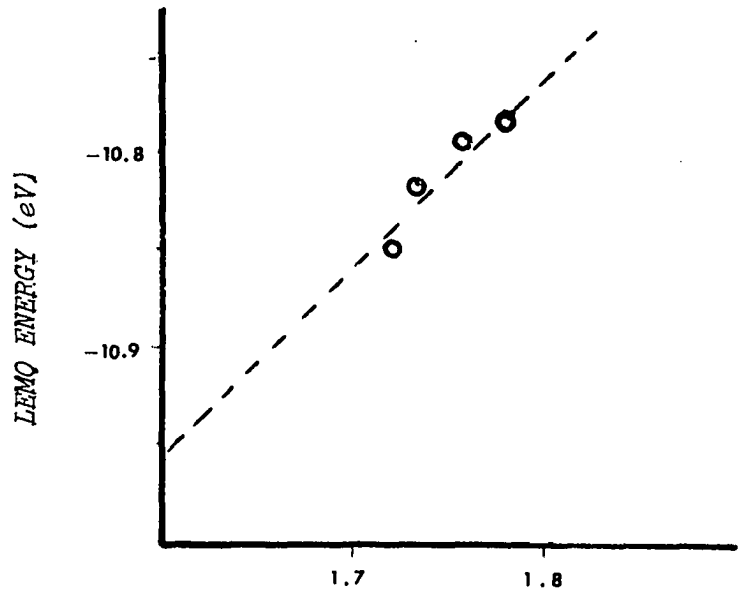

Figures 20b & 20c are respectively, plots of the n-π* ΔE values vs the LEMO values for Group I & II t-butyl Models.

(c)

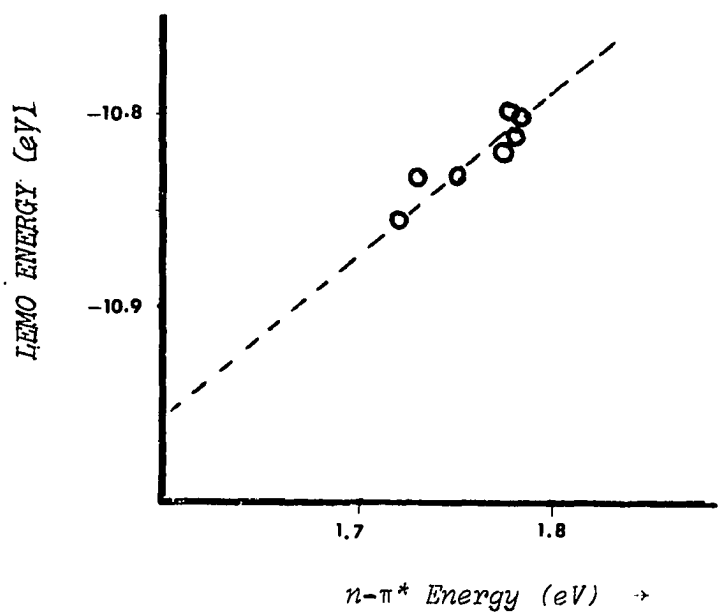

transition with the LEMO. In figure 20b & 20c a plot of the n-π^* energy values vs. LEMO values for the models of each group further substantiates this result. The transition value is proportional to the LEMO energy to a good approximation.

An analysis of the LEMO's of the 12 models reveals no striking differences. However, it is learned from the intermolecular interaction studies that through-space interactions can cause destabilization of the LEMO. The rotations of the respective t-butyl groups, i.e. changing the distance and orientation of the methyl groups with respect to the dicarbonyl system (the predominant location of the π^*) have a direct effect upon this type of interaction. Furthermore, we see that the 0^o rotation, which is the configuration most favorable for this through-space interaction, causes the greatest degree of destabilization of the LEMO in group I and group II.

The rotations (e.g. 50^o & 60^o) that provide less hindrance to the dicarbonyl system cause the least destabilization of the π^* MO. Although the π^* MO has some through-bond interaction, the through-space interactions also occur and are the major cause of the n-π^* energy flucturations arising from t-butyl rotation. Figure 21 shows the hybrid AO's making major contribution to the HOMO & LEMO of model XLI. The EHMO values for models XXXIX, XL & XLI are in table 24. Atomic coordinates are included in the appendix. See Guide, page 156.

The next EHMO calculations are made using coordinates of speculated DTCD structures (SDTCD). That is, different configurations of the CBD model with trans t-butyl di-substitution are used. The structures vary with respect to rotations of the respective t-butyl (methyl) carbons.

Figure 21 (a)

This illustration shows the orbitals making major contribution to the HOMO of a t-butyl Model- XLI. The HOMO extends throughout the t-butyl system.

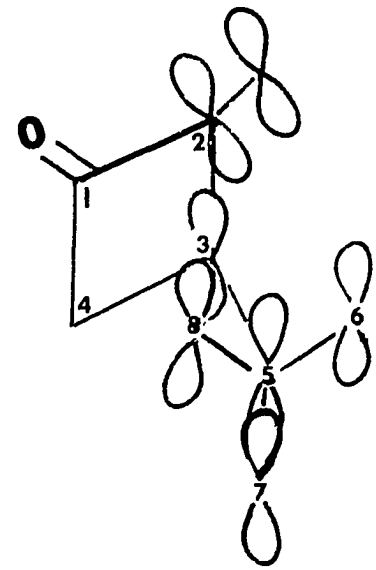

Figure 21 (b)

This illustration shows the orbitals for the LEMO of the same Model. (yz projection)

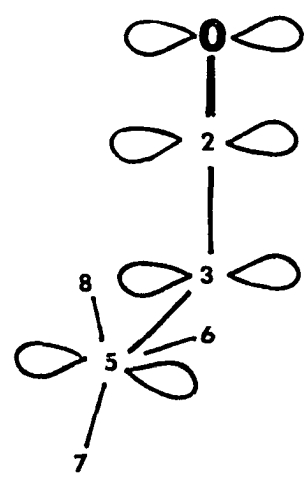

TABLE 24

EHMO Coefficients for the n & π^* Orbitals of CBD with mono t-butyl Substitution

Models XXXIX, XL, & XLI

	XXXIX		XL		XLI	
	TEE = -1072.581 eV		TEE = -1072.014 eV		TEE = -1072.921 eV	
MO(sym)	$\pi_S^*(A)$	$n_S(A)$	$\pi_S^*(A)$	$n_S(A)$	$\pi_S^*(A)$	$n_S(A)$
Energy (eV)	-10.832	-12.581	-10.855	-12.579	-10.833	-12.590
C_{ij}'s						
H(1)	-0.131	0.010	-0.129	0.016	0.129	0.007
H(2)	0.131	0.050	0.130	0.052	-0.129	0.061
H(3)	0.132	0.119	0.129	0.117	-0.128	0.108
H(4)	-0.017	0.024	0.019	-0.054	0.038	0.099
H(5)	-0.009	-0.059	-0.013	0.046	-0.010	0.007
H(6)	0.011	-0.010	-0.019	-0.012	-0.007	0.005
H(7)	0.003	0.027	-0.021	0.062	-0.012	0.007
H(8)	-0.032	0.098	0.022	-0.031	0.018	0.047
H(9)	0.009	-0.022	-0.021	0.077	0.015	-0.074
H(10)	0.012	-0.065	-0.029	-0.013	-0.008	-0.061
H(11)	0.022	0.029	-0.003	0.065	-0.005	0.007
H(12)	-0.044	0.058	0.017	-0.060	0.028	0.044
O(1,s)	0.001	-0.027	0.001	-0.027	-0.001	-0.027
O(2,s)	0.001	-0.004	-0.001	-0.004	0.000	-0.004
C(1,s)	-0.007	0.132	-0.007	0.131	0.006	0.128
C(2,s)	0.004	-0.000	0.004	0.002	-0.004	0.005
C(3,s)	-0.009	-0.034	-0.008	-0.031	0.009	-0.033
C(4,s)	-0.002	-0.040	-0.000	-0.038	-0.000	-0.042
C(5,s)	-0.038	0.018	-0.037	0.018	0.037	0.918
C(6,s)	-0.006	0.025	-0.002	0.012	-0.008	-0.586
C(7,s)	0.004	-0.055	0.009	-0.062	0.003	0.008
C(8,s)	0.010	-0.011	0.000	0.001	-0.001	0.007
O(1,x)	-0.005	0.224	-0.005	0.224	0.005	0.226
O(2,x)	0.005	-0.230	0.007	-0.234	-0.006	-0.233
C(1,x)	0.008	-0.304	0.007	-0.305	-0.007	-0.308
C(2,x)	-0.011	0.332	-0.010	0.333	0.009	0.335
C(3,x)	0.014	-0.074	0.016	-0.080	-0.017	-0.076
C(4,x)	-0.001	0.034	-0.003	0.040	0.006	0.033
C(5,x)	-0.058	0.060	-0.068	0.069	0.078	0.063
C(6,x)	-0.019	0.073	-0.014	0.041	-0.011	-0.013
C(7,x)	0.015	-0.100	0.004	-0.054	-0.018	-0.028
C(8,x)	-0.000	0.009	-0.021	-0.027	-0.004	0.029
O(1,y)	-0.319	-0.015	-0.319	-0.016	0.320	-0.013

TABLE 24

EHMO Coefficients for the n & π^* Orbitals of CBD with mono t-butyl Substitution

Models XXXIX, XL, & XLI

	XXXIX		XL		XLI	
	TEE = -1072.581 eV		TEE = -1072.014 eV		TEE = -1072.921 eV	
MO(sym)	π^*_S(A)	n_S(A)	π^*_S(A)	n_S(A)	π^*_S(A)	n_S(A)
Energy (eV)	-10.832	-12.581	-10.855	-12.579	-10.833	-12.590
C_{ij}'s						
O(2,y)	-0.305	-0.034	-0.309	-0.041	0.307	-0.035
C(1,y)	0.645	0.025	0.643	0.028	-0.646	0.022
C(2,y)	0.620	0.064	0.631	0.069	-0.621	0.062
C(3,y)	-0.090	0.079	-0.085	0.090	0.088	0.095
C(4,y)	-0.058	-0.010	-0.054	-0.003	0.054	-0.017
C(5,y)	0.136	-0.089	0.131	-0.107	-0.126	-0.105
C(6,y)	-0.010	-0.029	-0.003	0.005	0.004	0.025
C(7,y)	0.001	-0.013	0.001	0.023	0.013	-0.025
C(8,y)	-0.039	0.041	-0.009	0.000	0.004	0.013
O(1,z)	-0.000	-0.076	-0.001	-0.077	0.001	-0.083
O(2,z)	0.008	-0.215	0.009	-0.217	-0.007	-0.214
C(1,z)	-0.000	0.1400	0.001	0.142	-0.001	0.149
C(2,z)	-0.017	0.344	-0.018	0.342	0.016	0.339
C(3,z)	0.033	-0.407	0.029	-0.405	-0.030	-0.397
C(4,z)	0.001	-0.120	-0.003	-0.125	0.003	-0.130
C(5,z)	-0.074	0.271	-0.078	0.260	0.071	0.262
C(6,z)	-0.017	-0.102	0.011	-0.057	-0.032	-0.263
C(7,z)	0.023	-0.225	0.043	-0.025	0.055	-0.059
C(8,z)	-0.024	-0.043	-0.014	-0.044	-0.002	-0.044

The rotations of the t-butyl carbons are: 0^{o}, 30^{o}, 60^{o} and 90^{o}. The methyl hydrogens of each model are either in an eclipsed or staggered conformation. In all, there are seven SDTCD models studied. Table 25 lists the respective t-butyl rotations used for each. Five models with staggered methyl hydrogens are listed in group A. Two models with eclipsed (0^{o}) methyl hydrogens are in group B. Also included in the table are the corresponding LEMO, HOMO, n-π^{*} transition and total electronic energies. The EHMO coefficients and atomic coordinates for each model are listed in appendix. See guide, page 156.

As expected, the SDTCD molecular systems parallel, in many ways, the previous alkyl substituted CBD systems. The n and π^{*} molecular orbitals for all seven models are significantly destabilized relative to CBD. This is a result of interactions of these molecular orbitals with the alkyl network. The interactions are apparently those involving the sigma bonding MO's of the t-butyl system.

This explanation seems quite feasible on reviewing the MO network of the di-substituted system. The π-bonding MO energies of the isolated CBD model and the respective SDTCD models remain relatively equal (i.e. within 0.01 eV). No significant π-bonding interaction occurs due to di-t-butyl substitution. The σ MO energies on the same comparative basis vary significantly. There are 21 σ-bonding MO's between the HOMO and highest π-bonding MO of each SDTCD system, while there are only 5 in the case for CBD. Five MO's are within approximately 1.5 eV of the HOMO for each SDTCD system; there is only 1 in the case of CBD.

Figure 22 depicts the interactions resulting in a typical SDTCD system (EHMO results for number LI configuration in table 25 is

Table 25

Selected EHMO values for di-substituted t-butyl-CBD models. The rotation angle of the t-butyl is varied. C_2 symmetry is maintained except for model LIII. (the second t-butyl is rotated 60° out of symmetry.

Speculated DTCD structures (SDTCD)

Group A(staggered methyl hydrogens)

SDTCD Model	t-butyl rotation	LEMO(eV)	HOMO(eV)	n-π* ΔE	TEE(eV)
XLIX	0°	-10.698	-12.462	1.764	-1495.213
L	30°	-10.760	-12.487	1.727	-1495.308
LI	60°	-10.762	-12.485	1.722	-1495.958
LII	90°	-10.723	-12.478	1.754	-1495.908
LIII	90°	-10.742	-12.482	1.740	-1495.617

Group A(eclipsed methyl hydrogens)

LIV	0°	-10.661	-12.393	1.732	-1492.585
LV	60°	-10.801	-12..	1.689	-1494.583

Figure 22

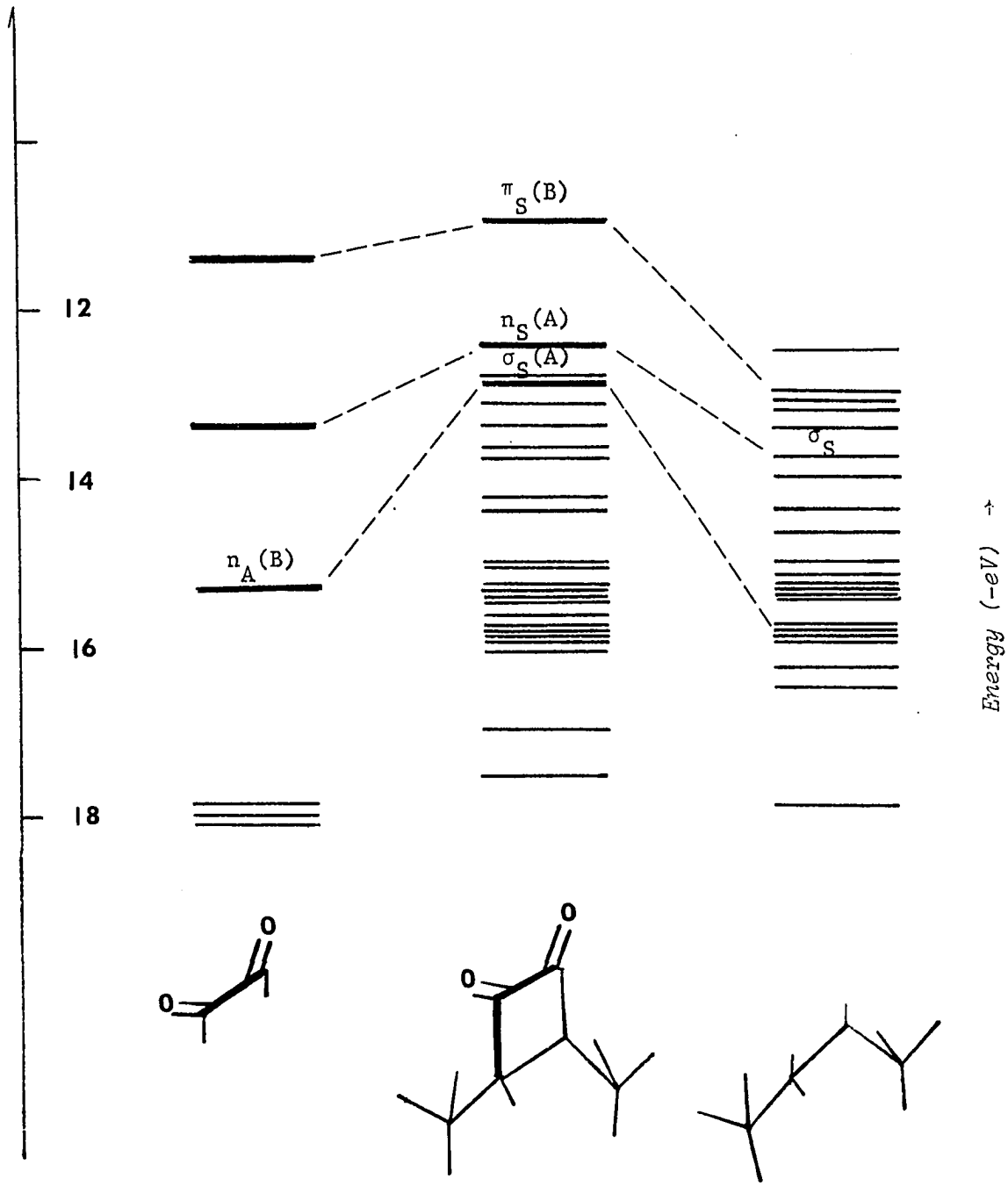

Figure 22. Energy diagram of a typical di-substituted t-butyl CBD system. (Gly-90 & 1,2 di-t-butyl ethane interaction).

TABLE 26

Selected EHMO's for CBD with di t-butyl Substitution (Staggered hydrogen) (60° rotation)

Model LI: C_2 Symmetry

TEE = -1495.958 eV

MO(sym)	π^*_S(B)	n_S(A)	σ_S(A)	n_A(B)	σ_A(B)
Energy (Ev)	-10.762	-12.484	-12.809	-12.862	-13.220
C_{ij}'s					
H(1)	0.124	0.053	-0.008	-0.128	-0.201
H(3)	0.036	0.079	-0.036	-0.083	0.056
H(4)	-0.010	-0.007	0.076	-0.035	0.031
H(5)	-0.007	0.001	-0.007	-0.018	0.099
H(6)	-0.012	-0.001	0.071	-0.022	0.093
H(7)	0.017	0.044	-0.047	-0.027	0.078
H(8)	0.015	-0.048	-0.014	0.084	0.021
H(9)	-0.007	-0.041	-0.022	0.073	-0.001
H(10)	-0.004	0.003	-0.011	-0.009	-0.111
H(11)	0.025	0.047	-0.108	-0.033	0.058
O(1,s)	-0.001	-0.017	0.013	0.028	0.007
C(1,s)	0.010	0.070	-0.039	-0.159	-0.016
C(4,s)	-0.008	-0.031	0.014	-0.005	0.051
C(5,s)	0.036	0.019	-0.014	-0.010	0.007
C(6,s)	-0.008	-0.040	-0.020	0.055	0.008
C(7,s)	0.003	0.003	0.007	0.018	0.049
C(8,s)	0.000	-0.002	0.061	-0.014	0.021
O(1,x)	-0.001	0.236	0.023	0.007	-0.044
C(1,x)	0.002	-0.332	-0.040	-0.032	0.053
C(4,x)	-0.010	0.102	-0.378	0.038	-0.029
C(5,x)	0.074	0.081	-0.294	-0.031	-0.106
C(6,x)	-0.012	-0.017	0.032	-0.009	0.025
C(7,x)	-0.019	-0.023	0.046	0.014	0.197
C(8,x)	-0.001	-0.009	0.290	-0.055	0.104
O(1,4)	0.310	0.018	-0.018	0.031	0.038
C(1,y)	-0.630	-0.034	0.028	-0.056	-0.051
C(4,y)	0.086	-0.099	0.139	-0.053	-0.238
C(5,y)	-0.121	-0.111	0.124	0.054	-0.337
C(6,y)	0.004	0.021	-0.013	-0.015	0.057
C(7,y)	0.013	-0.008	0.010	0.049	0.271
C(8,y)	0.003	0.014	-0.038	-0.010	0.061
O(1,z)	0.008	-0.148	-0.082	-0.178	0.018
C(1,z)	-0.016	0.252	0.091	0.245	-0.036
C(4,z)	0.031	-0.276	-0.102	-0.337	-0.003
C(6,z)	0.068	0.184	0.051	-0.277	-0.008
C(7,z)	-0.032	-0.174	-0.081	0.286	0.030
C(8,z)	0.056	-0.039	0.009	0.068	0.062

TABLE 26

Atomic Coordinates for Models LI & LVI

	LI			LVI		
	x	y	z	x	y	z
O(1)	1.624	0.0	2.367	-1.610	-0.030	2,377
O(2)	-1.624	0.0	2.367	1.610	-0.088	2.382
C(1)	0.775	0.0	1.532	0.781	-0.070	1.525
C(2)	-0.775	0.0	1.532	0.779	-0.070	-0.002
C(3)	-0.785	0.0	0.0	-0.779	0.014	1.525
C(4)	0.785	0.0	0.0	-0.770	0.125	0.001
C(5)	-1.511	1.250	-0.578	1.381	-1.323	-0.648
C(6)	-1.481	1.179	-2.133	0.779	-2.592	-0.049
C(7)	-0.776	2.533	-0.090	2.889	-1.322	-0.394
C(8)	-2.985	1.258	-0.075	1.132	-1.261	-2.153
C(9)	1.511	-1.250	-0.578	-1.370	1.427	-0.553
C(10)	1.478	-1.181	-2.133	-0.772	2.643	0.139
C(11)	0.776	=2.533	-0.090	-2.882	1.401	-0.306
C(12)	2.985	-1.258	-0.075	-1.118	1.471	-2.058
	Hydrogens			Hydrogens		
H(1)	-1.298	-0.883	-0.408	1.247	0.696	-0.377
H(2)	1.298	0.883	-0.408	-1.237	-0.611	-0.431
H(3)	-1.991	2.064	-2.541	1.162	-3.379	-0.380
H(4)	-0.434	1.163	-2.470	0.863	-2.625	0.951
H(5)	-1.994	0.263	-2.460	-0.202	-2.636	-0.176
H(6)	0.264	2.506	-0.445	3.330	-2.162	-0.819
H(7)	-1.289	3.416	-0.499	3.021	-1.422	0.609
H(8)	-0.798	2.562	1.008	3.332	-0.500	-0.762
H(9)	-2.988	1.298	1.023	0.179	-1.209	-2.330
H(10)	-3.485	0.341	-0.419	1.513	-0.428	-2.667
H(11)	-3.497	2.141	-0.484	1.511	-1.934	-2.582
H(12)	1.991	-2.064	-2.541	-1.502	0.678	-2.632
H(13)	1.990	-0.264	-2.461	-0.163	1.429	-2.235
H(14)	0.431	-1.166	-2.469	-1.493	2.172	-2.440
H(15)	1.289	-3.416	-0.499	-3.323	0.611	-0.734
H(16)	0.798	-2.562	1.008	-3.318	2.271	-0.671
H(17)	-0.264	-2.506	-0.445	-3.014	1.429	0.701
H(18)	3.497	-2.141	-0.484	0.210	2.698	0.021
H(19)	2.988	-1.298	1.023	-1.155	3.452	-0.134
H(20)	3.485	-0.341	-0.419	-0.860	2.603	1.139

used). Both the n and π^* MO's of CBD have the proper symmetry for interaction; however, the MO closest in energy to the σ-bonding MO's of the t-butyl system and therefore the most strongly affected is the HOMO (n). The over-all effect is a red shift of the n-π^* transition for all SDTCD models relative to the CBD system.

It is of interest to note that among each respective group (A & B), table 25, the staggered di-t-butyl species produces both the LTEE as well as the smallest n-π^* transition. Furthermore, the configurations with staggered methyl hydrogens (group A) are collectively the more stable species (relative to group B) and will be the structures henceforth considered.

In figure 23 the total electronic energy (TEE) values and n-π^* energy values of groups A are plotted vs. the di-t-butyl rotations. Only the conformations of C_2 point-group symmetry are considered. From figure 23b, the minimum n-π^* value may be expected to occur between a 50° and 60° rotation of the di-t-butyl groups. This too is the case in the mono t-butyl study.

Since both the minimum value for each of these energy parameters (n-π^* & LTEE) is desired, the optimum rotation appears to be in the proximity of 60°, the staggered di-t-butyl species.

A molecule such as DTCD may be expected to undergo a variety of conformations while in solution. To designate a specific conformation as the only conformation is probably not appropriate. However, it is anticipated that the most probable DTCD structure corresponds closely to the conformation predicted from the minimum n-π^* and TEE energy values. A reasonable conclusion, based on these two EHMO energy parameters, for the

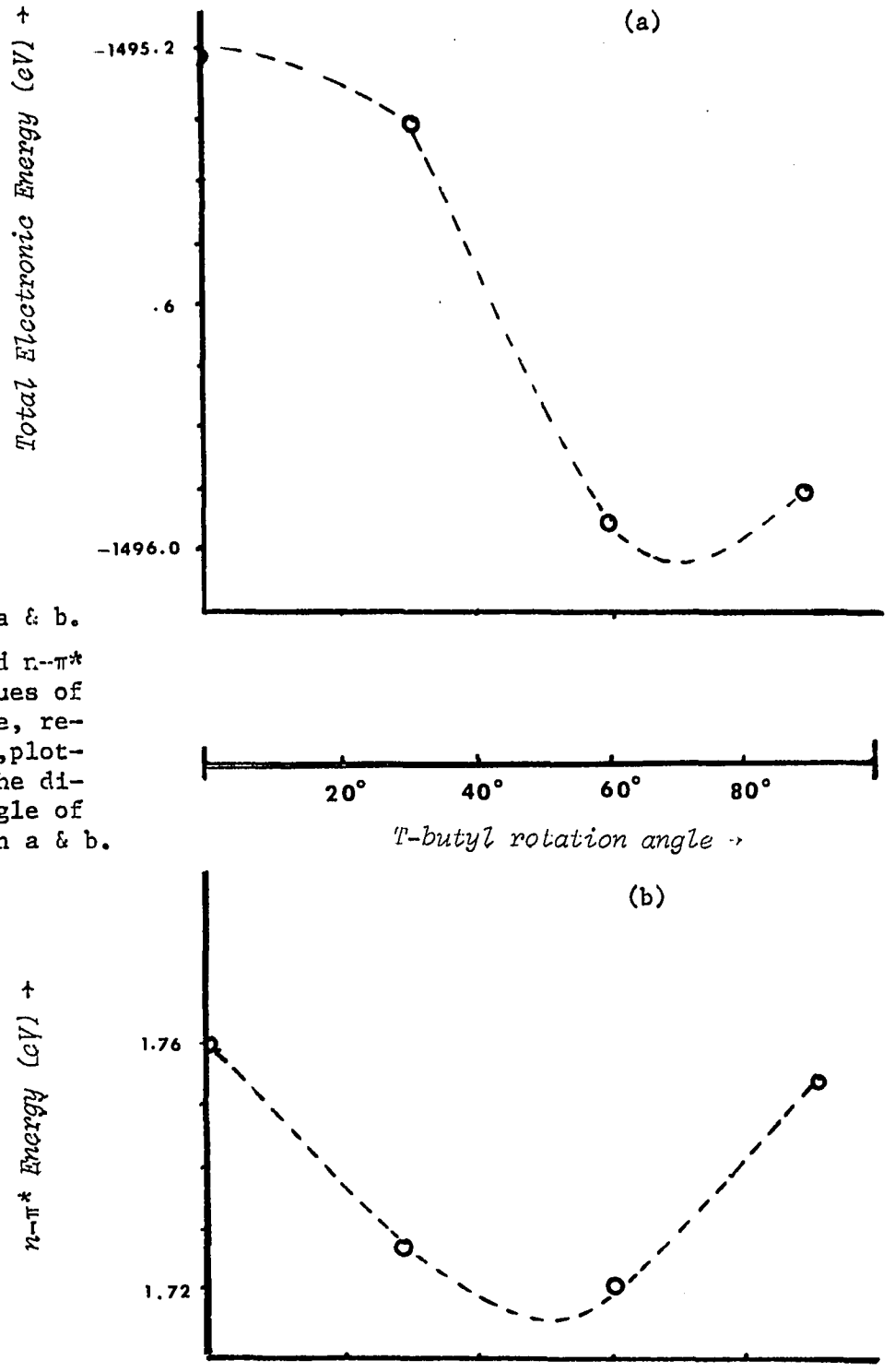

Figure 23 a & b.

The TEE and n--π* energy values of group A are, respectively, plotted vs, the di-t-butyl angle of rotation in a & b.

DTCD configuration in solution may be summarized as follows:

(1) a planar or near planar configuration of the cyclobutanedione portion.

(2) a 112-117° vertical angle and an approximate 120° horizontal angle of the vertex carbon.

(3) a 60 to 70° rotation of the t-butyl carbons.

(4) a staggered configuration of the methyl hydrogens.

This is also reasonable in view of the steric factors involved for larger or smaller rotation angles of the t-butyl group as borne out in table 25. The model producing the most destabilized π* MO and consequently the highest total electronic energy value (least stable) is the species with eclipsed t-butyl carbons. From the mono-substituted t-butyl systems, this π* destabilization was attributed to through-space interactions with the t-butyl diketone system. The eclipsed conformation is the configuration maximizing this type of interaction.

Summary

In this chapter, the Extended Huckel Molecular Orbital Theory was used to theoretically analyze a variety of alkyl substituted 1,2-cyclobutanedione (CBD) models, in order to probe for significant and consistent effects of alkyl substituents on the n and π* MO's of the diketone system. These effects were monitored to determine the dependence on the frequency of substitution and on the relative size and/or conformation of the substituent. The study was designed to provide insight into the query of the unusually large λ_{max} observed for the n-π* solution spectra of the 3,4-di-t-butyl substituted model.

The alkyl substituents studied were: methyl, ethyl, and t-butyl. A definite destabilization of the n & π* MO's was observed for all alkyl substitutions on the CBD model, and the magnitude of this effect varied with the size of the sigma network of the added substituent. The size of the sigma network, of course, varied with the size of the alkyl substituent or with the number of substituents used. The order of increasing influence (destabilization) on the n & π* MO's as far as frequency of substitution was: mono < di < tri ≈ tetra. The order of increasing influence as far as the size of the substituents was: -H < $-CH_3$ < $-C_2H_5$ < t-butyl.

The influence of each substituent was noticeably altered by its conformation. In general, however, there was a more pronounced effect due to substituent size. Figure 24 & 24a plot the LEMO & HOMO values of various glyoxal and di-substituted CBD systems. These values are listed from left to right according to increasing size of the substituent. The conformation of a particular substituent that produced

Figure 24

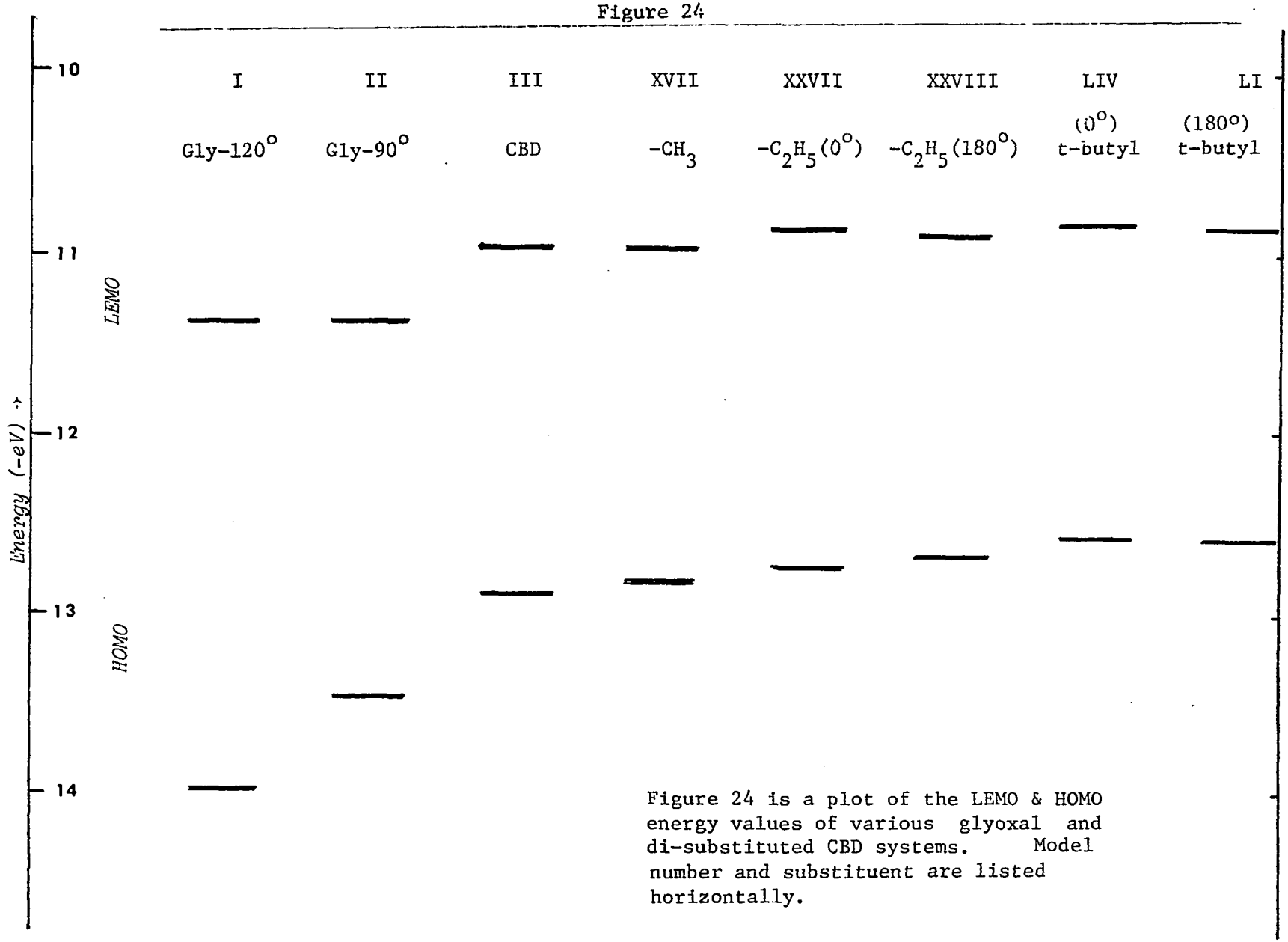

Figure 24 is a plot of the LEMO & HOMO energy values of various glyoxal and di-substituted CBD systems. Model number and substituent are listed horizontally.

Figure 24a

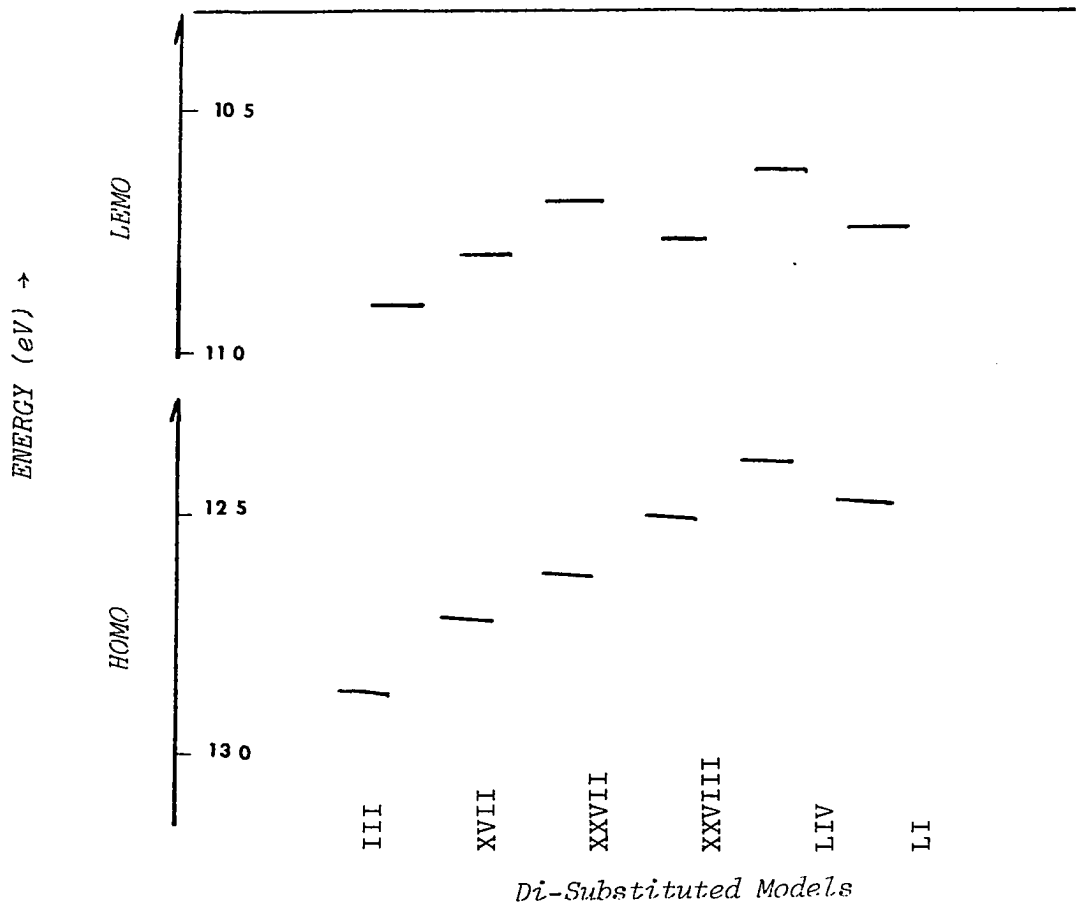

Figure 24a better illustrates (via larger energy scale) the variations of the HOMO & LEMO values for the CBD di-substituted series in figure 24.

Figure 25

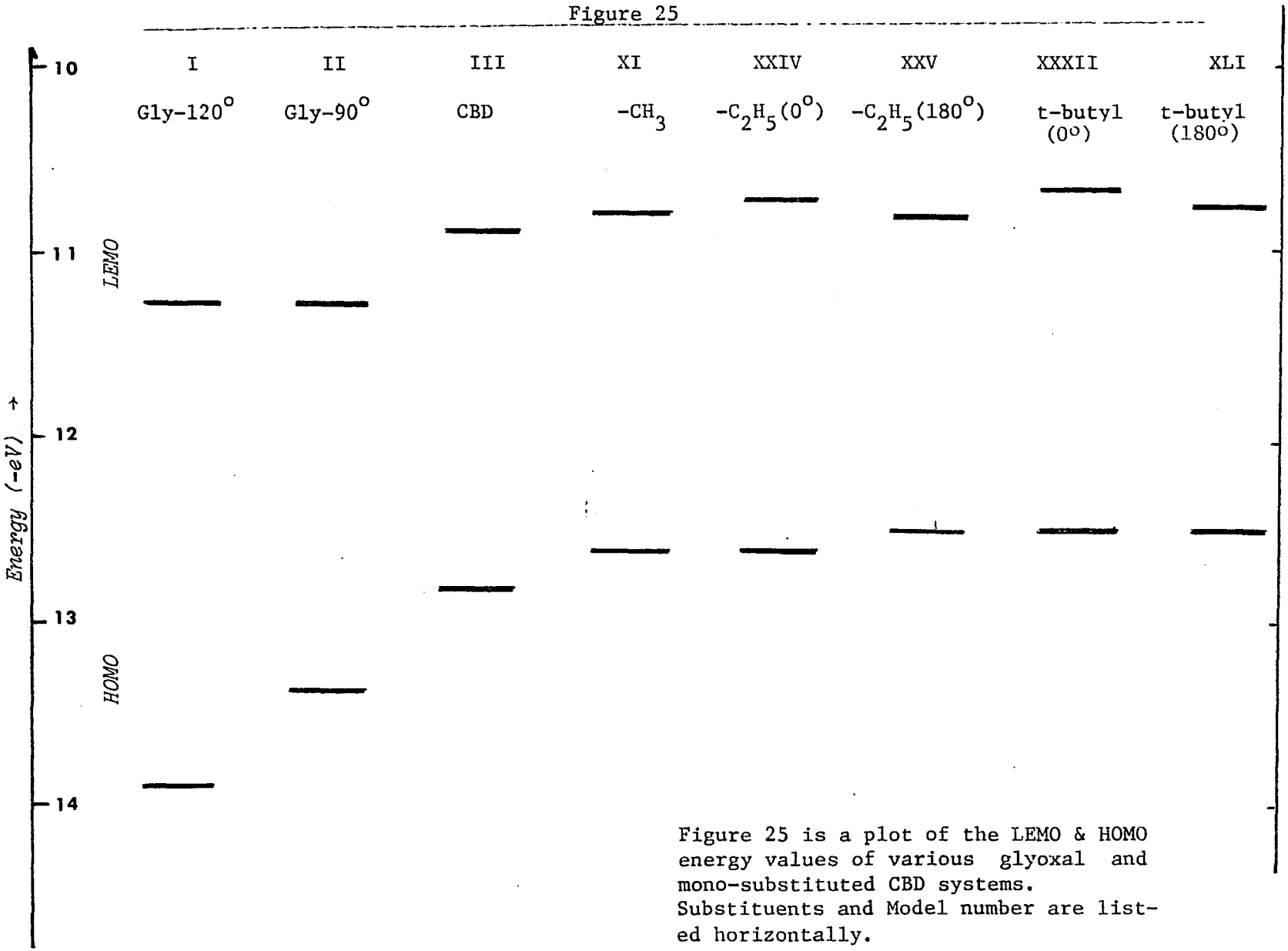

Figure 25 is a plot of the LEMO & HOMO energy values of various glyoxal and mono-substituted CBD systems.
Substituents and Model number are listed horizontally.

the most stable model (LTEE) is taken to be the most representative conformation for that substituent. There is a constant increase in energy for the n and π* MO with increasing size of the substituent. However in all cases, the increase for the n MO is approximately twice that of the π* MO. This, of course, produces an over-all decreasing n-π* energy value from left to right. The identical effect occurs for the mono-substituted model as well. Shown in figure 25 .

A through-bond interaction of the respective MO's of the CBD systems studied is the predominant cause of the observed destabilizations. The ordering of the two nonbonding MO energy levels, S above A (See Chapter III), found in these systems indeed supports this assertion. The observed destabilizations are most clearly due to the mixing of the n and π* MO's within the CBD system with the σ MO's of lower energy. This interaction is enhanced by the availability of σ MO's which have similar eneries and identical symmetries to those of the n and π* MO's[69]. This availability increases with the size of the σ frame. The larger σ frame has a larger number of σ MO's (S and A combinations) as well as more MO's with energy values closer to those of the n and π* MOs. Alkyl substitution on the ring increases the σ-frame. The larger number of S and A conbinations of the σ-bonding MO's induces an upward shift of the highest σ-bonding MO's and consequently increases nonbonding MO- σ MO interactions. Both the S and A combinations of the nonbonding MO's are destabilized. However, the S combination of the σ-bonding MO (σ_S) which is closer in energy to the nonbonding orbitals , in the dicarbonyl framework, causes the higher destabilization of the symmetric nonbonding MO, (n_S). Figure 26 gives

FIGURE 26. n & σ energies for various di-substituted CBD systems.

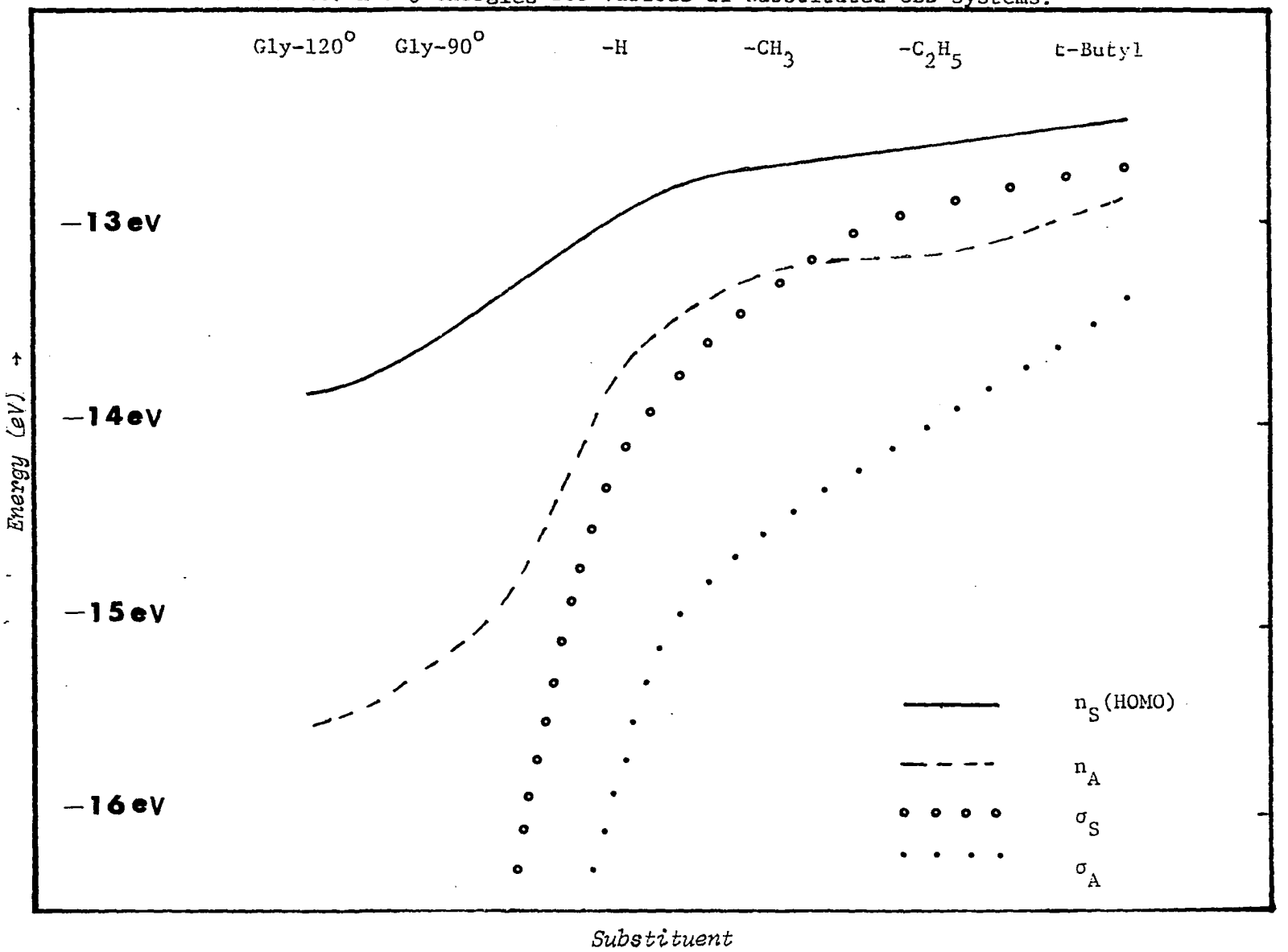

the energy values of the most available sigma MO's of the di-substituted systems with the proper symmetry for mixing. A plot of both nonbonding MO values (n_A and n_S) of the respective species are also included. It can be seen that the energy values of the highest available sigma MO's are in closer proximity to that of the n MO's (relative to π^*) as the size of the substituent increases. Consequently, a greater destabilization is observed for the n_S MO of the models with the larger substituent.

Over-all, the through-bond interaction was enhanced with the ring formation of CBD and with the size and number of alkyl substituents on the ring. Variations in this interaction were observed with variations of the substituent conformation. The physical picture of this through-bond phenomena is seen via through-bond coupling of the n and σ orbital lobes. It was found that this coupling is enhanced by certain favorable orbital orientations of the nonbonding lobes as well as by certain orbital orientations of the sigma frame. Some orientations of the substituent favored through-bond coupling, while with others important overlapping was to a lesser degree. The greater interaction of the nonbonding lobes was observed when the σ orbital lobes of the substituent were favored with the CBD system for interaction. This increased σ-σ interaction and consequently induced the upward shift of the σ MO energies.

This investigation could in no way simulate all possible configurations that could be encountered by an alkyl species in solution; however, this study did monitor interactions involved for a wide variety of selected conformations. An interesting observation in figure is that of the ethyl di-substituted species. Results from the 0^o and

180^{o} rotated models are presented. The HOMO interaction was maximized at the 180^{o} rotation. This configuration enhanced HOMO and σ MO mixing. The LEMO mixing was maximized at 0^{o} rotation, where through-space interaction was increased. Consequently the two configurations gave significantly different n-π^* energy values. The smallest n-π^* value occurs at the 180^{o} rotation, where n is more destabilized and π^* is less destabilized (relative to the 0^{o} rotation).

Since rotation of the ethyl group parallels that of a t-butyl, the isolation on this particular movement of the ethyl group gives some insight into the interactions involved for the t-butyl. The t-butyl group has three such terminal methyl groups, 120^{o} apart, simultaneously undergoing this type of rotation and this type of interaction. Just as in the case of ethyl substitution, the t-butyl group provided the smallest n-π^* transition when a terminal methyl carbon was rotated 180^{o} (staggered conformation).

Table 27 summarizes the n-π^* transition energies of the most stable 1,2-cyclobutanedione systems with 3,4 di-substitution. It is recalled that the observed empirical n-π^* transition value of DTCD is 49 mμ greater than that of CBD. EHMO predicts this difference to be approximately 84 mμ. The EHMO results indicate that the influence of the t-butyl group can indeed be expected to cause a shift in the n-π^* absorption spectra of CBD of the magnitude (49 mμ) and direction that is empirically observed. The calculated n-π^* energy values from the EHMO theory, as expected, are higher than the actual empirical values observed. However, the EHMO values are in qualitative agreement with the solution absorption spectra of the CBD and DTCD diketones.

Table

Calculated n-π^* transition energies of 1,2 cyclobutanedione with 3,4 di-substitution.

Substituent	Model Number	λ_{max} (mμ)	$\Delta\lambda_{max}$
-H-	III	636	-
$-CH_3$	XI	665	29
$-C_2H_5$ (0°)	XXVII	657	21
$-C_2H_5$ (180°)	XXVIII	716	80
-t-butyl (0°)	XLIX	717	81
-t-butyl (60°)	LI	720	84

It is of interest to note that the only other substituent predicted to cause such an enormous shift in the n-π^* transition (relative to CBD) is the di-ethyl substituent when constrained in a 180^o rotation. This, of course, is not a feasible expectation for an ethyl group when in solution. The ethyl group can have an expected path of rotation of over 180^o without incurring any significant hindrances from the adjacent (ring) hydrogen substituent or from the diketone system. The conformation of the t-butyl group ($50\text{-}70^o$ rotation), on the other hand, may be expected to be near that predicted by the EHMO calculations. A more constraining fluctuation in the rotation of the staggered t-butyl may indeed be anticipated, since a large degree of fluctuation (i.e. $> \pm 20^o$) would incur hindrances from the adjacent ring hydrogen or from the diketone network.

The chapter here has indicated, via EHMO Theory, that the n-π^* transition value of the CBD species is not only sensitive to the size of the alkyl substituent used but also sensitive to the conformation of the substituent as well. The study isolated an effect on the n and π^* MO's of the diketone system that is generally caused by alkyl substitution in the α position.

Chapter V

The Crystal Structure of 3,4 Di-t-butyl cyclobutanedione

The structure of 3,4 di-t-butyl cyclobutanedione (DTCD) is determined to support the MO and spectral studies of the compound. It appears as though the t-butyl groups play an important role in causing the high λ_{max} for DTCD since the corresponding absorption maximum of 487 mμ for 1,2 cyclobutanedione occurs near the normal absorption range.[68] It has been shown that sigma bonds play an important role in interactions in α-diketones. It is also known that such interactions depend on the conformation of the compound. Although the conformation of DTCD in solution may vary, comparison of the crystal conformation with the theoretical conformation prediction in chapter IV is of great interest. The ensuing crystal data may give insight into the probable occurrence of specific intermolecular interactions or of the existence of unusual bond lengths and angles for the DTCD system. The following information for the crystal structure parallels that of the publication.[90]

a. Experimental

The compound was obtained from Professor H. Wynberg who reported the synthesis and spectra.[1] A suitable data crystal was obtained by equilibrium diffusion of water into an ethanol-water solution of the compound. The crystal was enclosed in a thin-walled capillary because it proved too volatile at normal room temperature and pressure.

All X-ray data of the block-like (.4 x .4 x .3 mm) pink crystal were measured on a Nonius CAD-4 automatic diffractometer using Ni-filtered CuKα radiation (λ=1.5418 A^{o}), at room temperature (26^{o}C). The density measurement and cell volume data (Table 28) indicated that the unit cell contained four molecules. The molecule therefore contains a two-fold axis coincident with one of those of the space group. The least-squares cell dimensions were obtained from the averages of the ±2θ values of 40 reflections. The 1274 intensity data taken comprised all unique reflections with 2θ less than 150^{o}. The data were collected with θ-2θ scans in which the θ scan width, in degrees, was calculated as 1.0 + 0.1 tanθ . The maximum scan time was 150 sec with 2/3 of the time spent scanning the peak, while 1/6 each was considered indistinguishable from the background, having $I<2.0\ \sigma(I)$. For the purpose of least-squares refinement, these reflections were assigned a value equal to 1.4 times the square root of the total count (T). Secondary extinction corrections were made on the observed intensities according to the equation $I_{corrected} = I \exp(-C_{ext} \times P)$. The constant C_{ext} was determined to be 0.0000005 from the slope of a plot of log F_c/F_o versus P(net count) for reflections having a F_o greater than 30. Absorption corrections were omitted.

Table 28

Crystal Data

Formula: $C_{12}H_{20}O_2$

F.W. 196.29

Systematic Absences: hkℓ: $h + k = 2n + 1$
hoℓ: $\ell = 2n + 1 (h=2n + 1)$
oko: $k = 2n + 1$

Space group: C 2/c

a = 10.063(1)

b = 7.7273(5)

c = 16.190(2)

$\beta = 98.811(7)^{\circ}$

Density (obs) = 1.048 gm/cm^3

Density (calc)= 1.048 gm/cm^3

Z = 4

V = 1244.1 $A^{\circ 3}$

b. Structure Determination

The oxygen-oxygen and carbon-carbon (ring) vectors were identified on the v=0 section of the Patterson synthesis. By building a model it was possible to postulate carbon and oxygen atom positions and to compare interatomic vectors for these on the Patterson map. This model was used in an initial structure factor calculation. The temperature parameters of the nonhydrogen atoms were made isotropic and the R index ($R = \Sigma((||kF_o|-|F_c||)/\Sigma|kF_o|$) which had an initial value of 0.55, dropped to 0.16 after a few cycles of least-squares refinement. At this point the temperature parameters of the non-hydrogen atoms were made anisotropic and the R subsequently decreased to 0.12. All hydrogen atoms were located from a difference Fourier synthesis, and were included in the least-squares refinement. The extinction correction yielded the final R value of 0.060 for all data while the R for the reflections with $I>2\sigma(I)$, is 0.046. The final difference Fourier showed no negative or positive peaks greater than 0.15 e/A^{o3}. The parameter shifts in the final least-squares cycle were all less than 0.25σ.

All least-squares refinements were made using the block-diagonal least-squares program of Ahmed[73] while using 9x9 and 4x4 blocks. A logical routine[74] which may exclude certain reflections from least-squares refinement, was used during the refinement. The final positional and thermal parameters and their estimated standard deviations are given in Tables 29 and 30. The atomic scattering factors for C and O were taken from the International Tables for X-ray Crystallography[75]. The scattering factors for hydrogen atoms were those of Stewart, Davidson and Simpson[76].

Table 29

Parameters for the carbon and oxygen atoms

The x, y and z are expressed in fractions of the cell edges.

The anisotropic temperature factors are expressed in the form:

$$\exp\left[-2\pi^2(U_{11}h^2a^{*2}+U_{22}k^2b^{*2}+U_{33}\ell^2c^{*2}+2U_{12}hka^*b^*+2U_{13}h\ell a^*c^*+2U_{23}k\ell b^*c^*\right]$$

Standard deviations for the last digit are given in parentheses.

	x	y	z	U_{11}	U_{22}
O(1)	-0.1278(2)	-0.1238(2)	0.2988(1)	0.1217(12)	0.0758(8)
C(2)	-0.0602(2)	-0.0134(2)	0.2751(1)	0.0683(8)	0.0547(8)
C(3)	-0.0565(1)	0.1841(2)	0.2781(1)	0.0463(6)	0.0524(7)
C(4)	-0.0276(2)	0.2620(2)	0.3664(2)	0.0686(9)	0.0766(10)
C(5)	0.0955(2)	0.1783(4)	0.4172(1)	0.0807(12)	0.1644(22)
C(6)	-0.1500(2)	0.2296(3)	0.4099(1)	0.0901(13)	0.1220(17)
C(7)	-0.0082(3)	0.4567(3)	0.3585(2)	0.1662(23)	0.0828(14)

U_{33}	U_{23}	U_{13}	U_{12}
0.1643(17)	-0.0357(8)	0.0478(12)	0.0104(9)
0.0861(10)	-0.0100(7)	0.0123(8)	0.0049(8)
0.0589(8)	0.0000(5)	0.0133(5)	0.0025(6)
0.0594(8)	-0.0086(8)	0.0216(7)	-0.0065(8)
0.0638(10)	-0.0054(13)	0.0021(9)	-0.0025(12)
0.0782(12)	-0.0030(11)	0.0409(10)	-0.0003(11)
0.1053(16)	-0.0366(14)	0.0665(17)	-0.0398(12)

+The final F_o and F_c tables have been deposited with the British Library Lending Division as Supplementary Publication No. SUP(00000) (6 p., 1 microfiche). Copies may be obtained through the Executive Secretary, International Union of Crystallography, 13 White Friars, Chester CH1 1NZ, England.

Table 30

Parameters of the hydrogen atoms

The x, y and z are expressed in fractions of the cell edges.

Standard deviations for the last digit are given in parentheses.

	x	y	z	B
H(8)	-0.139(2)	0.236(2)	0.250(1)	5.3(3)
H(9)	0.177(2)	0.194(3)	0.391(1)	8.3(5)
H(10)	0.113(3)	0.218(3)	0.473(2)	10.8(7)
H(11)	0.088(3)	0.049(3)	0.420(2)	10.4(6)
H(12)	-0.134(2)	0.281(3)	0.470(2)	9.7(6)
H(13)	-0.157(2)	0.099(3)	0.417(1)	8.2(5)
H(14)	-0.234(2)	0.281(3)	0.378(2)	10.3(7)
H(15)	0.003(2)	0.509(4)	0.408(2)	11.5(7)
H(16)	0.066(2)	0.480(3)	0.328(1)	9.1(5)
H(17)	-0.088(4)	0.527(6)	0.325(3)	18.8(12)

A weighting scheme was used which assigns an experimental weight to each structure factor as defined below:

$$W_F = 1/\sigma_F^2$$

$$\sigma_F = 1/2\left[\frac{\sigma^2 + (0.04\ P)^2}{(P)\ (L_p)}\right]$$

in which

$\sigma = T^{1/2}V$

V = scan speed

T = total count

P = $(P_k - 2(R + L))$

R = right background count

L = left background count

L_p = Lorentz and Polarization corrections

P_k = peak count

In the structure factor analysis the average values of $W_F(\Delta F)^2$ did not show a significant variation with either $|F_o|$ or sin θ/λ, validating the weighting scheme used.

c. Description of the Structure

The bond distances are shown in figure 27 and Table 31. The bond angles are listed in Table 32. Figure 28 shows atom numbering scheme used.

Cyclobutane rings exist in both planar and puckered conformations. Infrared and Raman studies have indicated that the nonplanar conformation of these rings is more favorable than the planar conformation[77], but most of the reported centrosymmetrically substituted rings are planar in the solid state[78]. Therefore, it was not surprising to find that trans 3,4 di-t-butylcyclobutanedione has a nonplanar ring conformation (Table 33). The ring carbons are 0.028 A^{o} (over nine standard deviations) out of the least-squares plane, calculated for C(2), C(3), C(2') and C(3'). The dihedral angle between the plane through C(3), C(2) and C(2') and the plane through C(3), C(3') and C(2') is 174.3^{o}(2). The reported dihedral angles for puckered cyclobutane rings range from 145^{o} to 161^{o}.[79]

The dihedral angle of DTCD is large for puckered ring conformations, and this is probably due to the diketone substitution. The dihedral angle between the carbonyl groups, i.e., the torsion angle O(1)-C(2)-C(2')-O(1'), is 7.6^{o}.

Two long C-C bond lengths of 1.560(3) A^{o} are found for C(2)-C(2') and C(3)-C(3'). Long bond lengths in cyclobutane rings are common,[80] usually in the range from 1.547 to 1.58 A^{o}.[81] A short bond length of 1.527(2) A^{o} is observed for C(2)-C(3) which is symmetrically identical to the bond C(2')-C(3'). The shortening of this bond is consistent with the significant overlap of the p-π atomic orbital on C(2) with sigma-

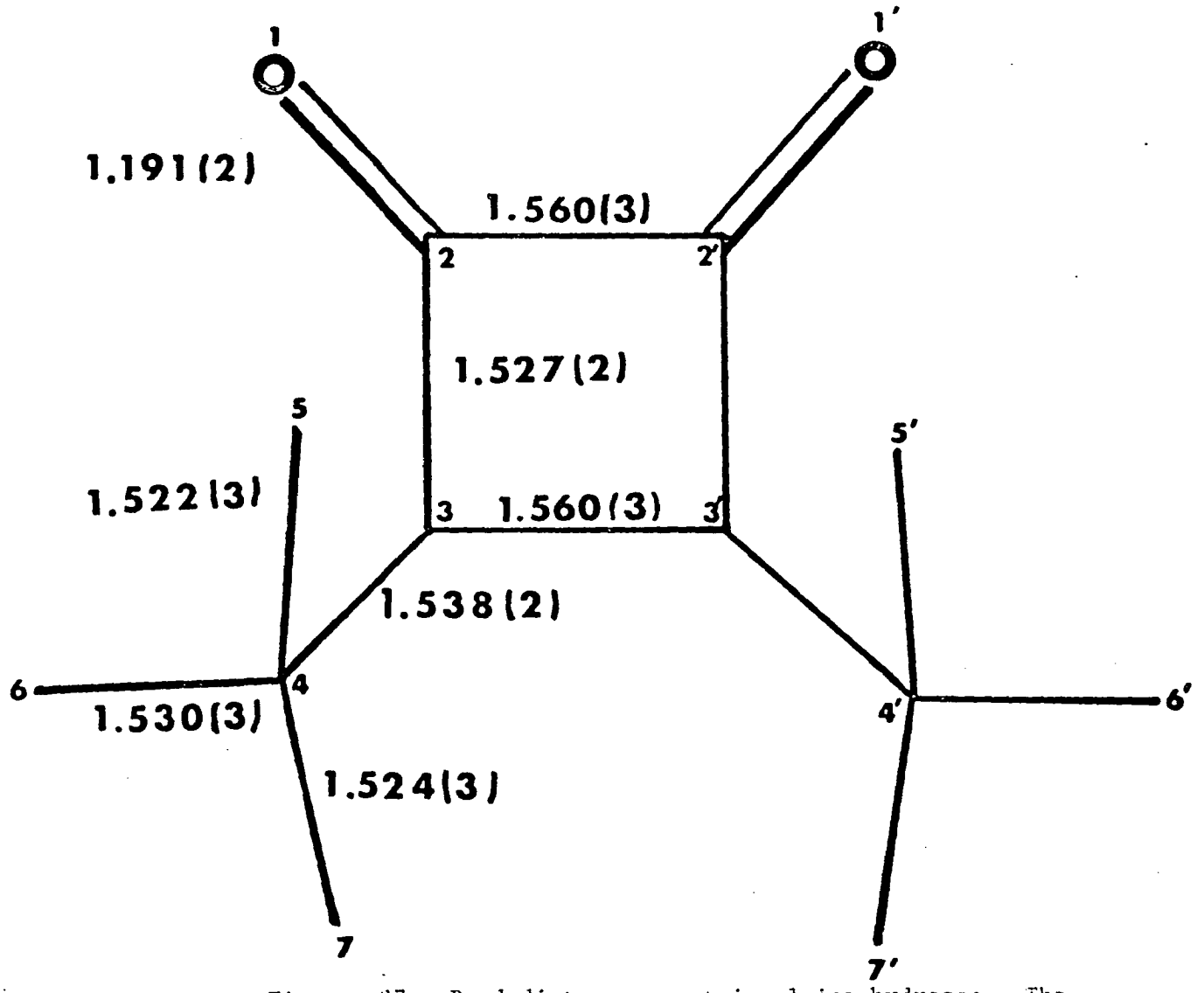

Figure 27. Bond distances, not involving hydrogen. The standard deviations of the last digits are given in parentheses.

Table 31

Carbon-hydrogen bond lengths

The standard deviations for the last digit are given in parentheses.

C(3)-H(8)	0.97(2) A°	C(6)-H(13)	1.02(2) A°
C(5)-H(9)	0.99(2)	C(6)-H(14)	1.00(3)
C(5)-H(10)	0.94(3)	C(7)-H(15)	0.88(3)
C(5)-H(11)	1.00(3)	C(7)-H(16)	0.97(2)
C(6)-H(12)	1.04(3)	C(7)-H(17)	1.05(5)

Table 32

Bond Angles

The standard deviations for the last digit are given in parentheses.

O(1)	C(2)	C(3)	136.0(2)°
O(1)	C(2)	C(2')	134.1(2)
C(3)	C(2)	C(2')	89.9(1)
C(2)	C(3)	C(3')	89.9(1)
C(2)	C(3)	C(4)	114.8(1)
C(4)	C(3)	C(3')	119.4(1)
C(4)	C(3)	H(8)	107.0(10)
C(3')	C(3)	H(8)	112.4(10)
C(2)	C(3)	H(8)	112.7(9)
C(3)	C(4)	C(5)	111.0(2)
C(3)	C(4)	C(6)	108.2(1)
C(3)	C(4)	C(7)	108.4(2)
C(5)	C(4)	C(6)	109.1(2)
C(5)	C(4)	C(7)	111.1(2)
C(6)	C(4)	C(7)	108.9(2)

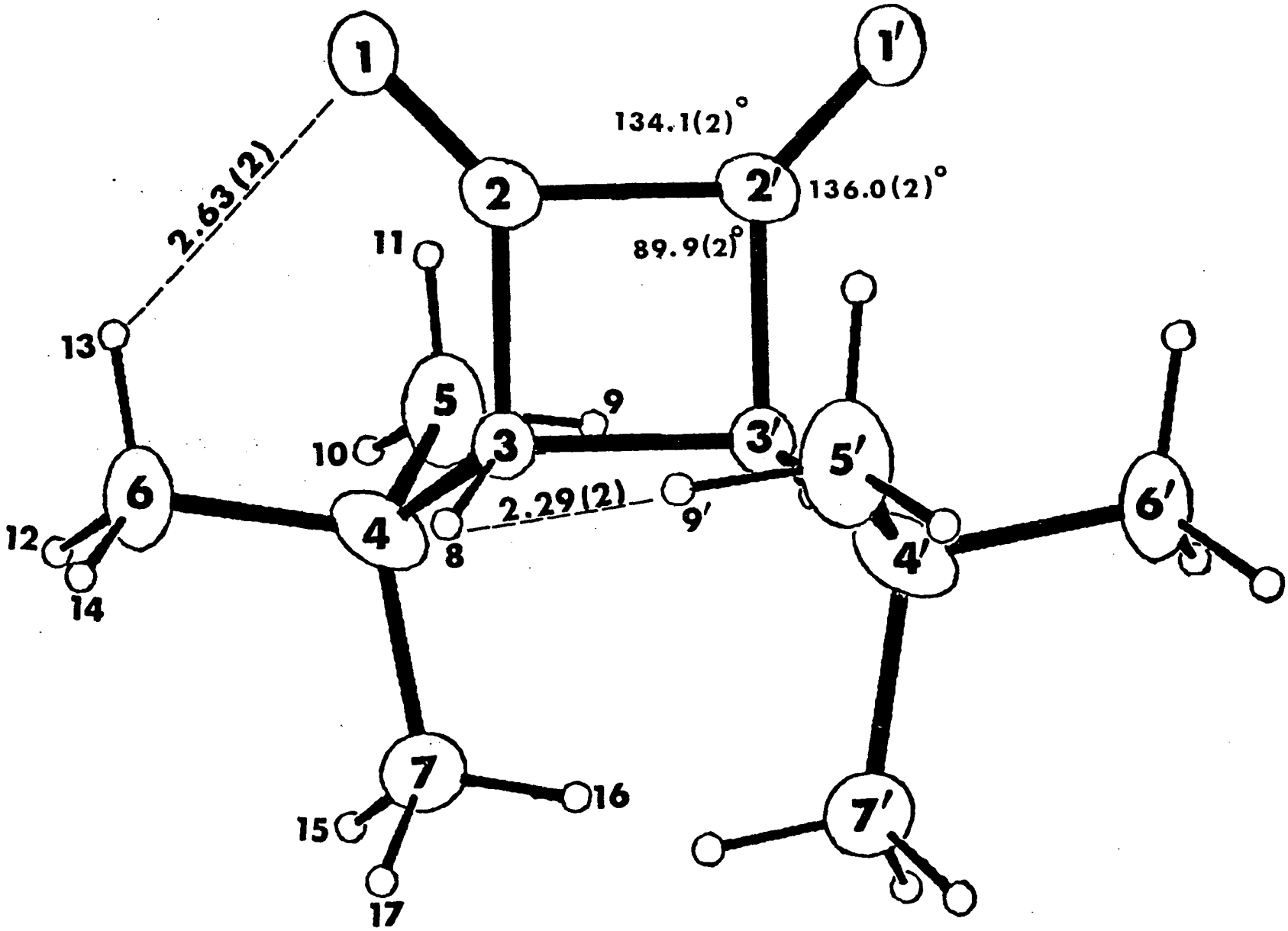

Figure 28. Intramolecular distances involving the hydrogen atoms. Atomic numbering scheme for Tables.

Table 33

Least-squares planes

I	C(2)	C(3)	C(2')	C(3')	5.494x + 0.000y + 12.052z = 3.013
II	C(3)	C(2)	C(2)		5.185x - 0.283y + 12.424z = 3.110
III	C(2')	C(3')	C(3)		-5.789x - 0.283y - 11.649z =-2.964
IV	O(1)	C(2)	C(3)	C(2')	5.123x - 0.338y + 12.492z = 3.124

x, y and z are fractional coordinates.

Distances from planes (A^{o})

Atom	(I)	(IV)
O(1)	-0.114	-0.004
C(2)	-0.028	0.009
C(3)	0.028	-0.002
O(1')	0.114	0.085
C(2')	0.028	-0.002
C(3')	-0.028	-0.125
C(4)	1.252	
C(5)	2.540	
C(6)	1.103	
C(7)	1.263	

hybrid orbitals on C(3) as reported for a similar diketone by Neely, Fink, van der Helm and Bloomfield.[82] Shirrell and Williams[78,81] have reported a short bond occurring in the ring of two other cyclobutanedione structures: the corresponding bond lengths are 1.515(6) A^o for 2,2,4,4-tetramethyl-3-thio-1,3-cyclobutanedione, and 1.507(2) for 2,2,4,4-tetramethyl-1,3-cyclobutanedione.

The shortest bond not involving hydrogen in the compound is, as expected, the carbonyl bond length, C(2)-O(1). The length of 1.191(2) A^o is shorter than the average carbonyl bond length of 1.215 A^o reported by Sutton[82]. This apparent shortening may well be caused in part or completely, by the high thermal motion of the oxygen atom (Table 29), although other short carbonyl bond lengths have been reported for similar systems.[83] Other atoms in the molecule show high thermal motion as well (Table 29). Two ring carbons, C(3) and C(3'), show the least thermal motion, while two t-butyl atoms, C(5) and C(7) show the highest. An apparent shortening of the C-C bonds occurs throughout the t-butyl groups. This is probably caused by the large thermal motion of the t-butyl carbons, especially for C(5) and C(7), which are involved in the shortest C-C bonds. It is interesting to note that the t-butyl carbon, C(6), closest to the oxygen, O(1), shows the least vibration of the three methyl groups. Also, the hydrogen H(13) bonded to C(6) (Figure 28) presents the shortest intramolecular distance between the oxygen atom and a methyl hydrogen atom. This distance of 2.63(2) A^o is comparable to the van der Waals distance of 2.6 A^o.[84]

A rigid body calculation was carried out using the method of Schomaker and Trueblood[85] with the appropriate restrictions imposed for a molecule with C_2 point symmetry. The R.M.S. ΔU_{ij} was 0.0043 A^{o2},

whereas the R.M.S. σU_{ij} was 0.0011 A^{o2}. This indicates that the molecule does not behave as a rigid body and the associated bond distance corrections can therefore not be made.

The shortest non-bonding intramolecular distance in DTCD occurs between two hydrogens. The nearly perfect staggering of the C-C and C-H bonds in the t-butyl group causes H(9') on C(5') to be only 2.29(2) A^{o} from the H(8) on C(3), (Figure 28). This is somewhat shorter than the van der Waals distance of 2.4 A^{o} between two hydrogen atoms, and suggests some intramolecular overlap.

The shortest intermolecular distance observed is the distance between the ring hydrogen, H(8), of one molecule and an oxygen atom (O") of a symmetry related molecule (-1/2-x, 1/2+y, 1/2-z) (Figure 30). While this distance of 2.59(2) indicates relatively little interaction, the fact that the ring hydrogen is the most acidic[86] and that the C(3)-H(8) and H(8)-O" vectors are colinear cannot be ignored. (C(3)-H(8)=0.97 A^{o}, C(3)-O"=3.55 A^{o}). A point of interest is that the only other intermolecular distances less than 3.00 A^{o} are also H-O" distances. These distances are 2.75 and 2.99 A^{o} and involve H(9) and H(17) respectively. All intermolecular distances not involving hydrogens are greater than 3.5 A^{o}.

The bond angles in the t-butyl group for the non-hydrogen atoms range from 108.2° to 111.1°, Table 32,and average 109.45°. The bond angles involving the methyl hydrogen atoms have an average value of 109.4°. All four of the angles in the cyclobutane ring are equal with a value of 89.9(1)°.

Atoms O(1), C(2), C(3) and C(2') are relatively coplanar. The three angles, O(1)-C(2)-C(3), O(1)-C(2)-C(2'), C(3)-C(2)-C(2'), in this plane

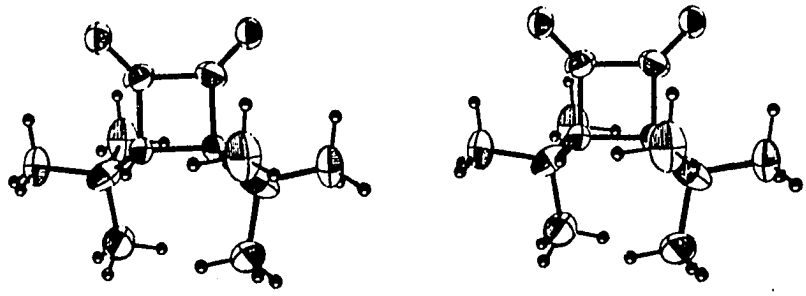

Figure 29. An ORTEP stereographic drawing of DTCD

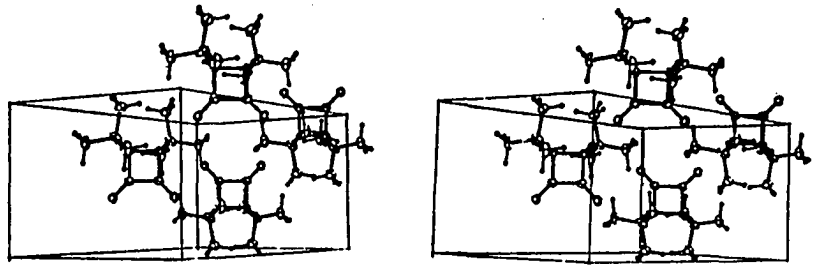

Figure 30. An ORTEP drawing of the packing of the molecules.

differ, as expected, from the normal 120°. The respective values of 136.0(2), 134.1(2)° and 89.9(1)° reflect the expected strain in four-membered rings. Similar angles for other ring diketones have been reported. Fink, et al.[83], reported the corresponding angles of 134.2(2)°, 135.5(2)° and 90.3(1)° for an α-diketone; Shirrell, et al.[81], reported 131.9(2)°, 134.6(2)° and 93.5(1)° for a 1,3 diketone.

The C-H bond distances average 0.99 A°, with the extremes being 0.88(3) A° for C(7)-H(15) and 1.05(5) A° for C(7)-H(17). The carbon involved in both cases, C(7), has the highest thermal motion for the molecule. Figure 29 is a stereographic drawing of DTCD. Figure 30 is an ORTEP drawing of the molecular packing.

Conclusion

The structure of DTCD provides information for at least three points of interest. Two of these were presented in the earlier investigations of de Groot, et al.[1] Point one occurs in the report of the compound's preparation from a mixture of dl and meso diesters. The reacting form was postulated to be dl and the structure determination indeed verifies that assumption. The second point arises in the comparison of the electronic spectrum of DTCD with those obtained for the tricyclo $(4.4.2.0)^{1,6}$dodeca-3,8-diene-11,12-dione (2DB), and its tetrahydro derivative (ODB). It was noted in chapter I that the DTCD spectrum corresponds closely to that of the unsaturated α-diketone (2DB) rather than to the saturated compound (ODB), as might be expected. Both the 536 mμ for DTCD and the 537.5 mμ for 2DB are above the expected maximum of 480 mμ for a n-π* transition for unsubstituted α-diketones. It is certainly not unreasonable to expect the spectral similarities of DTCD and 2DB to depend at least partially on some of the structural similarities of the two compounds. Some of these similarities are noted: both compounds have short carbonyl bond lengths of 1.19 A^{o}; both have C-C bond shortening occuring in the ring; both have nonplanar carbonyl dihedral angles, although the carbonyls of 2DB are in a planar ring, while the carbonyls of DTCD are in a nonplanar ring and both have 3,4 substitution of sigma bond networks. A theoretical comparison of the forementioned compounds is discussed in the following chapter (VI). Their similar n-π* transitions are discussed in detail.

The third, and perhaps more interesting, point is the comparison of the crystal conformation with that of the theoretical conformation. The crystal structure data reveals no unusual bond distances or angles for the DTCD structure, and intermolecular interactions appear negligible. EHMO calculations (chapter V) predict that the t-butyl substituents alone can be expected to cause a significant bathochromic shift in the n-π^* absorption spectrum of DTCD. It is of interest to determine whether the crystal structure version will support this theoretical interpretation. An EHMO analysis of the crystal form and a detailed comparison of the two species is also presented in chapter VI.

Chapter VI

Discussion

Salient points in this work, which deserve further emphasis, are presented below.

I. Evaluation of the influence of alkyl substituents in absorption spectra from empirical data is presented.

It is known that alkyl substituents such as methyl groups, etc. have significant bathochromic influences in the absorption spectra of various chromophoric groups (See chapter I). However, there is no direct empirical assessment of the magnitude of such effects in the n-π^* absorption spectra of substituted dicarbonyls. An indirect basis for assigning a quantitative value for this influence was presented in chapter I. This involved evaluating bathochromic effects of alkyl substitution in the absorption spectra of various chromophoric groups other than dicarbonyl. Alkyl substituted monocarbonyls and alkenes were among those considered. The average values deduced for a bathochromic shift caused by a methyl substitution and by a di-t-butyl substitution, respectively, are 12-15mμ and 44 mμ. These values seem quite reasonable in view of the red shift of 49 mμ observed for the DTCD compound.

II. The existence of a through-bond interaction in dicarbonyl is theoretically supported.

A through-bond mechanism is observed in CBD systems. This interaction is significantly enhanced by the four-membered ring formation as well as by alkyl substitution on the ring. Destabilization of both the symmetric and antisymmetric nonbonding MO's is observed. The influence of t-butyl substitution is shown to account for an unusually large red shift of the n-π^* transition of CBD. A bathochromic trend in the n-π^* absorption spectra for increased alkyl substitution on the CBD ring is established. Substituent as well as conformational effects are explained, respectively, in terms of an increasing destabilization of σ-orbitals and in terms of favorable orientations of the respective orbital lobes.

The through-bond mechanism for the CBD system is not uncommon for diketone models[21] and the explained physical phenomena are in accord with other such observations in the literature. Heilbronner and Martin[63] in a photoelectron spectroscopic study of π-orbital sequences in norbornadienes, showed that substitution of alkyl groups induced an upward shift of the orbital energies of the highest occuppied σ-orbitals, due to the enlargement of the σ-frame. This subsequently caused greater destabilization of the HOMO. Hoffmann, Imamura and Hebre[21] showed in a theoretical study of radical lobes of benzynes and didehydroconjugated molecules that through-bond interactions depend on the orientation of the σ bonds and on the orientation of the lobes themselves; thus inferring conformational effects.

Spafford and Vala[59] very recently reported a theoretical study of the n-π* transition of 1,3 cyclobutanedione. The interaction of the carbonyls' nonbonding n and π* antibonding orbitals are discussed qualitatively in terms of through-space and through-bond mechanisms. Through-bond interactions are shown to be the major cause of the large n orbital splitting. It was also shown that the simple extended Huckel theory gives more satisfactory results for the position, ordering, and spacing of the n and π* states than do CNDO methods.

III. More accurate n-π* transitions from EHMO data are predicted.

The EHMO method has revealed tremendous success with conformational predictions and qualitative interpretations for compounds in a common series. However, the quantitative predictions from the EHMO theory leave much to be desired. As expected, the n-π* energy values calculated in this study are much higher than the actual empirical values expected. Since the EHMO values are qualitatively correct for the known empirical values in the CBD series, improved theoretical n-π* values for the series are obtained by equating the empirically known values for CBD and DTCD to their respective EHMO values and obtaining an average proportionality factor. Table 34 lists these adjusted ΔE values for the CBD series. The predicted λ's are the best possible. It, of course, would be interesting to compare these values with the corresponding empirical values when more compounds of the CBD series are synthesized.

Table 34

n-π* Energy values for di-substituted 1,2 cyclobutanediones

Substituent	Expt. ΔE, eV	Expt. ΔE, mμ	EHMO ΔE, eV	EHMO# ΔE, eV	EHMO# ΔE, mμ	Error %
-H	2.54	487	1.95	2.54	479	2
$-CH_3$	-	-	1.86	2.47	502	-
$4(-CH_3)$[a]	-	-	1.82	2.42	512	-
$-C_2H_5(0^o)$	-	-	1.89	2.51	494	-
$-C_2H_5(180^o)$	-	-	1.73	2.30	539	-
$-C_2H_5$(ave.)	-	-	1.81	2.41	514	-
-t-butyl	2.31	536	1.70	2.26	548	2

[a] tetra methyl substituted
avg. proportionality factor = 1.33

IV. A crystal structure investigation reveals the stable conformation of DTCD as that which was theoretically predicted in chapter IV of this work via extended Huckel Theory.

Table 35

Predicted and Experimental Comparisons of Conformational Parameters of DTCD

	Vertex carbon angles of t-butyl		Rotation of t-butyl	Butane ring	Methyl hydrogens
	Vertical	Horizontal			
SDTCD(HMO)	112-117°	120°	60-70°	180°	staggered
CDTCD(Expt)	114.8°	119.4°	67.6°	174	staggered

The x-ray crystal structure of DTCD was determined to obtain the actual configuration of DTCD in the crystalline state and to rule out the possibilities of unusual intramolecular and intermolecular distances. Pertinent information on this work is reported in chapter V.

It is indeed gratifying to point out that the conformation determined for the crystalline species (CDTCD) closely parallels that which was predicted via HMO energy parameters (SDTCD). Two structures' conformation values are compared in table 35.

The molecular interactions in CDTCD, as may be expected, parallel those of the SDTCD systems. The n and π^* MO's are both significantly destabilized relative to CBD. The energy increases of the n and π^* MO's are 0.44 eV and 0.19 eV, respectively. The increase of the n MO is due to the same type of interactions postulated for the SDTCD system (figure 22). However, the interactions for CDTCD are more pronounced. This is probably due to its over-all shorter bond lengths. The C-C and C-H bond lengths for the CDTCD structure average 1.53 A^o and 0.99 A^o, respectively. The corresponding values for SDTCD are 1.54 A^o and 1.1 A^o. The over-all effect is a smaller n-π^* energy value for CDTCD than for the predicted SDTCD model. CDTCD is also the most stable (LTEE) of all the di-t-butyl species analyzed. The SDTCD model could obviously have been improved by bond length variations. Such variations should be considered in any future work of this type. The EHMO results and atomic coordinates of CDTCD are listed in appendix. (See page 156).

V. A theoretical basis for explaining the similar and unusual spectra (n-π^*) of DTCD and 2DB (See Chapter I) is provided.

The unusually large n-π^* λ_{max} values of both DTCD and 2DB are apparently due to through-bond mechanisms. However, the close similarities in these values are probably coincidental. (λ_{max} for DTCD = 536 mμ, λ_{max} for 2DB = 537 mμ).

The EHMO Theory predicts the n-π* ΔE for the crystal conformations of DTCD and 2DB to be 1.58 eV and 1.47 eV respectively. These are not as close as the respective empirical values, but both EHMO values are within 3% of the average value, 1.53 eV. (The 1.58 eV value for DTCD is obtained when using the same EHMO parameters as those used in the Neely study.[19]).

Since the ΔE values for the EHMO prediction are for single molecules, the fact that they are not exactly equivalent, as reflected in the respective solution absorption spectra, is not surprising. The empirical values are, of course, influenced by the presence of solvent and by the freedom of the species for conformational changes. Since both species cannot be expected to be influenced identically while in solution, their "similar" n-π* energy values in solution are certainly feasible. The small 3% difference in the theoretical values for the single molecules means that relatively small conformational or solvent effects could account for the experimental agreement.

It is of interest to note, however, that Fink[55] studied three different conformations of the 2DB species. The most stable conformation of the three was predicted to be the most prevalent in solution. This structure had both six-membered rings "endo" (ring up) to the four-membered ring. The structure which had both six-membered rings "exo" (ring down) to the four-membered ring was predicted to have an n-π* energy value of 1.57 eV. This value for 2DB reflects the similarities observed for the respective DTCD and 2DB empirical values. This, of course, suggests that, in solution, the 2DB compound resides more in the "exo" conformation, while the DTCD compound resides in the conformation predicted. The "exo"

conformation for 2DB, sterically, could be expected to be more stable while in solution. The difference in total energies of the "endo" and "exo" conformations is 0.24 eV. The difference of the 0^{o} and 60^{o} conformation of DTCD is 0.75 eV. The conformational change for the 2DB species would be more easily overcome, relative to DTCD. It is realized, however, that the suggestion of a new conformation for 2DB may be pushing the limits of accuracy of the EHMO method. An investigation featuring raman spectroscopy to determine solution conformers would be of special interest.

The molecular orbital and structural investigation of 3,4 di-t-butylcyclobutanedione and related compounds, covered in this study have revealed valuable information about the intramolecular interactions of alkyl-substituted dicarbonyls. The results will aid in expanding present knowledge of the electronic composition of dicarbonyls and specifically improve the interpretation of the $n-\pi^{*}$ absorption spectra of such systems. Although the final analysis and interpretations of this investigation apply directly to cyclobutanedione systems, the possible application of this work to carbonyl systems in general is clear.

BIBLIOGRAPHY

1. A. de Groot, D. Oudman and H. Wynberg, Tetrahedron Letters, 1529 (1969)

2. S. Nagakura and A. Kuboyana, J.Am.Chem.Soc., 76, 1003 (1954).

3. H. Booker, L. K. Evans, and A. E. Gillam, J. Chem. Soc., 1453(1940).

4. L. K. Evans and A. E. Gillam, J. Chem. Soc., 565 (1943).

5. N. J. Leonard and P.M. Mader, J.Am.Chem.Soc., 72, 1244 (1961).

6. R. B. Woodward, J. Am. Chem. Soc., 64, 72 (1942)

7. K. Dimroth and G. Troutmann, Chem. Ber. 69, 669 (1936)

8. R. Huhn and C. Brundmann, Chem. Ber. 70, 1318 (1937)

9. R. B. Woodward J. Am. Chem. Soc. 63, 1123 (1941)

10. L. K. Evans and A. E. Gillam, J.Chem.Soc., 815 (1941)

11. L.K. Evans and A.E. Gillam, J.Chem.Soc., 432-6 (1945)

12. J. B. Pazos and F. D. Greene, J.Am.Chem.Soc. 89, 1039 (1967)

13. N.J. Turro and W.B. Hammond, Tet. 24(18, 6017-28 (1968)

14. J.M. Conia and J. Core, Bull. Chem. Soc. (Fr), 2755 (1965)

15. H. Wynberg, S. Reiffers and J. Strating, Recueil 89, 982 (1970)

16. O. Sinanoglu, K. Wiberg, Sigma Molecular Orbital Theory, Prentice-Hall, Inc., New Jersey, 1970, pp. 3, 179-195, 225-227

17. R.Hoffmann, E.Heilbronner & G. Gleiter, J.Am.Chem.Soc., 92, 706(1970)

18. S.C.Neely, R.Fink, D. van der Helm and J.J. Bloomfield, J. Am. Chem Soc. 93, 4903-4905 (1971)

19. R. Hoffmann, J. Chem. Phys. 39, 1397 (1963)

20. R. Hoffmann, J. Chem. Phys. 40, 2474 (1963)

21. R. Hoffmann and W.N. Lipscomb, J. Chem. Phys. 36, 2179 (1962)

22. S.P. McGlynn, L.G. Vanquickenborne, M. Kinashita, D.G. Carroll, Introduction to Applied Quantum Chemistry, Holt Rinehart and Winston, Inc., 1972, pp. 72

23. A.G. Turner, Methods in Molecular Orbital Theory, Prentice-Hall, Inc., New Jersey, 1974, pp. 105

24. G. Scheibe, G. Roossler and F. Backenkahler, Ber., 58, 586 (1925)

25. R. Mulliken, J. Chem. Phys., 7, 121 (1939)

26 J.R. Hoyland, Molecular Orbital Studies in Chemical Pharmacology, edited by L.B. Kier, Springer-Verlag, N.Y., 1969, pp. 31-81

27. J.A. Pople, D.P. Santry, and G.A. Segal, J.Chem.Phys., 43, 5129(1965)

28. J.A. Pople and G.A. Segal, J. Chem. Physl, 44, 3289 (1966)

29. J. Del Bene and H.H. Jaffe, J.Chem. Phys., 48, 1807 (1968)

30. J. Del Bene and H. H. Jaffe, J.Chem.Physl, 48, 4050 (1968)

31. M.J.S. Dewar and G. Klopman, J.Am.Chem.Soc., 89, 3089 (1967)

32. J.A. Pople, D.L. Beveridge and P.A. Dobosh, J. Chem. Physl, 47, 2026 (1967)

33. R.S. Mulliken, J. Chem. Phys., 3, 564 (1934)

34. E. Huckel, Z. Physik, 70, 204 (1931)

35. A. Streitwieser, Molecular Orbital Theory for Organic Chemistry, J. Wiley and Sons, Inc., N. Y. , 1961, pp. 97-125.

36. M. W. Hanna, Quantum Mechanics in Chemistry, W.A. Benjamin, Inc., N. Y. 1966, pp. 193

37. K. Fukui, Modern Quantum Chemistry, Vol. I, O. Sinanogle, Ed, Academic Press, N. Y. , 1965

38. A.L. Companion, Chemical Bonding, McGraw Hill Co., 1964, pp. 40-43

39. A.A. Frost, J. Chem. Phys., 47, 3707 (1967)

40. H.A. Skinner and H.O. pritchard, Trans, Far.Soc., 49, 1254 (1953)

41. R. Hoffmann's Program QCPE Program 64, Quantum Chemistry Program Exchange, Indiana U.

43. J.N. Murrell, The Theory of the Electronic Spectra of Organic Molecules , John Wiley & Sons, Inc., N.Y. , 1963, pp. 158-174

44. R. Mason, Quart. Rev 15, 287 (1961)

45. G.J. Brealey and M. Kasha, J.Am.Chem.Soc., 77, 4462 (1955)

46. H. McConnell, J. Chem. Phys., 20, 700 (1952)

47. G.C. Pimentel, J. Am. Chem. Soc., 79, 3323 (1957)

48. R.C. Cookson and N.S. Wariyar, J.Chem.Soc., 3202 (1956)

49. D.Cowan, R. Gleiter, J. Hushmell, E. Heilbronner, V. Hornung, Angew. Chem. Int. Edit 10, 401 (1971)

50. H. Labhart and G. Wayniere, Helf,Chim.Acta 42, 2219 (1959)

51. E.I. Snyder and B. Franzus, J.Am.Chem.Soc., 86, 1166 (1964)

52. H. McMurry, J.Chem.Phys., 9, 231 and 241 (1941)

53. H. Birnbaum, R.C. Cookson and N.Levin, J.Chem.Soc., 1244 (1961)

54. T.R. Evans and P.A. Leermakers, J.Am.C-em.Soc., 89, 4380 (1967)

55. R. Fink, Ph.D. Dissertation, University of Ok, Norman, Ok

56. J.M. Foster and S.F. Boys, Rev. Mod. Phys., 32, 303 (1960)

57. J. R. Swenson and R. Hoffmann, Helf. Chim. Acta, 53, 233 (1970)

58. W.R. Wadt and W.A. Goddard IV. JACS 97, 2034 (1975)

59. J. Baiardo, R. Spafford, & M. Vala, JACS 98 17(1976), 5225-28

60. R. Spafford, J. Baiardo, J. Wrobel & M. Vala JACS 98:17 (1976) 5217-24

61. E. Heilbronner & A. Schmelzer, Helv,Chim Acta 58, 936=967 (1975)

62. E. Heilbronner & K.A. Muszkat JACS 92, 3818 (1970)

63. E. Heilbronner, H.D. Martin, Helf, Chim Acta 55, 1490-1502 (1972)

64. E. Heilbronner, Isr. J. Chem. 10, 143-156 (1972)

65. R. Hoffmann, Tet. Let. 43, 3819-3825 (1965)

66. E. Haselback, J.A. Hashmell, E. Heilbronner & V. Hornung, Angew Chem Int. Edit. 8, 878 (1969)

67. A.B. Anderson, J.Chem.Phys., 62, 1187-88 (1975)

68. H. Heine, Chem. Ber. 194, 2869-2872 (1971)

69. R. Hoffmann, Accts. of Chem. Res. 4, 1-9 (1971)

70. P. Bischof, J. Hashmal, E. Heilbronner, V. Hornung, Tet. Let. 4025(1969)

71. E. Heilbronner, K. Muszkat, JACS, 92, 3818 (1970)

72. R. Hoffmann, A. Imamura, W. Hehre, JACS, 90, 1499 (1968)

73. F.R. Ahmed (1966) S.F.L.S. Program, NRC-10 Ottawa; National Research Council

74. D. van der Helm, and H. B. Nicholas, Acta Cryst. B26, 1858-1866(1970)

75. International Tables for X-ray Crystallography (1962), Vol. III, pp. 202, 214, Birmingham: Kynoch Press.

76. R.F. Stewart, E.R. Davidson & W.T. Simpson, J.Chem.Physl, 42 3175-3187 (1965)

77. W.D. Rathjens, N.K. Freeman, W. D.. Guinn, K. S. Pitzer, JACS, 75 5634-42

78. C.D. Shirrell and D.E. Williams, Acta Cryst., B30, 1974-1978(1974)

79. C.D. Shirrell and D.E. Williams, Acta Cryst., B29, 1648-1653 (1973)

80. J.D. Dunita, and V. Schomaker, J.Chem. Phys., 20, 1703-1707 (1952)

81. C.D. Shirrell, and D.E. Williams, Acta Cryst., B30, 245-246 (1974)

82. L.E. Sutton, Tables of Interatomic Distances and Configuration in Molecules and IONs, Supplement 1956-59, The Chemical Soc. London 1965, pp. 514.

83. R. Fink, D. van der Helm, S.C. Neely, Acta Cryst. (in press) 1975

84. L. Pauling, The Nature of the Chemical Bond , p. 260, Cornell Univ. Press, Ithaca, N. Y. (1960)

85. V. Schomaker , and K.N. Trueblood, Acta Cryst. B24, 63-76 (1968)

86. K.F. Reid, Properties and Reactions of Bonds in Organic Molecules Amer. Elsevier Pub. Co., Inc., N.Y. pp. 349

87. J.J. Bloomfield, Tet. Let., 587-590 (1968)

88. J.J. Bloomfiedd, R.E. Moser, JACS., 90, 5625-5626 (1968)

89. C.K. Johnson, ORTEP Report ORNL-3794. Oak Ridge Natl. Lab, Oak Ridge, Tenn. (1965)

90. J.K. Coleman, S.C. Neely and Dick van der Helm, Acta Cryst., B32, 115-119(1976).

APPENDIX GUIDE

The APPENDIX GUIDE lists the location (Table No. & Page No.) of the EHMO & Coordinate values by Model No. for each respective model studied in this work. (*located in text)

Model No.	Description	EHMO Values		Atomic Coordinates	
		Table	Page	Table	Page
I	*gly-120	4a	45	4b	45
II	*gly-90	5a	48	5b	48
III	*CBD	6a	52	6b	52
IV	gly-120-1 methane	36	159	53	183
V	*gly-120-2 methanes	7a	58	7b	59
VI	gly-90-1 methane	36	159	53	183
VII	*gly-90-2 methanes	7a	58	7b	59
VIII	CBD-1 methane	37	160	54	184
IX	*CBD- 2 methanes	9a	64	9b	65
X	*CBD- 1 methyl (0^{o})	11a	69	11b	70
XI	*CBD- 1 methyl (60^{o})	11a	69	11b	70
XII	cis methyl CBD (0^{o})	38	161	55	185
XIII	trans methyl CBD(0^{o})	38	161	55	185
XIV	cis methyl CBD (30^{o})	39	162	56	186
XV	trans methyl CBD (30^{o})	39	162	56	186
XVI	*cis methyl CBD (60^{o})	13	74	15	76
XVII	*trans methyl CBD (60^{o})	14	75	15	76
XVIII	cis methyl CBD (90^{o})	40	163	56	186
XIX	trans methyl CBD (90^{o})	40	163	56	186
XX	cis methyl CBD (90^{o})	41	164	55	185
XXI	trans methyl CBD (90^{o})	41	164	55	185
XXII	*tri-methyl CBD	16a	80	16b	81
XXIII	*tetra-methyl CBD	17	82-83	57	187
XXIV	mono-ethyl CBD (0^{o})	42	165	58	188
XXV	mono-ethyl CBD (120^{o})	43	165	58	188
XXVI	mono-ethyl CBD (180^{o})	44	165	59	189
XXVII	*di-ethyl CBD (0^{o})	19	90	20	91
XXVIII	*di-ethyl CBD (180^{o})	19	90	20	91
XXIX	t-butyl CBD	43	166-7	60	190

APPENDIX GUIDE(Cont.)

Model No.	Description	EHMO Values Table	EHMO Values Page	Coordinates Table	Coordinates Page
XXX	t-butyl CBD	43	166-7	60	190
XXXI	t-butyl CBD	43	166-7	61	191
XXXII	t-butyl CBD	44	168-9	61	191
XXXIII	*t-butyl CBD	22	96-7	62	192
XXXIV	t-butyl CBD	44	168-9	61	191
XXXV	t-butyl CBD	44	168-0	61	191
XXXVI	t-butyl CBD	45	170-1	63	193
XXXVII	t-butyl CBD	45	170-1	63	193
XXXVIII	t-butyl CBD (0^{o})	45	170-1	63	193
XXXIX	*t-butyl CBD(30^{o})	24	106-7	63	193
XL	t-butyl CBD (50^{o})	24	106-7	64	194
XLI	t-butyl CBD (60^{o})	24	106-7	64	194
XLII	t-butyl CBD (70^{o})	46	172-3	64	194
XLIII	t-butyl CBD (80^{o})	46	172-3	64	194
XLIV	t-butyl CBD (90^{o})	46	172-3	65	195
XLV	t-butyl CBD (100^{o})	47	174-5	65	195
XLVI	t-butyl CBD (30^{o})	47	174-5	65	195
XLVII	t-butyl CBD (60^{o})	48	176-7	62	192
XLVIII	t-butyl CBD (90^{o})	47	174-5	65	195
XLIX	ci-t-butyl CBD (0^{o})	49	178	66	196
L	di-t-butyl CBD (30^{o})	49	178	66	196
LI	*di-t-butyl CBD (60^{o})	26a	111	26b	112
LII	di-t-butyl CBD (90^{o})	49	178	67	197
LIII	di-t-butyl CBD (90^{o})	50	179	67	197
LIV	di-t-butyl CBD 0^{o}	51	180	68	198
LV	di-t-butyl CBD 60^{o}	51	180	68	198
LVI	*di-t-butyl CBD (xtal)	52	181-2	26b	112
LVII	ethane		202		202
LXI	1,2 di-t-butyl ethane		203		203

APPENDIX

The following tables list the selected EHMO values, atomic coordinates and any other pertinent data relative to this investigation that for clarity was not located in the main text.

Table 36

Selected EHMO's for Glyoxal Interactions

Models: IV & VI
C_1 Symmetry

Model IV: Gly-120 with one methane
Model VI: Gly-90 with one methane

	Model IV			Model VI		
MO(sym.)	π_S^*(A)	n_S(A)	n_A(A)	π_S^*(A)	n_S(A)	n_A(A)
Energy (ev)	-11.167	-13.788	-14.924	-11.170	-13.348	-14.818
C_{ij}'s						
H(1)	-0.002	-0.278	0.268	-0.003	0.260	0.316
H(2)	0.026	-0.360	-0.213	0.028	0.304	-0.321
H(3)	0.036	-0.036	-0.206	0.036	0.022	-0.196
H(4)	0.012	-0.071	-0.257	0.011	0.031	-0.212
H(5)	-0.058	0.031	0.319	-0.056	-0.001	0.247
H(6)	-0.038	0.129	0.180	-0.037	-0.078	0.198
O(1,s)	0.006	0.007	-0.010	0.008	0.019	-0.005
O(2,s)	0.002	0.001	-0.027	0.002	0.021	0.007
C(1,s)	0.009	0.070	-0.147	0.006	-0.109	-0.177
C(2,s)	-0.002	0.110	0.045	-0.006	-0.132	0.118
C(3,s)	-0.028	0.021	0.036	-0.027	-0.014	0.036
O(1,x)	0.002	-0.294	0.111	0.001	0.318	0.083
O(2,x)	-0.003	0.292	-0.100	-0.004	-0.318	-0.041
C(1,x)	-0.013	0.348	-0.051	-0.011	-0.410	-0.020
C(2,x)	0.002	-0.335	0.096	0.003	0.404	0.063
C(3,x)	-0.043	0.053	0.192	-0.042	-0.035	0.188
O(1,y)	-0.312	-0.033	-0.200	-0.312	0.167	-0.160
O(2,y)	-0.342	-0.008	-0.013	-0.342	0.006	-0.013
C(1,y)	0.621	0.027	0.038	0.622	-0.019	0.039
C(2,y)	0.667	0.010	0.013	0.667	-0.008	0.013
C(3,y)	0.065	-0.124	-0.387	0.064	0.069	-0.442
O(1,z)	0.007	-0.263	-0.151	0.002	0.186	-0.197
O(2,z)	-0.001	-0.201	0.251	-0.003	0.161	0.258
C(1,z)	-0.022	0.266	0.151	-0.017	-0.267	0.220
C(2,z)	-0.000	0.198	-0.177	0.003	-0.230	-0.235
C(3,z)	-0.058	-0.083	0.143	-0.058	0.067	0.074
	TEE = -615.394 eV			TEE = -614.273 eV		

Table 37

Selected EHMO's for CBD Interaction

Model VIII: CBD & one methane

C_1 symmetry

MO(sym.)	π_S^*(A)	n_S(A)	σ_S(A)	n_A(A)
Energy (ev)	-10.873	-12.849	-13.509	-13.710
C_{ij}'s				
H(1)	-0.136	-0.079	0.049	0.134
H(2)	0.126	-0.088	-0.131	-0.122
H(3)	-0.123	-0.065	0.282	-0.239
H(4)	0.139	-0.072	0.220	0.073
H(5)	-0.025	0.002	0.221	-0.097
H(6)	0.045	0.024	0.035	0.069
H(7)	-0.005	-0.025	-0.218	0.054
H(8)	-0.020	-0.010	-0.190	0.032
O(1,s)	0.001	0.020	-0.004	0.039
O(2,s)	0.002	0.021	-0.014	-0.028
C(1,s)	-0.001	-0.912	-0.011	-0.211
C(2,s)	0.003	-0.083	0.136	0.170
C(3,s)	0.005	0.070	0.030	0.041
C(4,s)	-0.001	0.053	-0.078	-0.017
C(5,s)	-0.013	-0.004	-0.070	0.015
O(1,x)	-0.000	-0.282	0.045	-0.015
O(2,x)	0.001	0.280	-0.059	0.008
C(1,x)	-0.001	0.385	-0.068	-0.018
C(2,x)	-0.002	-0.389	0.028	-0.038
C(3,x)	-0.008	0.017	-0.378	0.156
C(4,x)	0.002	-0.021	0.331	-0.123
C(5,x)	-0.070	0.000	-0.126	0.005
O(1,y)	-0.321	0.001	0.011	-0.002
O(2,y)	-0.312	0.005	0.004	0.013
C(1,y)	0.645	-0.002	-0.013	0.001
C(2,y)	0.633	-0.002	0.031	-0.019
C(3,y)	-0.041	0.016	0.309	-0.093
C(4,y)	-0.054	-0.003	-0.074	0.028
C(5,y)	0.016	0.039	0.281	-0.051
O(1,z)	-0.001	0.175	-0.043	-0.271
O(2,z)	0.002	0.181	0.117	0.227
C(1,z)	0.001	-0.274	0.082	0.308
C(2,z)	-0.007	-0.286	-0.152	-0.272
C(3,z)	0.006	0.308	0.188	0.390
C(4,z)	-0.001	0.294	-0.076	-0.445
C(5,z)	-0.018	-0.013	0.051	-0.072

Table 38

EHMO Coefficients for the n & π^* Orbitals of CBD with Methyl Disubstitution. Models XII & XIII.

	XII		XIII	
TEE = -861.120 eV			TEE = -861.378 eV	
MO(sym)	π^*_S(A'')	n_S(A')	π^*_S(A')	n_S(A)
Energy (eV)	-10.813	-12.698	-10.805	-12.669
C_{ij}'s				
H(1)	0.126	-0.100	-0.125	0.075
H(6)	-0.020	-0.061	0.021	0.062
H(7)	0.014	0.072	-0.029	-0.063
H(8)	0.027	0.049	-0.015	-0.068
O(1,s)	0.001	0.021	-0.001	-0.020
C(1,s)	-0.001	-0.083	0.012	0.079
C(4,s)	-0.006	0.057	-0.003	-0.051
C(6,s)	-0.043	-0.021	0.042	0.022
O(1,x)	-0.009	-0.269	-0.001	0.265
C(1,x)	0.015	0.375	0.003	-0.372
C(4,x)	-0.007	-0.065	-0.011	0.056
C(6,x)	0.054	0.052	0.049	0.047
O(1,y)	0.313	-0.025	0.313	-0.014
C(1,y)	-0.635	0.038	0.634	0.919
C(4,y)	0.074	0.018	-0.075	0.036
C(6,y)	-0.107	-0.055	0.114	0.083
O(1,z)	0.006	0.168	0.009	-0.168
C(1,z)	-0.015	-0.277	-0.019	0.278
C(4,z)	0.023	0.300	0.028	-0.304
C(6,z)	-0.081	-0.088	0.088	0.106

TABLE 39

EHMO Coefficients for the n & π^* Orbitals of CBD with Methyl Disubstitution Models:

	XIV		XV	
TEE = -861.163 eV			TEE = -861.417 eV	
MO(sym)	$\pi^*_S(A'')$	$n_S(A')$	$\pi^*_S(B)$	$n_s(A)$
Energy (eV)	-10.8232	-12.6879	-10.8186	-12.6738
C_{ij}'s				
H(1)	-0.1298	0.0935	-0.129	-0.071
H(6)	-0.0146	-0.0151	0.016	0.022
H(7)	0.0218	0.0539	-0.022	-0.050
H(8)	-0.0267	-0.0967	0.027	0.098
O(1,s)	-0.0012	-0.0204	0.001	0.020
C(1,s)	0.0017	0.0800	-0.009	-0.079
C(4,s)	0.0057	-0.0532	0.004	0.050
C(6,s)	0.0409	0.0195	0.039	-0.023
O(1,x)	0.0077	0.2678	0.000	-0.265
C(1,x)	-0.0131	-0.3749	-0.002	0.372
C(4,x)	0.0102	0.0448	0.011	-0.051
C(6,x)	-0.0582	-0.0369	-0.053	0.045
O(1,y)	0.2137	-0.0230	0.313	0.013
C(1,y)	-0.6344	0.0345	-0.633	-0.018
C(4,y)	0.0761	0.0185	0.077	-0.039
C(6,y)	-0.1185	-0.0568	-0.125	0.084
O(1,z)	-0.0048	-0.1716	-0.007	0.169
C(1,z)	0.0120	0.2806	0.014	-0.278
C(4,z)	-0.0197	-0.3039	-0.024	0.303
C(6,z)	0.0669	0.0961	0.069	-0.105

TABLE 40

EHMO Coefficients for the n & π^* Orbitals of CBD Dimethyl Substitution. Models XVIII & XIX.

	XVIII		XIX	
	TEE = -861.376 eV		TEE = -861.516 eV	
MO(sym)	π^*_S(A'')	n_S(A')	π^*_S(B)	n_S(A)
Energy (eV)	-10.816	-12.709	-10.810	-12.679
C_{ij}'s				
H(1)	-0.124	0.095	0.122	-0.070
H(6)	0.002	-0.025	-0.002	0.025
H(7)	-0.035	-0.086	-0.012	-0.050
H(8)	0.011	0.053	0.038	0.096
O(1,s)	-0.001	-0.020	-0.001	0.020
C(1,s)	0.001	0.081	0.011	-0.079
C(4,s)	0.004	-0.054	-0.004	0.050
C(6,s)	0.043	0.019	0.042	-0.023
O(1,x)	0.009	0.269	-0.001	-0.265
C(1,x)	-0.015	-0.375	0.003	0.371
C(4,x)	0.012	0.050	-0.009	-0.052
C(6,x)	-0.069	-0.043	0.068	-0.051
O(1,y)	0.314	-0.025	-0.313	0.013
C(1,y)	-0.635	0.039	0.634	-0.019
C(4,y)	0.074	0.021	-0.075	-0.043
C(6,y)	-0.102	-0.062	0.103	-0.087
O(1,z)	-0.006	-0.172	0.009	0.170
C(1,z)	0.015	0.279	-0.018	-0.278
C(4,z)	-0.020	-0.302	0.028	0.303
C(6,z)	0.080	0.081	0.085	-0.103

TABLE 41

EHMO Coefficients for the n & π^* orbitals of CBD with Methyl Disubstitution.

Models(TEE)	XX(-861.376 eV)		XXI(-861.465 eV)	
MO(sym)	$\pi_S^*(A)$	$n_S(A)$	$\pi_S^*(A)$	$n_S(A)$
Energy (ev)	-10.819	-12.695	-10.814	-12.676
C_{ij}'s				
H(1)	-0.130	-0.098	-0.130	0.072
H(2)	-0.124	-0.090	0.123	0.069
H(3)	-0.015	0.014	-0.016	-0.023
H(4)	-0.026	0.097	-0.028	-0.100
H(5)	0.021	-0.052	0.023	0.051
H(6)	0.002	0.022	-0.002	-0.024
H(7)	-0.036	0.089	0.038	-0.094
H(8)	0.013	-0.054	-0.012	0.049
O(1,s)	-0.002	0.020	0.001	-0.020
O(2,s)	-0.001	0.021	-0.001	-0.021
C(1,s)	0.002	-0.076	-0.011	0.076
C(2,s)	0.000	-0.084	0.011	0.083
C(3,s)	0.001	0.053	-0.004	-0.051
C(4,s)	0.005	0.054	0.005	-0.051
C(5,s)	0.043	-0.018	0.040	0.025
C(6,s)	0.040	-0.020	-0.043	0.023
O(1,x)	0.008	-0.268	-0.001	0.265
O(2,x)	-0.009	0.269	0.002	-0.266
C(1,x)	-0.014	0.375	-0.001	-0.372
C(2,x)	0.015	-0.374	-0.004	0.371
C(3,x)	-0.010	0.044	0.012	-0.051
C(4,x)	0.012	-0.046	0.009	0.053
C(5,x)	0.069	-0.038	-0.054	-0.048
C(6,x)	-0.056	0.039	-0.068	0.048
O(1,y)	0.314	0.024	0.314	-0.012
O(2,y)	0.314	0.025	0.313	0.014
C(1,y)	-0.635	-0.037	-0.635	0.017
C(2,y)	-0.634	-0.038	-0.634	-0.021
C(3,y)	0.075	-0.021	0.076	-0.042
C(4,y)	0.076	-0.019	0.077	0.041
C(5,y)	-0.102	0.061	-0.125	-0.088
C(6,y)	-0.121	0.058	-0.104	0.084
O(1,z)	-0.005	0.176	-0.007	-0.173
O(2,z)	-0.007	0.169	0.010	-0.167
C(1,z)	0.012	-0.286	0.015	0.284
C(2,z)	0.016	-0.275	-0.019	0.273
C(3,z)	-0.023	0.297	0.027	-0.297
C(4,z)	-0.019	0.311	-0.026	-0.311
C(5,z)	0.083	-0.087	0.069	0.109
C(6,z)	0.067	-0.097	-0.086	0.101

TABLE 42

EHMO Coefficients for the n & π^* Orbitals of CBD with Ethyl Mono-Substitution Models XXIV, XXV & XXVI

	XXIV		XXV		XXVI	
	TEE = -860.727 eV		TEE = -861.221 eV		TEE = -861.418 eV	
MO(sym)	π^*_S(A)	n_S(A)	π^*_S(A)	n_S(A)	π^*_S(A)	n_S(A)
Energy (eV)	-10.824	-12.712	-10.830	-12.693	-10.856	-12.634
H(1)	-0.113	0.045	0.133	-0.037	0.128	-0.013
H(2)	0.125	0.116	-0.129	-0.094	-0.129	-0.065
H(3)	0.138	0.057	-0.132	-0.064	-0.126	-0.112
H(4)	0.013	-0.002	-0.028	0.032	-0.023	0.049
H(5)	-0.014	-0.011	0.052	-0.081	0.017	-0.071
H(6)	-0.021	-0.031	-0.011	-0.002	0.027	-0.067
H(7)	0.023	-0.088	0.019	-0.081	-0.001	-0.026
H(8)	0.001	-0.096	-0.023	0.086	0.013	-0.020
O(1,s)	0.001	-0.024	-0.001	0.024	-0.002	0.027
C(2,s)	0.003	-0.009	0.000	0.012	0.000	0.009
C(1,s)	0.005	0.117	0.007	-0.117	0.007	-0.127
C(2,s)	0.008	0.037	-0.006	-0.032	0.007	0.040
C(3,s)	0.001	-0.056	0.008	0.044	-0.000	0.045
C(4,s)	-0.003	-0.049	0.004	0.045	-0.005	-0.012
C(5,s)	0.039	0.034	0.041	-0.017	0.039	-0.014
C(6,s)	-0.022	0.026	-0.016	0.028	-0.011	0.047
O(1,x)	-0.0039	0.261	0.006	-0.254	0.005	-0.240
O(2,x)	0.003	-0.264	-0.007	0.255	-0.006	0.242
C(1,x)	0.004	-0.356	-0.010	0.347	-0.008	0.326
C(2,x)	-0.011	0.371	0.013	-0.366	-0.015	0.066
C(3,x)	-0.002	-0.037	-0.010	0.046	0.002	-0.030
C(4,x)	-0.007	0.020	-0.001	-0.021	0.011	-0.352
C(5,x)	-0.045	0.033	0.052	-0.033	0.076	-0.068
C(6,x)	-0.030	0.035	-0.005	-0.041	-0.004	0.031
O(1,y)	-0.324	-0.009	0.319	0.019	0.320	0.015
O(2,y)	-0.298	-0.012	0.307	0.041	0.309	0.041
C(1,y)	0.654	0.014	-0.644	-0.031	-0.644	-0.025
C(2,y)	0.620	0.031	-0.622	-0.062	0.083	-0.077
C(3,y)	-0.061	0.022	0.087	-0.067	0.052	0.016
C(4,y)	-0.055	-0.001	0.061	-0.000	-0.623	-0.063
C(5,y)	0.110	-0.047	-0.123	0.124	-0.120	0.120
C(6,y)	0.042	-0.07-	0.024	-0.091	0.003	-0.054
O(1,z)	-0.001	-0.127	-0.000	0.121	0.001	0.096
O(2,z)	0.006	-0.213	-0.010	0.210	-0.009	0.217
C(1,z)	0.002	0.210	0.001	-0.201	-0.001	-0.168
C(2,z)	-0.021	0.336	0.023	-0.333	-0.030	0.406
C(3,z)	0.080	-0.377	-0.035	0.390	0.003	0.154
C(4,z)	-0.001	-0.210	-0.003	0.203	0.020	-0.347
C(5,z)	-0.080	0.170	0.095	-0.158	0.081	-0.207
C(6,z)	-0.056	-0.107	-0.033	0.085	-0.048	0.206

TABLE 43

EHMO Coefficients for the n & π* Orbitals of CBD with Mono t-butyl Substitution (0° rotation)

Models XXIX, XXX, & XXXI

	XXIX		XXX		XXXI	
	TEE = -1070.346 eV		TEE = -1070.610 eV		TEE = -1070.665 eV	
MO(sym)	π^*_S(A)	n_S(A)	π^*_S(A)	n_S(A)	π^*_S(A)	n_S(A)
Energy (eV)	-10.646	-12.484	-10.719	-12.530	-10.769	-12.558
C_{ij}'s						
H(1)	0.150	-0.035	-0.153	-0.061	-0.155	-0.088
H(2)	-0.142	-0.079	0.136	-0.081	0.130	-0.084
H(3)	-0.092	-0.128	0.103	-0.126	0.115	-0.122
H(4)	0.043	0.085	-0.028	0.071	-0.015	0.059
H(5)	-0.022	-0.037	0.013	-0.036	0.005	-0.035
H(6)	0.004	-0.001	-0.006	0.002	-0.009	0.005
H(7)	0.014	-0.033	-0.015	-0.038	-0.015	-0.041
H(8)	-0.019	0.041	0.018	0.039	0.018	0.035
H(9)	0.022	-0.086	-0.019	-0.077	-0.017	-0.066
H(10)	0.015	-0.013	-0.016	-0.016	-0.017	-0.018
H(11)	0.046	-0.090	-0.046	-0.092	-0.047	-0.094
H(12)	-0.052	0.061	0.057	0.080	0.060	0.100
O(1,s)	-0.003	0.028	0.002	0.026	0.001	0.023
O(2,s)	-0.008	0.002	0.005	0.008	0.003	0.012
C(1,s)	0.006	-0.123	-0.002	-0.111	0.001	-0.097
C(2,s)	-0.012	-0.019	0.004	-0.036	-0.002	-0.053
C(3,s)	0.002	0.019	-0.004	0.023	-0.006	0.026
C(4,s)	0.009	0.046	-0.009	0.047	-0.007	0.046
C(5,s)	0.038	-0.019	-0.036	-0.016	-0.034	-0.012
C(6,s)	0.034	-0.015	-0.026	-0.013	-0.018	-0.010
C(7,s)	-0.006	0.049	0.004	0.048	0.002	0.047
C(8,s)	-0.026	0.036	0.026	-0.036	0.026	0.037
O(1,x)	0.010	-0.224	-0.009	-0.234	-0.009	-0.240
O(2,x)	-0.013	0.225	0.012	0.235	0.009	0.241
C(1,x)	-0.012	0.311	0.014	0.325	0.015	0.337
C(2,x)	0.026	-0.327	-0.021	-0.338	-0.016	-0.345
C(3,x)	0.001	0.131	0.000	0.123	0.001	0.111
C(4,x)	0.015	-0.105	-0.019	-0.110	-0.023	-0.111
C(5,x)	0.037	-0.100	-0.037	-0.101	-0.037	-0.099
C(6,x)	0.035	0.005	-0.024	0.004	-0.013	0.005
C(7,x)	-0.028	0.143	0.024	0.141	0.019	0.136
C(8,x)	-0.057	-0.018	-0.061	-0.014	0.064	0.050
O(1,y)	0.324	0.033	-0.317	0.034	-0.312	0.037
O(2,y)	0.274	0.028	-0.293	0.031	-0.303	0.031
C(1,y)	-0.666	-0.056	0.648	-0.057	0.635	-0.060
C(2,y)	-0.600	-0.088	0.615	-0.074	0.624	-0.063

TABLE 43 (continued)

EHMO Coefficients for the n & π* Orbitals of CBD with Mono t-butyl Substitutiin (9°, rotation)

Models XXIX, XXX, & XXXI

	XXIX		XXX		XXXI	
	TEE = -1070.346 eV		TEE = -1070.610 eV		TEE = -1070.665 eV	
MO(sym)	π^*_S(A)	n_S(A)	π^*_S(A)	n_S(A)	π^*_S(A)	n_S(A)
Energy (eV)	-10.646	-12.484	-10.719	-12.530	-10.769	-12.558
C_{ij}'s						
C(3,y)	0.065	-0.128	-0.064	-0.105	-0.066	-0.082
C(4,y)	0.086	-0.015	-0.088	-0.032	-0.090	-0.050
C(5,y)	-0.114	0.144	0.119	0.117	0.122	0.092
C(6,y)	-0.088	0.022	0.060	0.030	0.034	0.030
C(7,y)	-0.002	-0.033	0.005	-0.022	0.007	-0.011
C(8,y)	0.066	-0.095	-0.066	-0.099	-0.065	-0.105
C(1,z)	-0.001	0.083	0.005	0.104	0.008	0.125
O(2,z)	-0.014	0.194	0.010	0.186	0.005	0.175
C(1,z)	0.007	-0.159	-0.013	-0.189	-0.018	-0.219
C(2,z)	0.042	-0.320	-0.029	-0.305	-0.015	-0.286
C(3,z)	-0.066	0.380	0.045	0.358	0.027	0.331
C(4,z)	-0.014	0.140	0.020	0.181	0.025	0.223
C(5,z)	0.091	-0.231	-0.089	-0.221	-0.090	-0.204
C(6,z)	0.085	0.140	-0.090	0.106	-0.088	0.076
C(7,z)	-0.009	0.120	0.006	0.119	0.003	0.115
C(8,z)	-0.009	0.087	0.015	0.084	0.022	0.085

TABLE 44

EHMO Coefficients for the n & π^* Orbitals of CBD with Mono-t-butyl Substitution

Models XXXII, XXXIV, XXXV

	XXXII		XXXIV		XXXV	
	TEE = -1070.665 eV		TEE = -1071.271 eV		TEE = -1070.243 eV	
MO(sym)	π_S^*(A)	n_S(A)	π_S^*(A)	n_S(A)	π_S^*(A)	n_S(A)
Energy (eV)	-10.731	-12.492	-10.808	-12.595	-10.779	-12.463
C_{ij}'s						
H(1)	0.139	0.009	-0.143	-0.053	-0.130	-0.005
H(2)	-0.141	0.060	0.133	-0.059	0.137	0.051
H(3)	-0.111	0.122	0.133	-0.122	0.133	0.109
H(4)	0.031	-0.079	-0.009	0.057	-0.017	-0.085
H(5)	-0.018	0.016	0.002	-0.017	0.013	0.007
H(6)	0.010	0.003	-0.014	0.005	-0.019	0.011
H(7)	0.012	0.021	-0.013	-0.031	-0.009	0.015
H(8)	-0.017	-0.044	0.015	0.042	0.013	-0.046
H(9)	0.023	0.094	-0.016	-0.083	-0.022	0.099
H(10)	0.019	0.012	-0.023	-0.015	-0.021	0.009
H(11)	0.038	0.090	-0.036	-0.088	-0.035	0.093
H(12)	-0.040	-0.038	0.046	0.060	0.035	-0.030
O(1,s)	-0.002	-0.028	0.001	0.025	0.002	-0.027
O(2,s)	-0.007	0.002	0.001	0.007	0.004	0.009
C(1,s)	0.010	0.130	-0.001	-0.115	-0.011	0.133
C(2,s)	-0.015	-0.001	0.001	-0.027	0.016	-0.012
C(3,s)	0.004	-0.021	-0.007	0.031	-0.008	-0.017
C(4,s)	0.008	-0.037	-0.007	0.043	-0.010	-0.030
C(5,s)	0.039	0.019	-0.036	-0.014	-0.041	0.020
C(6,s)	0.026	0.026	-0.012	-0.023	-0.015	0.027
C(7,s)	-0.004	-0.045	-0.001	0.045	0.001	-0.044
C(8,s)	-0.021	-0.039	0.021	0.036	0.020	-0.043
O(1,x)	0.009	0.216	-0.005	-0.238	-0.009	0.207
O(2,x)	-0.009	-0.224	0.005	0.241	0.006	-0.227
C(1,x)	-0.013	-0.297	0.009	0.328	0.013	-0.285
C(2,x)	0.026	0.319	-0.011	-0.345	-0.024	0.305
C(3,x)	-0.001	-0.095	0.001	0.081	0.003	-0.079
C(4,x)	-0.005	0.051	-0.002	-0.058	0.022	0.020
C(5,x)	0.058	0.086	-0.057	-0.081	-0.078	0.088
C(6,x)	0.039	0.021	-0.013	-0.026	-0.031	0.035
C(7,x)	-0.025	-0.130	0.013	0.126	0.016	-0.124
C(8,x)	-0.038	0.049	0.048	-0.006	0.023	0.049
O(1,y)	0.325	-0.029	-0.316	0.022	-0.323	-0.029

TABLE 44 (continued)

EHMO Coefficients for the n & π^* Orbitals of CBD with Mono-t-butyl Substitution

Models XXXII, XXXIV, XXXV

	XXXII		XXXIV		XXXV	
	TEE = -1070.665 eV		TEE = -1071.271 eV		TEE = -1070.243 eV	
MO(sym)	π^*_S(A)	n_S(A)	π^*_S(A)	n_S(A)	π^*_S(A)	n_S(A)
Energy (eV)	-10.731	-12.492	-10.808	-12.595	-10.779	-12.463
C_{ij}'s						
O(2,y)	0.280	-0.027	-0.304	0.022	-0.288	-0.021
C(1,y)	-0.662	0.049	0.640	-0.036	0.655	0.048
C(2,y)	-0.606	0.094	0.623	-0.050	0.609	0.104
C(3,y)	0.076	0.110	-0.077	-0.059	-0.095	0.107
C(4,y)	0.069	-0.003	-0.073	-0.019	-0.060	-0.011
C(5,y)	-0.115	-0.121	0.120	0.068	0.116	-0.107
C(6,y)	-0.062	-0.045	0.022	0.062	0.032	-0.039
C(7,y)	-0.012	0.016	0.017	0.001	0.024	-0.002
C(8,y)	0.047	0.103	-0.045	-0.087	-0.040	0.119
C(1,z)	0.001	-0.071	0.004	0.106	-0.000	-0.062
O(2,z)	-0.015	-0.211	0.004	0.202	0.015	-0.217
C(1,z)	0.001	0.135	-0.008	-0.186	0.001	0.119
C(2,z)	0.043	0.343	-0.013	-0.323	-0.041	0.349
C(3,z)	-0.066	-0.410	0.026	0.375	0.063	-0.420
C(4,z)	-0.006	-0.113	0.015	0.180	0.005	-0.097
C(5,z)	0.090	0.259	-0.088	-0.242	-0.090	0.276
C(6,z)	0.054	-0.160	-0.066	0.095	-0.019	-0.185
C(7,z)	-0.012	-0.117	0.001	0.122	0.012	-0.116
C(8,z)	-0.015	-0.109	0.021	0.100	0.022	-0.122

TABLE 45

EHMO Coefficients for the n & π^* orbitals for CBD with mono t-butyl Substitution

Models XXXVI, XXXVII & XXXVIII

	XXXVI		XXXVII		XXXVIII	
	TEE = -1070.969 eV		TEE = -1071.295 eV		TEE = -1072.533 eV	
MO(sym)	π^*_S(A)	n_S(A)	π^*_S(A)	n_S(A)	π^*_S(A)	n_S(A)
Energy (eV)	-10.806	-12.537	-10.820	-12.594	-10.801	-12.579
C_{ij}'s						
H(1)	0.132	-0.014	0.133	0.035	-0.133	-0.021
H(2)	-0.134	-0.047	-0.131	0.044	0.134	-0.053
H(3)	-0.144	-0.112	-0.154	0.115	0.126	-0.125
H(4)	0.008	0.068	0.001	-0.058	0.002	-0.020
H(5)	-0.005	-0.005	0.000	0.006	-0.028	0.051
H(6)	0.019	-0.002	0.020	-0.004	-0.002	0.029
H(7)	0.009	-0.020	0.009	0.025	0.012	0.042
H(8)	-0.012	0.046	-0.010	-0.033	-0.028	-0.085
H(9)	0.018	-0.096	0.014	0.092	-0.002	-0.032
H(10)	0.024	-0.011	0.027	0.011	0.028	0.051
H(11)	0.032	-0.091	0.030	0.088	0.009	-0.033
H(12)	-0.037	0.036	-0.039	-0.043	-0.051	-0.075
O(1,s)	-0.001	0.026	0.000	-0.025	0.001	0.027
O(2,s)	-0.001	-0.001	-0.000	-0.004	0.001	0.006
C(1,s)	0.006	-0.128	0.001	0.121	-0.007	-0.127
C(2,s)	-0.009	0.001	-0.002	0.011	0.007	-0.006
C(3,s)	0.008	0.025	0.009	-0.031	-0.008	0.035
C(4,s)	0.009	0.034	0.008	-0.037	-0.004	0.041
C(5,s)	0.039	-0.017	0.038	0.015	-0.038	-0.017
C(6,s)	0.011	-0.030	0.029	0.029	-0.013	-0.029
C(7,s)	0.002	0.044	0.005	-0.045	0.002	0.040
C(8,s)	-0.019	0.040	-0.019	-0.036	0.019	0.031
O(1,x)	0.006	-0.220	0.003	0.231	-0.006	-0.227
O(2,x)	-0.004	0.231	-0.002	-0.238	0.007	0.231
C(1,x)	-0.009	0.302	-0.006	-0.317	0.009	0.309
C(2,x)	0.014	-0.324	0.006	0.338	-0.014	-0.335
C(3,x)	-0.001	0.069	-0.001	-0.060	0.009	0.076
C(4,x)	-0.019	-0.020	-0.015	0.022	0.002	-0.046
C(5,x)	0.076	-0.079	0.074	0.072	-0.051	-0.074
C(6,x)	0.020	-0.048	0.009	0.053	-0.044	-0.030
C(7,x)	-0.007	0.122	0.000	-0.120	0.012	0.133
C(8,x)	-0.028	-0.039	-0.032	0.025	0.000	-0.053
O(1,y)	0.320	0.021	0.318	-0.016	-0.321	0.021

TABLE 45 (continued)

EHMO Coefficients for the n & π^* Orbitals for CBD with mono t-butyl Substitution

Models XXXVII & XXXVIII

	XXXVI		XXXVII		XXXVIII	
	TEE = -1070.969 eV		TEE = -1071.295 eV		TEE = -1072.533 eV	
MO(sym)	π_S^*(A)	n_S(A)	π_S^*(A)	n_S(A)	π_S^*(A)	n_S(A)
Energy (eV)	-10.806	-12.537	-10.820	-12.594	-10.801	-12.579
C_{ij}'s						
O(2,y)	0.298	0.022	0.304	-0.015	-0.302	0.039
C(1,y)	-0.648	-0.035	-0.642	0.026	0.649	-0.035
C(2,y)	-0.616	-0.070	-0.619	0.043	0.617	-0.070
C(3,y)	0.093	-0.076	0.096	0.045	-0.085	-0.074
C(4,y)	0.061	0.002	0.062	0.007	-0.061	-0.000
C(5,y)	-0.117	0.080	-0.119	-0.051	0.124	0.075
C(6,y)	-0.021	0.060	-0.009	-0.069	-0.006	0.079
C(7,y)	-0.025	0.009	-0.026	-0.018	0.000	0.016
C(8,y)	0.037	-0.105	0.036	0.090	-0.027	-0.081
O(1,z)	-0.001	0.078	-0.003	-0.095	-0.001	0.083
O(2,z)	-0.010	0.217	-0.004	-0.213	0.011	0.210
C(1,z)	0.001	-0.142	0.003	0.166	-0.003	-0.151
C(2,z)	0.025	-0.345	0.009	0.337	-0.025	-0.338
C(3,z)	0.041	0.411	-0.023	-0.394	0.040	0.400
C(4,z)	0.008	0.127	-0.011	-0.158	0.002	0.135
C(5,z)	0.086	-0.273	0.086	0.264	-0.097	-0.262
C(6,z)	0.035	0.144	0.043	-0.112	-0.012	0.139
C(7,z)	0.004	0.121	0.003	-0.126	0.014	0.121
C(8,z)	0.022	0.116	-0.024	-0.109	0.039	0.103

TABLE 46

EHMO Coefficients for the n & π* Orbitals of CBD with mono t-butyl Substitution

Models XLII, XLIII, & XLIV

	XLII		XLIII		XLIV	
	TEE = -1072.334 eV		TEE = -1072.974 eV		TEE = -1072.889 eV	
MO(sym)	π_S^*(A)	n_S(A)	π_S^*(A)	n_A(A)	π_S^*(A)	n_A(A)
Energy (eV)	-10.837	-12.575	-10.820	-12.600	-10.813	-12.600
C_{ij}'s						
H(1)	0.128	-0.014	-0.129	0.013	-0.130	0.017
H(2)	-0.129	-0.060	0.130	0.065	0.1309	0.064
H(3)	-0.122	-0.110	0.123	0.109	0.122	0.114
H(4)	-0.021	0.049	-0.028	0.058	-0.028	0.065
H(5)	0.018	-0.065	0.013	-0.055	0.014	-0.051
H(6)	0.015	0.005	-0.000	0.016	-0.001	0.021
H(7)	0.024	-0.081	0.017	-0.014	0.020	-0.025
H(8)	-0.025	0.032	-0.042	0.095	-0.044	0.091
H(9)	0.020	-0.057	0.004	0.020	0.003	0.025
H(10)	0.019	0.005	-0.005	-0.017	-0.015	-0.029
H(11)	-0.007	-0.049	-0.024	-0.065	-0.023	-0.057
H(12)	0.006	0.076	-0.000	0.040	0.005	0.035
O(1,s)	-0.001	0.027	0.001	-0.027	0.002	-0.027
O(2,s)	-0.000	0.006	0.000	-0.006	0.001	-0.006
C(1,s)	0.005	-0.129	-0.007	0.125	-0.007	0.124
C(2,s)	-0.006	-0.006	0.006	0.010	0.007	0.011
C(3,s)	0.003	0.028	-0.007	-0.033	-0.007	-0.034
C(4,s)	-0.001	0.042	0.000	-0.043	-0.001	-0.044
C(5,s)	0.036	-0.019	-0.037	0.018	-0.038	0.017
C(6,s)	0.004	0.004	0.001	-0.008	0.001	-0.017
C(7,s)	-0.009	0.060	0.013	-0.053	0.015	-0.048
C(8,s)	0.016	-0.012	-0.011	0.019	-0.013	0.023
O(1,x)	0.004	-0.225	-0.005	0.230	-0.006	0.230
O(2,x)	-0.006	0.229	0.007	-0.234	0.007	-0.234
C(1,x)	-0.005	0.307	0.007	-0.313	0.008	-0.314
C(2,x)	0.009	-0.335	-0.011	0.338	-0.013	0.339
C(3,x)	-0.010	0.087	0.014	-0.077	0.012	-0.078
C(4,x)	0.001	-0.046	-0.004	0.040	-0.002	0.445
C(5,x)	0.066	-0.090	-0.078	0.073	-0.073	0.079
C(6,x)	0.018	0.023	0.008	-0.038	0.009	-0.975
C(7,x)	0.003	0.000	0.012	0.035	0.012	0.050
C(8,x)	0.060	0.052	0.009	-0.031	-0.003	-0.026
O(1,y)	0.320	0.009	-0.322	-0.016	-0.322	-0.018

TABLE 46(continued)

EHMO Coefficients for the n & π^* Orbitals of CBD with mono tu-butyl Substitution

Models XLII, XLIII, & XLIV

	XLII		XLIII		XLIV	
	Tee = -1072.334 eV		TEE = -1072.974 eV		TEE = -1072.889 eV	
MO(sym)	$\pi_S^*(A)$	$n_S(A)$	$\pi_S^*(A)$	$n_A(A)$	$\pi_S^*(A)$	$n_A(A)$
Energy (eV)	-10.837	-12.575	-10.820	-12.600	-10.813	-12.600
C_{ij}'s						
O(2,y)	0.308	0.038	-0.305	-0.038	-0.303	-0.039
C(1,y)	-0.645	-0.017	0.650	0.027	0.651	0.031
C(2,y)	-0.622	-0.061	0.619	0.066	0.619	0.069
C(3,y)	0.071	-0.105	-0.084	0.096	-0.083	0.091
C(4,y)	0.050	0.011	-0.053	-0.013	-0.055	-0.009
C(5,y)	-0.119	0.113	0.116	-0.101	0.115	-0.094
C(6,y)	0.005	-0.011	-0.002	0.016	-0.001	0.009
C(7,y)	0.011	-0.052	-0.010	0.058	-0.012	0.071
C(8,y)	-0.017	0.038	0.005	-0.062	0.009	-0.076
O(1,z)	0.001	0.080	-0.001	-0.088	-0.001	-0.089
O(2,z)	-0.009	0.211	0.009	-0.211	0.010	-0.210
C(1,z)	-0.000	-0.146	0.001	0.158	-0.000	0.159
C(2,z)	0.019	-0.336	-0.021	0.335	-0.023	0.335
C(3,z)	-0.026	0.399	0.034	-0.394	0.037	-0.394
C(4,z)	0.003	0.125	-0.003	-0.141	-0.001	-0.143
C(5,z)	0.075	-0.259	-0.084	0.252	-0.092	0.250
C(6,z)	-0.004	0.031	0.008	-0.026	0.010	-0.034
C(7,z)	-0.033	0.245	0.038	-0.230	0.042	-0.200
C(8,z)	0.062	0.081	-0.041	-0.086	-0.027	-0.102

TABLE 47

EHMO Coefficients for the n & π* Orbitals of CBD with mono t-butyl Substitution

Models XLV, XLVI, & XLVIII

	XLV		XLVI		XLVIII	
	TEE = -1072.748 eV		TEE = -1071.195 eV		TEE = -1072.200 eV	
MO(sym)	π^*_S(A)	n_S(A)	π^*_S(A)	n_S(A)	π^*_S(A)	n_S(A)
Energy (eV)	-10.807	-12.594	-10.822	-12.556	-10.789	-12.556
C_{ij}'s						
H(1)	-0.132	-0.020	-0.137	0.023	-0.132	0.019
H(2)	0.132	-0.061	0.134	0.050	0.135	0.066
H(3)	0.122	-0.119	0.130	0.125	0.117	0.106
H(4)	-0.028	-0.072	0.008	-0.062	0.018	-0.047
H(5)	0.014	0.047	-0.022	-0.011	-0.019	0.080
H(6)	-0.002	-0.025	-0.004	0.032	-0.011	0.006
H(7)	0.024	0.036	-0.020	0.089	-0.018	0.039
H(8)	-0.046	-0.086	0.018	-0.034	0.030	-0.036
H(9)	0.003	-0.030	-0.018	0.043	-0.028	0.090
H(10)	-0.023	0.040	-0.032	-0.008	-0.003	0.005
H(11)	-0.019	0.046	-0.021	0.077	0.007	0.029
H(12)	0.008	-0.029	0.038	-0.050	-0.023	-0.081
O(1,s)	0.001	0.027	0.001	-0.027	0.001	-0.027
O(2,s)	0.001	0.006	-0.001	-0.001	0.001	-0.006
C(1,s)	-0.007	-0.125	-0.008	0.128	-0.004	0.126
C(2,s)	0.007	-0.011	0.004	0.004	0.008	0.011
C(3,s)	-0.007	0.034	-0.012	-0.030	-0.001	-0.026
C(4,s)	-0.002	0.043	-0.006	-0.036	-0.001	-0.045
C(5,s)	-0.038	-0.017	-0.038	0.017	-0.036	0.019
C(6,s)	0.002	0.026	-0.001	0.020	-0.004	-0.023
C(7,s)	0.018	0.043	0.009	-0.059	0.010	-0.054
C(8,s)	-0.013	-0.026	0.018	-0.015	-0.027	0.018
O(1,x)	-0.006	-0.230	-0.006	0.223	-0.003	0.227
O(2,x)	0.007	0.234	0.009	-0.241	0.006	-0.227
C(1,x)	0.009	0.314	0.011	-0.305	0.003	-0.312
C(2,x)	-0.014	-0.338	-0.014	0.329	-0.009	0.335
C(3,x)	0.011	0.078	0.016	-0.081	-0.000	-0.093
C(4,x)	-0.000	-0.047	-0.006	0.045	0.003	0.053
C(5,x)	-0.065	-0.082	-0.064	0.061	-0.059	0.096
C(6,x)	0.010	0.106	-0.009	0.064	-0.011	-0.083
C(7,x)	0.011	-0.057	0.019	-0.103	0.001	0.038
C(8,x)	-0.019	0.014	0.035	0.002	-0.067	-0.038
O(1,y)	-0.321	0.020	-0.316	-0.025	-0.322	-0.010
O(2,y)	-0.303	0.040	-0.308	-0.036	-0.301	-0.029

TABLE 47 (continued)

EHMO Coefficients for the n & π* Orbitals of CBD with mono t-butyl Substitution

Models XLV, XLVI, & XLVII

	XLV		XLVI		XLVII	
	TEE = -1072.748 eV		TEE = -1071.195 eV		TEE = -1072.200 eV	
MO(sym)	π^*_S(A)	n_S(A)	π^*_S(A)	n_S(A)	π^*_S(A)	n_S(A)
Energy (eV)	-10.807	-12.594	-10.822	-12.556	-10.789	-12.556
C_{ij}'s						
C(1,y)	0.650	-0.033	-.639	0.042	0.653	0.017
C(2,y)	0.619	-0.071	0.620	0.078	0.616	0.052
C(3,y)	-0.083	-0.084	-0.094	0.079	-0.059	0.108
C(4,y)	-0.057	0.005	-0.070	0.007	-0.053	-0.010
C(5,y)	0.116	0.084	0.134	-0.095	0.108	-0.113
C(6,y)	-0.001	0.000	0.001	-0.012	-0.001	0.012
C(7,y)	-0.016	-0.079	0.016	0.006	-0.022	0.081
C(8,y)	0.006	0.086	-0.037	0.048	0.04]	-0.057
O(1,z)	-0.001	0.088	-0.000	-0.079	-0.001	-0.085
O(2,z)	0.011	0.209	0.010	-0.217	0.009	-0.205
C(1,z)	-0.001	-0.159	-0.001	0.145	0.000	0.155
C(2,z)	-0.025	-0.335	-0.021	0.340	-0.024	0.330
C(3,z)	0.039	0.395	0.037	-0.402	0.032	-0.391
C(4,z)	0.000	0.143	0.006	-0.132	-0.001	-0.134
C(5,z)	-0.098	-0.251	-0.086	0.263	-0.077	0.259
C(6,z)	0.012	0.054	0.011	-0.109	-0.004	-0.049
C(7,z)	0.046	0.167	0.043	-0.213	0.021	-0.201
C(8,z)	-0.015	0.118	0.020	-0.047	-0.098	-0.120

TABLE 48

Selected EHMO's for CBD with Mono t-Butyl Substitution, eclipsed hydrogens (60° rotation)

Model XLVII (C_1 Symmetry)

TEE = -1072.252 eV

MO(sym)	π_S^*(A)	n_S(A)	σ_S(A)	n_A(A)	σ_A(A)
Energy (eV)	-10.853	-12.581	-13.353	-13.353	-14.038
C_{ij}'s					
H(1)	-0.128	-0.056	0.086	0.138	0.059
H(2)	0.128	-0.014	-0.010	0.146	-0.098
H(3)	-0.126	-0.114	0.036	-0.056	-0.194
H(4)	-0.024	0.031	-0.103	-0.071	-0.122
H(5)	0.021	-0.068	-0.034	-0.066	0.139
H(6)	0.022	-0.073	0.104	-0.038	-0.064
H(7)	0.025	0.010	0.102	0.073	0.091
H(8)	-0.005	0.068	-0.112	0.048	0.066
H(9)	-0.003	-0.058	-0.027	-0.076	0.121
H(10)	0.017	0.009	0.103	0.069	0.127
H(11)	0.016	-0.056	0.106	-0.054	-0.061
H(12)	-0.021	0.051	0.005	0.067	-0.141
O(1,s)	-0.001	0.027	-0.018	0.010	0.002
O(2,s)	0.000	0.005	-0.004	-0.037	0.011
C(1,s)	0.006	-0.130	0.061	-0.073	0.005
C(2,s)	-0.005	-0.003	0.005	0.202	-0.024
C(3,s)	0.006	0.030	0.020	-0.029	0.059
C(4,s)	-0.001	0.040	-0.046	-0.076	0.018
C(5,s)	0.037	-0.018	0.007	-0.002	0.001
C(6,s)	-0.009	0.062	0.012	0.060	0.015
C(7,s)	0.008	-0.007	0.011	-0.018	-0.091
C(8,s)	0.003	-0.004	-0.084	-0.030	0.024
O(1,x)	0.004	-0.225	-0.024	0.155	-0.025
O(2,x)	-0.006	0.231	0.025	-0.150	0.020
C(1,x)	-0.006	0.306	0.044	-0.225	0.030
C(2,x)	0.009	-0.334	-0.037	0.174	-0.033
C(3,x)	-0.014	0.083	-0.345	-0.046	-0.019
C(4,x)	0.002	-0.042	0.336	0.082	-0.051
C(5,x)	0.068	-0.080	0.421	0.047	-0.165
C(6,x)	0.001	0.026	-0.077	-0.023	0.030
C(7,x)	0.045	0.043	-0.113	0.024	0.229
C(8,x)	0.017	-0.011	-0.389	-0.119	0.130
O(1,y)	0.320	0.012	0.000	0.004	-0.012
O(2,y)	0.309	0.041	-0.032	0.020	-0.066
C(1,y)	-0.644	-0.021	0.001	-0.007	0.019
C(2,y)	-0.622	-0.065	0.050	-0.029	0.092

TABLE 48 (continued)

Selected EHMO's for CBD with Mono t-Butyl Substitution, eclipsed hydrogens (60° rotation)

Model XLVII (C_1 Symmetry)

TEE = -1072.252 eV

MO(sym)	π^*_S(A)	n_S(A)	σ_S(A)	n_A(A)	σ_A(A)
Energy (eV)	-10.853	-12.581	-13.269	-13.353	-14.038
C_{ij}'s					
C(3,y)	0.078	-0.098	0.189	-0.033	0.285
C(4,y)	0.050	0.008	-0.031	0.000	-0.067
C(5,y)	-0.126	0.114	-0.147	-0.014	-0.483
C(6,y)	0.005	-0.037	0.027	0.022	0.112
C(7,y)	-0.004	0.021	-0.016	0.059	0.397
C(8,y)	0.004	-0.009	0.042	0.002	0.114
O(1,z)	0.001	0.078	0.117	-0.241	0.024
O(2,z)	-0.009	0.214	0.045	0.089	-0.011
C(1,z)	-0.001	-0.143	-0.126	0.329	-0.040
C(2,z)	0.018	-0.340	-0.045	-0.097	-0.002
C(3,z)	-0.026	0.403	0.007	0.167	-0.060
C(4,z)	0.004	0.124	0.205	-0.409	0.039
C(5,z)	0.075	-0.259	-0.041	-0.314	-0.065
C(6,z)	-0.039	0.253	0.061	0.308	0.079
C(7,z)	0.038	0.059	-0.020	0.091	0.136
C(8,z)	-0.008	0.039	0.104	0.101	-0.024

TABLE 49

EHMO Coefficients for the n & π^* Orbitals of CBD with di t-butyl Substitution (C_2 Symmetry)

Models XLIX, L, LII

	XLIX		L		LII	
MO(sym)	π_S^*(B)	n_S(A)	π_S^*(B)	n_S(A)	π_S^*(B)	n_S(A)
Energy (eV)	-10.698	-12.462	-10.760	-12.487	-10.723	-12.477
C_{ij}'s						
H(1)	-0.126	-0.080	-0.131	0.067	-0.119	-0.064
H(3)	0.003	-0.027	-0.016	0.033	-0.027	-0.060
H(4)	-0.028	0.039	-0.010	-0.042	0.014	0.032
H(5)	-0.003	0.016	0.011	-0.003	-0.002	-0.009
H(6)	0.012	0.026	0.002	0.007	0.019	0.033
H(7)	-0.027	-0.068	-0.030	0.077	-0.042	-0.077
H(8)	-0.002	-0.016	0.009	-0.014	0.003	-0.012
H(9)	0.027	0.049	0.013	-0.042	-0.015	0.025
H(10)	0.008	-0.008	0.022	-0.000	-0.024	0.039
H(11)	-0.049	-0.066	-0.044	0.052	0.007	-0.039
O(1,s)	0.001	0.018	0.001	-0.018	0.001	0.018
C(1,s)	-0.014	-0.070	-0.011	0.071	-0.013	-0.070
C(4,s)	0.003	0.031	0.006	-0.032	0.005	0.031
C(5,s)	-0.039	-0.017	0.037	0.018	-0.037	-0.018
C(6,s)	-0.013	-0.015	0.007	0.008	0.001	0.018
C(7,s)	0.002	0.032	-0.004	-0.038	0.015	0.034
C(8,s)	0.019	0.022	-0.010	-0.008	-0.013	-0.013
O(1,x)	0.001	-0.236	-0.000	0.239	0.001	-0.234
C(1,x)	-0.005	0.335	-0.002	-0.337	-0.004	0.333
C(4,x)	0.011	-0.108	0.013	0.104	0.009	-0.112
C(5,x)	-0.050	-0.087	-0.055	-0.080	-0.070	-0.095
C(6,x)	-0.044	-0.011	-0.020	-0.020	0.007	0.080
C(7,x)	0.011	0.110	0.014	0.074	0.010	-0.015
C(8,x)	-0.000	-0.012	-0.001	0.013	-0.001	0.017
O(1,y)	-0.305	-0.013	-0.307	0.014	-0.308	-0.017
C(1,y)	0.630	0.027	0.628	-0.030	0.633	0.326
C(4,y)	-0.090	0.065	-0.094	-0.079	-0.082	0.091
C(5,y)	0.123	0.077	0.133	0.093	0.110	0.103
C(6,y)	-0.007	0.041	-0.010	0.006	-0.001	-0.006
C(7,y)	-0.000	0.014	0.001	0.006	-0.013	-0.049
C(8,y)	-0.026	-0.054	-0.038	-0.032	0.010	0.038
O(1,z)	-0.010	0.147	-0.007	-0.149	-0.010	0.147
C(1,z)	0.024	-0.255	0.016	0.255	0.022	-0.252
C(4,z)	-0.035	0.283	0.030	-0.282	-0.037	0.278
C(5,z)	-0.095	-0.182	0.072	0.181	-0.090	-0.178
C(6,z)	-0.013	0.085	0.017	-0.052	0.009	0.026
C(7,z)	0.013	0.092	-0.021	-0.152	0.041	0.132
C(8,z)	0.038	0.063	0.022	-0.015	-0.028	0.066

TABLE 50

EHMO Coefficients for the n & π* Orbitals of CBD with di t-butyl Substitution

Model LIII (C_1 Symmetry)

TEE = -1495.617 eV

MO(sym)	π_S^*(A)	n_S(A)		π_S^*(A)	n_S(A)
Energy (eV)	-10.742	-12.482		-10.742	-12.482
C_{ij}'s			C_{ij}'s		
H(1)	-0.129	-0.071	C(3,x)	0.011	0.104
H(2)	0.120	-0.060	C(4,x)	0.011	-0.109
H(3)	-0.027	-0.055	C(5,x)	-0.070	-0.086
H(4)	0.014	0.031	C(6,x)	0.007	0.074
H(5)	-0.001	-0.009	C(7,x)	0.012	-0.013
H(6)	0.019	0.032	C(8,x)	-0.001	0.016
H(7)	-0.042	-0.074	C(9,x)	-0.055	0.086
H(8)	0.003	-0.011	C(10,x)	-0.021	0.022
H(9)	-0.014	0.023	C(11,x)	0.015	-0.077
H(10)	-0.024	0.038	C(13,x)	-0.001	-0.011
H(11)	0.006	-0.037	O(1,y)	-0.309	-0.014
H(12)	0.015	-0.035	O(2,y)	-0.305	0.016
H(13)	0.010	0.044	C(1,y)	0.634	0.031
H(14)	-0.011	0.003	C(2,y)	0.627	-0.031
H(15)	0.031	-0.081	C(3,y)	-0.086	-0.085
H(16)	-0.009	0.015	C(4,y)	-0.089	0.084
H(17)	-0.003	-0.008	C(5,y)	0.111	0.095
H(18)	0.042	-0.054	C(6,y)	-0.001	-0.005
H(19)	-0.012	0.044	C(7,y)	-0.012	-0.047
H(20)	-0.021	-0.001	C(8,y)	0.008	0.037
O(1,s)	0.001	0.016	C(9,y)	0.131	-0.101
O(2,s)	-0.000	0.019	C(10,y)	-0.009	-0.006
C(1,s)	-0.011	-0.063	C(11,y)	0.001	-0.006
C(2,s)	0.013	-0.078	C(12,y)	-0.037	0.033
C(3,s)	-0.004	0.031	O(1,z)	-0.008	0.156
C(4,s)	0.008	0.032	O(2,z)	0.010	0.140
C(5,s)	-0.037	-0.017	C(1,z)	0.017	-0.266
C(6,s)	0.001	0.017	C(2,z)	-0.022	-0.241
C(7,s)	0.015	0.033	C(3,z)	0.034	0.264
C(8,s)	-0.012	-0.012	C(4,z)	-0.034	0.296
C(9,s)	0.037	-0.020	C(5,z)	-0.089	-0.169
C(10,s)	0.007	-0.008	C(6,z)	0.009	0.024
C(11,s)	-0.005	0.040	C(7,z)	0.041	0.126
C(12,s)	-0.009	0.008	C(8,z)	-0.029	0.064
O(1,x)	-0.000	-0.237	C(9,z)	0.073	-0.191
O(2,x)	0.001	0.235	C(10,z)	0.017	0.054
C(1,x)	-0.003	0.336	C(11,z)	-0.021	0.169
C(2,x)	-0.004	-0.333	C(12,z)	0.022	0.017

TABLE 51

EHMO Coefficients for the n & π* Orbitals of CBD with di t-butyl Substitution Models LIV & LV (C_2 Symmetry)

	LIV		LV	
MO(sym)	π^*_S(B)	n_S(A)	π^*_S(B)	n_S(A)
Energy (eV)	-10.660	-12.392	-7.279	-10.801
C_{ij}'s				
H(1)	0.130	0.093	-0.120	-0.064
H(3)	0.013	-0.001	0.024	0.029
H(4)	0.018	-0.046	-0.020	-0.048
H(5)	-0.009	0.026	-0.022	-0.053
H(6)	0.012	0.032	-0.024	0.001
H(7)	-0.016	-0.032	0.005	0.048
H(8)	0.018	0.060	0.004	-0.040
H(9)	0.020	0.015	-0.016	-0.002
H(10)	0.034	0.068	-0.014	-0.044
H(11)	-0.040	-0.062	0.019	0.040
O(1,s)	-0.002	-0.016	0.002	0.018
C(1,s)	-0.012	0.069	-0.011	-0.070
C(4,s)	-0.001	-0.021	0.006	0.030
C(5,s)	0.039	0.017	-0.036	-0.017
C(6,s)	-0.001	-0.039	0.010	0.041
C(7,s)	-0.019	-0.027	-0.008	-0.005
C(8,s)	0.018	0.011	-0.003	0.001
O(1,x)	-0.001	0.232	0.001	-0.238
C(1,x)	-0.006	-0.330	-0.003	0.337
C(4,x)	0.003	0.125	0.011	-0.097
C(5,x)	-0.057	-0.104	-0.065	-0.077
C(6,x)	0.015	0.115	0.001	0.019
C(7,x)	0.037	0.031	-0.042	0.022
C(8,x)	-0.025	-0.004	-0.018	0.007
O(1,y)	-0.229	0.000	-0.311	-0.021
C(1,y)	0.631	-0.019	0.630	0.034
C(4,y)	-0.089	-0.056	-0.074	0.085
C(5,y)	0.120	0.084	0.120	0.106
C(6,y)	0.014	0.001	-0.008	-0.026
C(7,y)	-0.042	-0.071	0.005	0.012
C(8,y)	0.039	0.028	-0.003	-0.012
O(1,z)	-0.006	-0.146	-0.010	0.151
C(1,z)	0.020	0.254	0.018	-0.255
C(4,z)	-0.031	-0.284	-0.030	0.280
C(5,z)	0.085	0.172	-0.073	-0.180
C(6,z)	-0.004	-0.094	0.039	0.169
C(7,z)	-0.016	-0.058	-0.036	0.032
C(8,z)	0.066	-0.074	0.008	0.023

TABLE 52

Selected EHMO's for CBD with Di-t-butyl substitution (crystal)

C_2 Symmetry

Model LVI

TEE = -1498.626 eV

MO(sym)	$\pi_S^*(B)$	$n_S(A)$	$\sigma_S(A)$	$n_A(B)$	$\sigma_A(B)$
Energy (eV)	-10.721	-12.421	-12.700	-12.869	-13.118
C_{ij}'s					
H(1)	0.118	-0.061	0.056	-0.107	-0.201
H(2)	-0.117	-0.061	0.055	0.100	-0.202
H(3)	-0.012	-0.041	0.036	-0.031	0.098
H(4)	-0.014	0.047	0.030	0.078	-0.020
H(5)	0.005	0.005	-0.088	-0.017	0.056
H(6)	-0.026	-0.055	0.079	-0.051	0.089
H(7)	0.009	0.039	0.040	0.084	-0.025
H(8)	0.004	-0.000	0.011	-0.005	-0.084
H(9)	0.012	0.013	-0.086	-0.039	0.038
H(10)	0.008	0.008	0.024	0.005	-0.097
H(11)	-0.031	-0.072	0.010	-0.083	0.073
H(12)	-0.008	0.009	0.023	-0.008	-0.094
H(13)	-0.012	0.013	-0.087	0.040	0.032
H(14)	0.032	-0.073	0.010	0.085	0.070
H(15)	-0.004	0.000	0.009	0.002	-0.080
H(16)	0.026	-0.056	0.080	0.053	0.087
H(17)	-0.009	0.039	0.041	-0.084	-0.021
H(18)	-0.005	0.005	-0.089	0.018	0.051
H(19)	0.012	-0.042	0.037	0.035	0.098
H(20)	0.014	0.048	0.031	-0.079	-0.018
O(1,s)	-0.002	0.020	-0.015	0.027	0.009
O(2,s)	0.002	0.020	-0.015	-0.027	0.010
C(1,s)	0.002	-0.073	0.047	0.157	-0.027
C(2,s)	-0.010	0.063	-0.025	-0.003	0.069
C(3,s)	-0.002	-0.071	0.048	-0.158	-0.022
C(4,s)	0.010	0.032	-0.024	0.005	0.070
C(5,s)	-0.034	-0.018	0.010	-0.009	0.009
C(6,s)	-0.002	-0.006	0.010	-0.015	-0.053
C(7,s)	0.000	0.007	-0.066	-0.011	0.012
C(8,s)	0.007	0.038	0.032	0.060	0.001
C(9,s)	0.034	-0.018	0.010	0.009	0.008
C(10,s)	0.002	-0.006	0.010	0.013	-0.052
C(11,s)	-0.000	0.007	-0.066	0.011	0.010
C(12,s)	-0.007	0.038	0.032	-0.059	0.003
O(1,x)	0.009	0.241	0.013	-0.004	0.081

TABLE 52 (cont.)
Model LVI

TEE = -1498.626 eV

MO(sym)	π_S^*(B)	n_S(A)	σ_S(A)	n_A(B)	σ_A(B)
Energy (eV)	-10.721	-12.421	-12.700	-12.869	-13.118
C_{ij}'s					
O(2,x)	0.009	-0.241	-0.013	-0.009	-0.081
C(1,x)	-0.029	0.345	0.028	0.038	0.103
C(2,x)	-0.004	-0.121	0.375	-0.036	-0.007
C(3,x)	-0.029	-0.344	-0.027	0.031	-0.104
C(4,x)	-0.005	0.120	-0.375	-0.035	0.009
C(5,x)	0.062	0.073	-0.298	-0.007	0.041
C(6,x)	-0.008	-0.018	0.074	-0.014	-0.125
C(7,x)	-0.002	-0.034	0.309	0.050	-0.059
C(8,x)	-0.013	0.007	0.076	0.067	-0.040
C(9,x)	0.062	-0.072	0.299	-0.008	-0.031
C(10,x)	-0.009	0.017	-0.073	-0.009	0.119
C(11,x)	-0.002	0.034	-0.310	0.051	0.049
C(12,x)	-0.013	-0.008	-0.077	0.069	0.035
O(1,y)	0.310	0.002	-0.017	-0.011	-0.051
O(2,y)	0.311	-0.011	0.011	-0.022	0.049
C(1,y)	-0.636	0.023	-0.017	0.037	-0.070
C(2,y)	0.093	0.098	-0.085	0.070	-0.300
C(3,y)	-0.631	-0.006	0.025	0.022	0.074
C(4,y)	0.092	-0.120	0.080	0.103	0.294
C(5,y)	-0.114	-0.111	0.064	-0.074	0.344
C(6,y)	0.013	-0.007	0.025	-0.031	-0.252
C(7,y)	0.005	0.021	-0.032	0.019	-0.068
C(8,y)	0.012	0.045	0.012	0.057	-0.078
C(9,y)	-0.119	0.127	-0.061	-0.105	-0.340
C(10,y)	0.010	0.002	-0.021	-0.018	0.243
C(11,y)	0.006	-0.023	0.029	0.025	0.067
C(12,y)	0.014	-0.058	-0.020	0.079	0.076
O(1,z)	0.030	0.142	0.078	-0.173	0.042
O(2,z)	-0.007	0.139	0.079	0.174	0.039
C(1,z)	0.009	-0.245	-0.085	-0.241	-0.071
C(2,z)	-0.000	0.270	0.094	0.333	0.023
C(3,z)	-0.055	-0.249	-0.085	0.239	-0.073
C(4,z)	0.006	0.265	0.100	-0.323	0.054
C(5,z)	-0.075	-0.182	-0.071	-0.283	0.055
C(6,z)	-0.045	0.047	-0.005	0.066	0.049
C(7,z)	0.004	0.020	0.062	0.063	-0.035
C(8,z)	0.026	0.159	0.125	0.280	-0.027
C(9,z)	0.067	-0.175	-0.077	0.276	0.022
C(10,z)	0.045	0.047	-0.006	-0.066	0.066
C(11,z)	-0.004	0.019	0.064	-0.061	0.027
C(12,z)	-0.025	0.157	0.125	-0.273	-0.012

TABLE 53

Atomic Coordinates (Å) for Models IV & VI

	Model IV			Model VI		
	x	y	z	x	y	z
O(1)	-1.624	0.0	2.368	-1.624	0.0	2.368
O(2)	1.624	0.0	2.368	1.624	0.0	2.368
C(1)	-0.775	0.0	1.533	-0.775	0.0	1.533
C(2)	0.775	0.0	1.533	0.775	0.0	1.533
C(3)	-2.014	2.135	0.600	-2.014	2.135	0.600
H(1)	1.325	0.0	0.580	0.786	0.0	0.433
H(2)	-1.325	0.0	0.580	-0.786	0.0	0.433
H(3)	-3.108	2.228	0.537	-3.108	2.228	0.537
H(4)	-1.548	3.128	0.526	-1.548	3.128	0.526
H(5)	-1.737	1.656	1.551	-1.737	1.656	1.551
H(6)	-1.659	1.510	-0.232	-1.659	1.510	-0.232

TABLE 54

Atomic Coordinates (A^{o}) for Model VIII

Model VIII: CBD & one methane

	x	y	z
O(1)	1.624	0.0	2.368
O(2)	-1.624	0.0	2.368
C(1)	0.775	0.0	1.533
C(2)	-0.775	0.0	1.533
C(3)	-0.786	0.0	0.0
C(4)	0.786	0.0	0.0
C(5)	-2.014	2.135	0.600
H(1)	1.298	0.883	-0.408
H(2)	-1.298	-0.883	-0.408
H(3)	-1.298	0.883	-0.408
H(4)	1.298	-0.883	-0.408
H(5)	-2.369	2.760	1.543
H(6)	-2.288	2.606	-0.355
H(7)	-2.475	1.138	0.666
H(8)	-0.920	2.036	0.656

TABLE 55

Atomic Coordinates for Models XII, XIII, XX & XXI

	XII			XIII		
	x	y	z	x	y	z
O(1)	1.624	0.0	2.367	1.624	0.0	2.367
O(2)	-1.624	0.0	2.367	-1.624	0.0	2.367
C(1)	0.775	0.0	1.532	0.775	0.0	1.532
C(2)	-0.775	0.0	1.532	-0.775	0.0	1.532
C(3)	-0.785	0.0	0.0	-0.785	0.0	0.0
C(4)	0.785	0.0	0.0	0.785	0.0	0.0
C(5)	-1.497	-1.258	-0.578	1.497	1.258	-0.578
C(6)	1.497	-1.258	-0.578	-1.497	-1.258	-0.578
	Hydrogens			Hydrogens		
H(1)	-1.285	0.890	-0.408	-1.285	0.890	-0.408
H(2)	1.285	0.890	-0.408	1.285	-0.890	-0.408
H(3)	-0.783	-1.819	-1.199	1.845	1.887	0.254
H(4)	-1.845	-1.887	0.254	2.353	0.936	-1.188
H(5)	-2.353	-0.936	-1.188	0.783	1.819	-1.199
H(6)	1.845	-1.887	0.254	-1.845	-1.887	0.254
H(7)	2.353	-0.936	-1.188	-0.783	-1.819	-1.199
H(8)	0.783	-1.819	-1.199	-2.353	-0.936	-1.188
	XX			XXI		
O(1)	1.298	-0.883	-0.408	1.624	0.0	2.367
O(2)	-1.298	-0.883	-0.408	-1.624	0.0	2.367
C(1)	0.777	2.057	-0.717	0.775	0.0	1.532
C(2)	1.965	0.985	-1.544	-0.775	0.0	1.532
C(3)	2.291	1.569	0.128	-0.785	0.0	0.0
C(4)	-2.571	1.017	-0.705	0.785	0.0	0.0
C(5)	-1.065	1.505	-1.550	1.511	1.250	-0.578
C(6)	-1.391	2.089	0.121	-1.511	-1.250	-0.578
	Hydrogens			Hydrogens		
H(1)	1.298	-0.883	-0.408	1.298	-0.883	-0.408
H(2)	-1.298	-0.883	-0.408	-1.298	0.883	-0.408
H(3)	0.777	2.057	-0.717	0.777	2.057	-0.717
H(4)	1.965	0.985	-1.544	1.965	0.985	-1.544
H(5)	2.291	1.569	0.128	2.291	1.569	0.128
H(6)	-2.571	1.017	-0.705	-2.579	-1.017	-0.705
H(7)	-1.065	1.505	-1.550	-1.065	-1.505	-1.550
H(8)	-1.391	2.089	0.121	-1.391	-2.089	0.121

TABLE 56

Atomic Coordinates for Models XVIII, XIX, XIV & XV

	XVIII			XIX		
	x	y	z	x	y	z
O(1)	1.624	0.0	2.367	1.624	0.0	2.367
O(2)	-1.624	0.0	2.367	-1.624	0.0	2.367
C(1)	0.775	0.0	1.532	0.775	0.0	1.532
C(2)	-0.775	0.0	1.532	-0.775	0.0	1.532
C(3)	-0.785	0.0	0.0	-0.785	0.0	0.0
C(4)	0.785	0.0	0.0	0.785	0.0	0.0
C(5)	-1.511	1.250	-0.578	1.511	1.250	-0.578
C(6)	1.511	1.250	-0.578	-1.511	-1.250	-0.578
	Hydrogens			Hydrogens		
H(1)	1.298	-0.883	-0.408	1.298	-0.883	-0.408
H(2)	-1.298	-0.883	-0.408	-1.298	0.883	-0.408
H(3)	2.579	1.017	-0.705	-2.579	-1.017	-0.705
H(4)	1.391	2.089	0.121	-1.065	-1.505	-1.550
H(5)	1.065	1.505	-1.550	-1.391	-2.089	0.121
H(6)	-2.571	1.017	-0.705	2.579	1.017	-0.705
H(7)	-1.065	1.505	-1.550	1.391	2.089	0.121
H(8)	-1.391	2.089	0.121	1.065	1.505	-1.550
	XIV			XV		
O(1)	1.624	0.0	2.367	1.624	0.0	2.367
O(2)	-1.624	0.0	2.367	-1.624	0.0	2.367
C(1)	0.775	0.0	1.532	0.775	0.0	1.532
C(2)	-0.775	0.0	1.532	-0.775	0.0	1.532
C(3)	-0.785	0.0	0.0	-0.785	0.0	0.0
C(4)	0.785	0.0	0.0	0.785	0.0	0.0
C(5)	-1.511	1.250	-0.578	-1.511	-1.250	-0.578
C(6)	1.511	1.250	-0.578	1.511	1.250	-0.578
	Hydrogens			Hydrogens		
H(1)	1.298	-0.883	-0.408	1.298	-0.883	-0.408
H(2)	-1.298	-0.883	-0.408	-1.298	0.883	-0.408
H(3)	0.777	2.057	-0.717	0.777	2.057	-0.717
H(4)	1.965	0.985	-1.544	2.291	1.569	0.128
H(5)	2.291	1.569	0.128	1.964	0.985	-0.544
H(6)	-0.777	2.057	-0.717	-0.777	-2.057	-0.717
H(7)	-2.291	1.569	0.128	-2.291	-1.569	9.128
H(8)	-1.965	0.985	-1.544	-1.965	-0.985	-1.544

TABLE 57

Atomic Coodinates for XXIII

	x	y	z
O(1)	1.624	0.0	2.367
O(2)	-1.624	0.0	2.367
C(1)	0.775	0.0	1.532
C(2)	-0.775	0.0	1.532
C(3)	-0.785	0.0	0.0
C(4)	0.785	0.0	0.0
C(5)	1.497	1.258	-0.578
C(6)	-1.497	1.258	-0.578
C(7)	-1.497	-1.258	-0.578
C(8)	1.497	-1.258	-0.578
		Hydrogens	
H(1)	1.845	1.887	0.254
H(2)	2.353	0.936	-1.188
H(3)	0.783	1.819	-1.199
H(4)	-0.783	-1.819	-1.199
H(5)	-1.845	-1.887	0.254
H(6)	-2.353	-0.936	-1.188
H(7)	1.845	-1.887	0.254
H(8)	2.353	-0.936	-1.188
H(9)	0.783	-1.819	-1.199
H(10)	-1.845	1.887	0.254
H(11)	-2.353	0.936	-1.188
H(12)	-0.783	1.819	-1.199

TABLE 58

Atomic Coordinates for Models XXIV & XXV

	XXIV			XXV		
	x	y	z	x	y	z
O(1)	1.624	0.0	2.367	1.624	0.0	2.367
O(2)	-1.624	0.0	2.36	-1.624	0.0	2.367
C(1)	0.775	0.0	1.532	0.775	0.0	1.532
C(2)	-0.775	0.0	1.532	-0.775	0.0	1.532
C(3)	-0.785	0.0	0.0	-0.785	0.0	0.0
C(4)	0.785	0.0	0.0	0.785	0.0	0.0
C(5)	-1.511	1.250	-0.578	-1.511	1.250	-0.578
C(6)	-2.014	2.134	0.600	-0.510	2.055	-1.457
	Hydrogens			Hydrogens		
H(1)	1.298	0.883	-0.408	1.298	0.883	-0.408
H(2)	-1.298	-0.883	-0.408	-1.298	-0.883	-0.408
H(3)	1.298	-0.883	-0.408	1.298	-0.883	-0.408
H(4)	-3.108	2.227	0.536	0.340	2.370	-0.834
H(5)	-1.548	3.128	0.526	-1.023	2.939	-1.866
H(6)	-1.736	1.656	1.550	-0.157	1.413	-2.278
H(7)	-0.604	1.819	-1.199	-1.866	1.875	0.254
H(8)	-2.364	0.918	-1.188	-2.364	0.918	-1.188

TABLE 59

Atomic Coordinates for Model XXVI

	x	y	z
O(1)	1.624	0.0	2.367
O(2)	-1.624	0.0	2.367
C(1)	0.775	0.0	1.532
C(3)	-0.785	0.0	0.0
C(4)	0.785	0.0	0.0
C(2)	-0.775	0.0	1.532
C(5)	-1.511	1.250	-0.578
C(6)	-1.481	1.179	-2.133
		Hydrogens	
H(1)	1.298	0.883	-0.408
H(2)	1.298	-0.883	-0.408
H(3)	-1.298	-0.883	-0.408
H(4)	-0.954	0.263	-2.440
H(5)	-0.954	2.063	-2.521
H(6)	-2.514	1.162	-2.511
H(7)	-0.992	2.156	-0.233
H(8)	-2.552	1.256	-0.223

TABLE 60

Atomic Coordinates for Models XXIX & XXX

	XXIX			XXX		
	x	y	z	x	y	z
O(1)	1.624	0.0	2.367	1.624	0.0	2.367
O(2)	-1.624	0.0	2.367	-1.624	0.0	2.367
C(1)	0.775	0.0	1.532	0.775	0.0	1.532
C(2)	-0.775	0.0	1.532	-0.775	0.0	1.532
C(3)	-0.785	0.0	0.0	-0.785	0.0	0.0
C(4)	0.785	0.0	0.0	0.785	0.0	0.0
C(5)	-1.298	1.399	-0.451	-1.283	1.356	-0.579
C(6)	-1.601	2.255	0.804	-1.623	2.312	0.592
C(7)	-2.588	1.217	-1.291	-2.548	1.104	-1.439
C(8)	-0.203	2.085	-1.307	-0.162	1.972	-1.455
	Hydrogens			Hydrogens		
H(1)	1.298	0.883	-0.408	1.298	0.883	-0.408
H(2)	1.298	-0.883	-0.408	1.298	-0.883	-0.408
H(3)	-1.298	-0.883	-0.408	-1.298	-0.883	-0.408
H(4)	-1.379	1.662	1.703	-1.428	1.795	1.543
H(5)	-2.663	2.540	0.795	-2.684	2.593	0.528
H(6)	-0.970	3.156	0.784	-0.991	3.209	0.517
H(7)	-3.414	1.750	-0.798	-3.388	1.674	-1.017
H(8)	-2.822	0.144	-1.360	-2.780	0.029	-1.427
H(9)	-2.422	1.630	-2.297	-2.351	1.433	-2.470
H(10)	0.092	3.027	-0.822	0.118	2.951	-1.040
H(11)	-0.607	2.290	-2.309	-0.537	2.094	-2.483
H(12)	0.664	1.413	-1.383	0.706	1.298	-1.451

TABLE 61

Atomic Coordintes for Models XXXI, XXXII, XXXIV, XXXV

	XXXI			XXXII		
	x	y	z	x	y	z
C(5)	-1.265	1.303	-0.703	-1.533	1.289	-0.450
C(6)	-1.639	2.351	0.375	-1.980	2.078	0.806
C(7)	-2.503	0.979	-1.577	-2.772	0.887	-1.289
C(8)	-0.118	1.847	-1.593	-0.574	2.156	-1.304
	Hydrogens					
H(1)	1.298	0.883	-0.408	1.298	0.883	-0.408
H(2)	1.298	-0.883	-0.408	1.298	-0.883	-0.408
H(3)	-1.298	-0.883	-0.408	-1.298	-0.883	-0.409
H(4)	-1.473	1.914	1.371	-1.656	1.532	1.705
H(5)	-2.697	2.624	0.257	-3.076	2.174	0.798
H(6)	-1.005	3.240	0.246	-1.515	30.75	0.787
H(7)	-3.355	1.581	-1.227	-3.678	1.268	-0.796
H(8)	-2.737	-0.091	-1.483	-2.816	-0.209	-1.360
H(9)	-2.276	1.223	-2.625	-2.680	1.323	-2.295
H(10)	0.151	2.857	-1.251	-0.446	3.134	-0.818
H(11)	-0.462	1.884	-2.637	-1.008	2.289	-2.306
H(12)	0.750	1.177	-1.507	0.397	1.646	-1.381
	XXXIV			XXXV		
C(5)	-1.484	1.201	-0.702	-1.745	1.140	-0.448
C(6)	-2.034	2.166	0.378	-2.322	1.838	0.809
C(7)	-2.047	0.668	-1.576	-2.896	0.530	-1.289
C(8)	-0.449	1.937	-1.591	-0.951	2.161	-1.302
	Hydrogens					
H(1)	1.298	0.883	-0.408	1.298	0.883	-0.408
H(2)	1.298	-0.883	-0.408	1.298	-0.883	-0.408
H(3)	-1.298	-0.883	-0.408	-1.298	-0.883	-0.408
H(4)	-1.795	1.764	1.373	-1.911	1.355	1.707
H(5)	-3.124	2.252	0.260	-3.418	1.743	0.800
H(6)	-1.564	3.153	0.249	-2.038	2.901	0.791
H(7)	-3.591	1.112	-1.226	-3.854	0.747	-0.795
H(8)	-2.692	-0.427	-1.484	-2.749	-0.557	-1.360
H(9)	-2.466	0.949	-2.624	-2.881	9.977	-2.294
H(10)	-0.359	2.978	-1.248	-0.995	3.147	-0.814
H(11)	-0.794	1.914	-2.635	-1.402	2.218	-2.304
H(12)	0.522	1.428	-1.505	0.093	1.838	-1.379

TABLE 62

Atomic Coordinates for Models XXXIII & XLVII

	XXXIII			XLVII		
	x	y	z	x	y	z
O(1)	1.624	0.0	2.367	1.624	0.0	2.367
O(2)	-1.624	0.0	2.367	-1.624	0.0	2.367
C(1)	0.775	0.0	1.532	0.775	0.0	1.532
C(2)	-0.775	0.0	1.532	-0.775	0.0	1.532
C(3)	-0.785	0.0	0.0	-0.785	0.0	0.0
C(4)	0.785	0.0	0.0	0.785	0.0	0.0
C(5)	-1.511	1.250	-0.578	-1.511	1.250	-0.578
C(6)	-2.014	2.134	0.600	-1.481	1.179	-2.133
C(7)	-2.718	0.780	-1.442	-0.776	2.533	-0.090
C(8)	-0.510	2.055	-1.457	-2.985	1.258	-0.075
	Hydrogens			Hydrogens		
H(1)	1.298	0.883	-0.408	1.298	-0.883	-0.408
H(2)	1.298	-0.883	-0.408	1.298	0.883	-0.408
H(3)	-1.298	-0.883	-0.408	-1.298	-0.883	-0.408
H(4)	-1.736	1.656	1.550	-0.954	0.263	-2.440
H(5)	-1.548	3.128	0.526	-0.954	2.063	-2.521
H(6)	-3.108	2.227	0.536	-2.514	1.162	-2.511
H(7)	-3.645	1.196	-1.019	-1.480	3.150	0.487
H(8)	-2.761	-0.318	-1.431	0.073	2.240	0.542
H(9)	-2.582	1.140	-2.473	-0.417	3.094	-0.965
H(10)	-0.402	3.068	-1.041	-3.162	2.179	0.499
H(11)	-0.900	2.111	-2.484	-3.659	1.222	-0.943
H(12)	0.462	1.542	-1.454	-3.150	0.379	0.564

TABLE 63

Atomic Coordinates for Models XXXVI, XXXVII, XXXVIII, XXXIX

XXXVI						
	x	y	z	x	y	z
C(5)	-1.717	1.105	-0.576	-1.682	1.062	-0.700
C(6)	-2.363	1.884	0.597	-2.391	1.916	0.380
C(7)	-2.820	0.438	-1.437	-2.735	0.336	-1.575
C(8)	-0.875	2.069	-1.451	-0.791	1.968	-1.588
	Hydrogens			Hydrogens		
H(1)	1.298	0.883	-0.408	1.298	0.883	-0.408
H(2)	1.298	-0.883	-0.408	1.298	-0.883	-0.408
H(3)	-1.298	-0.883	-0.408	-1.298	-0.883	-0.408
H(4)	-2.003	1.463	1.547	-2.086	1.560	1.375
H(5)	-3.457	1.786	0.533	-3.480	1.811	0.262
H(6)	-2.077	2.944	0.524	-2.100	2.969	0.253
H(7)	-3.804	0.686	-1.014	-3.741	0.609	-1.225
H(8)	-2.671	-0.651	-1.428	-2.589	-0.749	-1.484
H(9)	-2.748	0.817	-2.468	-2.606	0.646	-2.623
H(10)	-0.945	3.085	-1.033	-0.882	3.008	-1.244
H(11)	-1.269	2.058	-2.478	-1.127	1.887	-2.633
H(12)	0.171	1.733	-1.447	0.253	1.635	-1.504
XXXVIII				XXXIX		
C(5)	-1.511	1.250	-0.578	-1.511	1.250	-0.578
C(6)	-2.014	2.134	0.699	-2.615	1.702	0.421
C(7)	-2.718	0.780	-1.442	-2.154	0.875	-1.945
C(8)	-0.510	2.055	-1.457	-0.472	2.393	-0.775
	Hydrogens			Hydrogens		
H(1)	1.298	0.883	-0.408	1.298	0.883	-0.408
H(2)	1.298	-0.883	-0.408	1.298	-0.883	-0.408
H(3)	-1.298	-0.883	-0.408	-1.298	-0.883	-0.408
H(4)	-2.522	3.020	0.191	-3.128	2.586	0.012
H(5)	-1.151	2.448	1.205	-2.146	1.953	1.384
H(6)	-2.711	1.547	1.216	-3.334	0.881	0.557
H(7)	-3.409	0.205	-0.809	-1.362	0.548	-2.636
H(8)	-3.253	1.665	-1.820	-2.667	1.758	-2.354
H(9)	-2.347	0.149	-2.263	-2.876	0.060	-1.790
H(10)	0.340	2.370	-0.834	-0.021	2.638	0.197
H(11)	-0.157	1.413	-2.278	0.304	2.053	-1.475
H(12)	-1.023	2.939	-1.866	-0.985	3.276	-1.183

TABLE 64

Atomic Coordinates for Models XL, XLI, XLII, XLIII

XL				XLI		
	x	y	z	x	y	z
C(5)	-1.511	1.250	-0.578	-1.511	1.250	-0.578
C(6)	-2.895	1.400	0.118	-1.481	1.179	-2.133
C(7)	-1.706	1.059	-2.111	-0.776	2.533	-0.090
C(8)	-0.640	2.512	-0.307	-2.985	1.258	-0.075
	Hydrogens			Hydrogens		
H(1)	1.298	0.883	-0.408	1.298	0.883	-0.408
H(2)	1.298	-0.883	-0.408	1.298	-0.883	-0.408
H(3)	-1.298	-0.883	-0.408	-1.298	=0.883	-0.408
H(4)	-3.019	0.586	0.847	-1.991	2.064	-2.541
H(5)	-3.687	1.345	-0.642	-0.434	1.163	-2.470
H(6)	-2.934	2.372	0.631	-1.994	0.263	-2.460
H(7)	-2.782	1.085	-2.341	0.264	2.506	-0.445
H(8)	-1.283	0.087	-2.407	-1.289	3.416	-0.499
H(9)	-1.189	1.871	-2.642	-0.798	2.562	1.008
H(10)	-1.217	3.219	0.307	-2.988	1.298	1.023
H(11)	-0.377	2.978	-1.268	-3.485	0.341	-0.419
H(12)	0.272	2.209	0.225	-3.497	2.141	-0.484
XLII				XLIII		
C(5)	-1.511	1.250	-0.578	-1.511	1.250	-0.578
C(6)	-3.036	1.128	-0.290	-3.049	1.015	-0.520
C(7)	-1.263	1.314	-2.114	-1.061	1.460	-2.053
C(8)	-0.942	2.528	0.105	-1.132	2.496	0.274
	Hydrogens			Hydrogens		
H(1)	1.298	0.883	-0.408	1.298	0.883	-0.408
H(2)	1.298	-0.883	-0.408	1.298	-0.883	-0.408
H(3)	-1.298	-0.883	-0.408	-1.298	-0.883	-0.408
H(4)	-3.225	0.189	0.249	-3.562	1.898	-0.929
H(5)	-3.582	1.127	-1.246	-3.348	0.858	0.526
H(6)	-3.355	1.985	0.321	-3.298	0.126	-1.119
H(7)	-2.231	1.269	-2.635	0.027	1.614	-2.077
H(8)	-0.639	0.459	-2.412	-1.570	2.346	-2.461
H(9)	-0.752	2.258	-2.355	-1.326	0.567	-2.639
H(10)	-1.759	3.050	0.623	-0.042	2.641	0.231
H(11)	-0.507	3.182	-0.664	-1.447	2.327	1.315
H(12)	-0.170	2.232	0.830	-1.629	3.382	-0.145

TABLE 65

Atomic Coordinates for Models XLIV, XLV, XLVI, XLVIII

	XLIV			XLV		
	x	y	z	x	y	z
C(5)	-1.511	1.250	-0.578	-1.511	1.250	-0.578
C(6)	-3.022	0.921	-0.757	-2.957	0.849	-0.995
C(7)	-0.879	1.611	-1.954	-0.724	1.764	-1.819
C(8)	-1.341	2.438	0.412	-1.562	2.357	0.514
	Hydrogens			Hydrogens		
H(1)	1.298	0.883	-0.408	1.298	0.883	-0.408
H(2)	1.298	-0.883	-0.408	1.298	-0.883	-0.408
H(3)	-1.298	-0.883	-0.408	-1.298	-0.883	-0.408
H(4)	-3.535	1.804	-1.066	-3.469	1.732	-1.403
H(5)	-3.450	0.658	0.220	-3.495	0.479	-0.110
H(6)	-3.124	0.073	-1.451	-2.903	0.059	-1.759
H(7)	0.188	1.830	-1.811	0.296	2.033	-1.509
H(8)	-1.389	2.497	-2.360	-1.234	2.650	-2.225
H(9)	-0.999	0.758	-2.638	-0.688	0.967	-2.576
H(10)	-0.268	2.651	0.536	-0.534	2.621	0.805
H(11)	-1.782	2.163	1.381	-2.111	1.974	1.387
H(12)	-1.853	3.322	0.004	-2.074	3.240	0.106
	XLVI			XLVIII		
C(5)	-1.511	1.250	-0.578	-1.511	1.250	-0.578
C(6)	-2.615	1.702	0.421	-3.022	0.921	-0.757
C(7)	-2.154	0.875	-1.945	-0.879	1.611	-1.954
C(8)	-0.472	2.393	-0.775	-1.341	2.438	0.412
	Hydrogens			Hydrogens		
H(1)	1.298	0.883	-0.408	1.298	0.883	-0.408
H(2)	1.298	-0.883	-0.408	1.298	-0.883	-0.408
H(3)	-1.298	-0.883	-0.408	-1.298	-0.883	-0.408
H(4)	-2.611	1.027	1.289	-3.201	-0.120	-0.451
H(5)	-2.405	2.732	0.745	-3.289	1.032	-1.819
H(6)	-3.593	1.660	-0.081	-3.615	1.617	-0.146
H(7)	-1.727	1.518	-2.730	-0.469	2.630	-1.903
H(8)	-1.937	-0.180	-2.166	-0.076	0.894	-2.179
H(9)	-3.241	1.030	-1.884	-1.657	1.558	-2.730
H(10)	-0.772	3.258	-0.165	-2.334	2.773	0.745
H(11)	-0.446	2.674	-1.838	-0.820	3.261	-0.100
H(12)	9.517	2.035	-0.457	-0.747	2.103	1.276

TABLE 66

Atomic Coordinates for Models XLIX & L

	XLIX			L		
	x	y	z	x	y	z
O(1)	1.624	0.0	2.367	1.624	0.0	2.367
O(2)	-1.624	0.0	2.367	-1.624	0.0	2.367
C(1)	0.775	0.0	1.532	0.775	0.0	1.532
C(2)	-0.775	0.0	1.532	-0.775	0.0	1.532
C(3)	-0.785	0.0	0.0	-0.785	0.0	0.0
C(4)	0.785	0.0	0.0	0.785	0.0	0.0
C(5)	-1.511	1.250	-0.578	1.511	-1.250	-0.578
C(6)	-2.014	2.134	0.600	2.615	-1.702	0.421
C(7)	-2.718	0.780	-1.442	2.154	-0.875	-1.945
C(8)	-0.510	2.055	-1.457	0.472	-2.393	-0.775
C(9)	1.511	-1.250	-0.578	-1.511	1.250	-0.578
C(10)	2.014	-2.134	0.600	-2.615	1.702	0.421
C(11)	0.510	-2.055	-1.457	-2.154	0.875	-1.945
C(12)	2.718	-0.780	-1.442	-0.472	2.393	-0.775
	Hydrogens			Hydrogens		
H(1)	1.298	0.883	-0.408	1.298	0.883	-0.408
H(2)	-1.298	-0.883	-0.408	-1.298	-0.883	-0.408
H(3)	-2.522	3.020	0.191	-3.128	2.586	0.012
H(4)	-1.151	2.448	1.205	-2.146	1.953	1.384
H(5)	-2.711	1.547	1.216	-3.334	0.881	0.557
H(6)	-3.409	0.205	-0.809	-1.362	0.548	-2.636
H(7)	-3.253	1.665	-1.820	-2.667	1.758	-2.354
H(8)	-2.347	0.149	-2.263	-2.876	0.060	-1.790
H(9)	0.340	2.370	-0.834	-0.021	2.638	0.197
H(10)	-0.157	1.413	-2.278	0.304	2.053	-1.475
H(11)	-1.023	2.939	-1.866	-0.985	3.276	-1.183
H(12)	2.522	-3.020	0.191	3.128	-2.586	0.012
H(13)	2.711	-1.547	1.216	2.146	-1.953	1.384
H(14)	1.151	-2.448	1.205	3.334	-0.881	0.557
H(15)	-0.340	-2.370	-0.834	2.667	-1.758	-2.354
H(16)	1.023	-2.939	-1.866	2.877	-0.060	-1.790
H(17)	0.157	-1.413	-2.278	1.362	-0.548	-2.636
H(18)	3.409	-0.205	-0.809	0.985	-3.276	-1.183
H(19)	2.347	-0.149	-2.263	0.021	-2.638	0.197
H(20)	3.253	-1.665	-1.820	-0.304	-2.053	-1.475

TABLE 67

Atomic Coordinates for Models LII & LIII

	LII			LIII		
	x	y	z	x	y	z
O(1)	1.624	0.0	2.367	1.624	0.0	2.367
O(2)	-1.624	0.0	2.367	-1.624	0.0	2.367
C(1)	0.775	0.0	1.532	0.775	0.0	1.532
C(2)	-0.775	0.0	1.532	-0.775	0.0	1.532
C(3)	-0.785	0.0	0.0	-0.785	0.0	0.0
C(4)	0.785	0.0	0.0	0.785	0.0	0.0
C(5)	-1.511	1.250	-0.578	-1.511	1.250	-0.578
C(6)	-3.022	0.921	-0.757	-3.022	0.921	-0.757
C(7)	-0.879	1.611	-1.954	-0.879	1.611	-1.954
C(8)	-1.341	2.438	0.412	-1.341	2.438	0.412
C(9)	1.511	-1.250	-0.578	1.511	-1.250	-0.578
C(10)	3.022	-0.921	-0.757	2.615	-1.702	0.421
C(11)	0.879	-1.611	-1.954	2.154	-0.875	-1.945
C(12)	1.341	-2.438	0.412	0.472	-2.393	-0.775
	Hydrogens			Hydrogens		
H(1)	1.298	0.883	-0.408	1.298	0.883	-0.408
H(2)	-1.298	-0.883	-0.408	-1.298	-0.883	-0.408
H(3)	-3.535	1.804	-1.166	-3.535	1.804	-1.166
H(4)	-3.450	0.658	0.220	-3.450	0.658	0.220
H(5)	-3.124	0.073	-1.451	-3.124	0.073	-1.451
H(6)	0.188	1.830	-1.811	0.188	1.830	-1.811
H(7)	-1.389	2.497	-2.360	-1.389	2.497	-2.360
H(8)	-0.999	0.758	-2.638	-0.999	0.758	-2.638
H(9)	-0.268	2.651	0.536	-0.268	2.651	0.536
H(10)	-1.782	2.163	1.381	-1.782	2.163	1.381
H(11)	-1.853	3.322	0.004	-1.853	3.322	0.004
H(12)	3.535	-1.804	-1.166	3.128	-2.586	0.012
H(13)	3.450	-0.658	0.220	2.146	-1.953	1.384
H(14)	3.124	-0.073	-1.451	3.334	-0.881	0.557
H(15)	1.389	-2.497	-2.360	2.668	-1.758	-2.354
H(16)	0.999	-0.758	-2.638	2.877	-0.060	-1.790
H(17)	-0.188	-1.830	-1.811	1.362	-0.548	-2.636
H(18)	1.853	-3.322	0.004	0.985	-3.276	-1.183
H(19)	0.268	-2.651	0.536	0.021	-2.638	0.197
H(20)	1.782	-2.163	1.381	0.304	-2.053	-1.475

TABLE 68

Atomic Coordinates for Models LIV & LV

	LIV			LV		
	x	y	z	x	y	z
O(1)	1.624	0.0	2.367	1.624	0.0	2.367
O(2)	-1.624	0.0	2.367	-1.624	0.0	2.367
C(1)	0.775	0.0	1.532	0.775	0.0	1.532
C(2)	-0.775	0.0	1.532	-0.775	0.0	1.532
C(3)	-0.785	0.0	0.0	-0.785	0.0	0.0
C(4)	0.785	0.0	0.0	0.785	0.0	0.0
C(5)	1.511	-1.250	-0.578	-1.511	1.250	-0.578
C(6)	2.718	-0.780	-1.442	-1.481	1.179	-2.133
C(7)	0.510	-2.055	-1.457	-0.776	2.533	-0.090
C(8)	2.014	-2.134	0.600	-2.985	1.258	-0.075
C(9)	-1.511	1.250	-0.578	1.511	-1.250	-0.578
C(10)	-2.718	0.780	-1.442	1.481	-1.179	-2.133
C(11)	-0.510	2.055	-1.457	0.776	-2.533	-0.090
C(12)	-2.014	2.134	0.600	2.985	-1.258	-0.075
	Hydrogens			Hydrogens		
H(1)	-1.298	-0.883	-0.408	1.298	0.883	-0.408
H(2)	1.298	0.883	-0.408	-1.298	-0.883	-0.408
H(3)	1.548	-3.128	0.526	-0.954	0.263	-2.440
H(4)	1.736	-1.656	1.550	-0.954	2.063	-2.521
H(5)	3.108	-2.227	0.536	-2.514	1.162	-2.511
H(6)	3.645	-1.196	-1.019	-1.480	3.150	0.487
H(7)	2.761	0.318	-1.431	0.073	2.240	0.542
H(8)	2.582	-1.140	-2.473	-0.417	3.094	-0.965
H(9)	0.402	-3.068	-1.041	-3.126	2.179	9.499
H(10)	0.900	-2.111	-2.484	-3.659	1.222	-0.943
H(11)	-0.462	-1.542	-1.454	-3.150	0.379	0.564
H(12)	-1.548	3.128	0.526	0.954	-0.263	-2.440
H(13)	-1.736	1.656	1.550	0.954	-2.063	-2.521
H(14)	-3.108	2.227	0.536	2.514	-1.162	-2.511
H(15)	-3.645	1.196	-1.019	1.480	-3.150	0.487
H(16)	-2.761	-0.318	-1.431	-0.073	-2.240	0.542
H(17)	-2.582	1.140	-2.473	0.417	-3.094	-0.965
H(18)	-0.402	3.068	-1.041	3.162	-2.179	0.499
H(19)	-0.900	2.111	-2.484	3.659	-1.222	-0.943
H(20)	0.462	1.542	-1.454	3.150	-0.379	0.564

SUPPLEMENTARY DATA

SUPPLEMENTARY DATA contains tables of data, not located in the main text but is pertinent to theoretical study.

Contents

Selected EHMO's for CBD with Di t-butyl substitution (Crystal) (C_2 symmetry)

The valence state ionization potentials of oxygen 2s & 2p are 32.3 & 14.8 respectively.

Model LVI

MO(sym)	π_S^*(B)	n_S(A)		π_S^*(B)	n_S(A)
Energy (eV)	-10.507	-12.075		-10.507	-12.075
C_{ij}'s					
H(1)	0.112	-0.064	C(3,x)	-0.028	-0.349
H(2)	-0.111	-0.064	C(4,x)	-0.005	0.084
H(3)	-0.010	-0.025	C(5,x)	0.060	0.044
H(4)	-0.014	0.033	C(6,x)	-0.009	-0.017
H(5)	0.004	0.002	C(7,x)	-0.001	-0.013
H(6)	-0.024	-0.034	C(8,x)	-0.013	0.007
H(7)	0.009	0.059	C(9,x)	-0.043	0.009
H(8)	0.004	-0.002	C(10,x)	-0.009	0.016
H(9)	0.012	0.010	C(11,x)	-0.002	0.013
H(10)	0.007	0.008	C(12,x)	-0.013	-0.008
H(11)	-0.029	-0.051	O(1,y)	0.407	-0.011
H(13)	-0.012	0.011	O(2,y)	0.409	-0.005
H(14)	0.029	-0.052	C(1,y)	-0.607	0.009
H(15)	-0.004	-0.002	C(2,y)	0.083	0.052
H(16)	0.024	-0.034	C(3,y)	-0.603	0.007
H(17)	-0.009	0.028	C(4,y)	0.082	-0.072
H(18)	-0.005	0.002	C(5,y)	-0.106	-0.072
H(19)	0.011	-0.025	C(6,y)	0.011	-0.017
H(20)	0.014	0.033	C(7,y)	0.005	0.013
O(1,s)	-0.003	0.012	C(8,y)	0.011	0.033
O(2,s)	0.003	0.012	C(9,y)	-0.111	0.083
C(1,s)	0.002	-0.076	C(10,y)	0.007	0.013
C(2,s)	-0.009	0.044	C(11,y)	0.005	-0.014
C(3,s)	-0.002	-0.075	C(12,y)	0.012	-0.042
C(4,s)	0.009	0.044	O(1,z)	0.040	0.228
C(5,s)	-0.033	-0.016	O(2,z)	-0.011	0.225
C(6,s)	-0.003	-0.007	C(1,z)	0.010	-0.026
C(7,s)	00.000	0.004	C(2,z)	-0.002	0.007
C(8,s)	0.007	0.032	C(3,z)	-0.054	-0.228
C(9,s)	0.033	-0.016	C(4,z)	0.008	0.255
C(10,s)	0.003	-0.007	C(5,z)	-0.071	-0.137
C(11,s)	-0.000	0.004	C(6,z)	-0.036	0.036
C(12,s)	-0.007	0.032	C(7,z)	0.005	0.016
O(1,x)	0.013	0.382	C(8,z)	0.023	0.126
O(2,x)	0.0127	-0.382	C(9,z)	0.062	-0.132
C(1,x)	-0.029	0.350	C(10,z)	0.042	0.037
C(2,x)	-0.005	-0.085	C(11,z)	-0.005	0.015
H(12)	-0.007	0.008	C(12,z)	-0.022	0.124

Selected MO energies for the following isolated alkyl Models. LVII, LVIII, LIX & LX

Model No.	Isolated alkyl model
LVII	Ethane
LVIII	Butane
LIX	T-butyl
LX	Di-t-butyl
LXI	1,2 di-t-butyl ethane

σ-Molecular Orbital Energies
*(antibonding)

LVII	LVIII	LIX	LX	LXI
0.725*	0.197*	0.903*	00.864*	-9.256*
-14.131	-13.394	-13.538	-13.520	-12.256
-14.131	-13.622	-13.559	-13.534	-13.069
-14.840	-13.996	-14.183	-13.541	-13.187
-15.972	-14.643	-15.081	-13.570	-13.269
-16.473	-15.170	-15.335	-13.998	-13.468
-21.604	-15.539	-15.359	-14.337	-13.748
	-15.785	-15.849	-15.062	-14.026
	-15.897	-15.870	-15.076	-14.494
	-16.476	-16.307	-15.279	-14.665
	-19.791	-19.490	-15.278	-15.042
	-22.185	-23.734	-15.334	-15.178
			-15.336	-15.250
			-15.406	-15.326
			-15.840	-15.340
			-15.839	-15.426
			-15.842	-15.712
			-15.854	-15.821
			-15.870	-15.896
			-16.224	-16.338
			-16.387	-16.570
			-19.392	-17.994
			-19.579	-18.566
			-23.683	-21.445
				-23.684

Selected EHMO's for isolated ethane. LVII

Atomic Coordinates

	x	y	z
C(1)	-0.786	0.0	0.0
C(2)	0.786	0.0	0.0
H(1)	-0.778	0.0	1.100
H(2)	0.778	0.0	1.100
H(3)	-1.298	-0.883	-0.408
H(4)	-1.298	0.883	-0.408
H(5)	1.298	0.883	-0.408
H(6)	1.298	-0.883	-0.408

C_{2v} Symmetry

σ-Molecular Orbitals

C_{ij}'s	-14.131	-14.131	-14.840	-15.972
H(1)	0.132	-0.423	0.000	0.000
H(2)	0.156	0.414	0.000	0.00
H(3)	0.125	0.156	0.341	0.286
H(4)	0.125	0.156	-0.341	-0.286
H(5)	0.116	-0.164	0.341	-0.286
H(6)	0.116	-0.164	-0.341	0.286
C(1,s)	-0.073	-0.033	0.000	0.000
C(2,s)	-0.073	0.033	0.000	0.000
C(1,x)	-0.528	-0.010	0.000	0.000
C(1,y)	0.000	0.000	-0.387	-0.387
C(1,z)	0.162	-0.434	0.000	0.000

Selected EHMO's for isolated 1,2 di-t-butyl ethane LXI

(C_2 Symmetry)

Atomic Coordinates

	x	y	z
C(1)	0.786	0.0	0.0
C(2)	1.512	-1.250	-0.578
C(3)	1.478	-1.181	-2.133
C(4)	0.777	-2.533	-0.091
C(5)	2.985	-1.258	-0.076
C(6)	-0.786	0.0	0.0
C(7)	-1.512	1.251	-0.578
C(8)	-1.481	1.250	-0.578
C(9)	-0.777	2.533	-0.091
C(10)	-2.985	1.258	-0.076

σ- Molecular Orbitals

(2-fold related elements not shown)

	A	B	B	A
C_{ij}'s	-12.256	-13.069	-13.187	-13.269
C(1,s)	0.019	-0.016	-0.040	-0.063
C(2,s)	-0.004	-0.012	-0.014	0.040
C(3,s)	0.021	0.060	0.023	-0.004
C(4,s)	-0.032	-0.017	-0.002	0.038
C(5,s)	-0.123	-0.014	-0.034	0.008
C(1,x)	0.309	-0.088	0.029	0.217
C(2,x)	-0.275	0.043	-0.017	0.016
C(3,x)	0.045	0.008	0.013	-0.032
C(4,x)	-0.055	-0.012	0.069	0.080
C(5,x)	0.029	0.009	-0.026	0.138
C(1,y)	-0.193	0.141	0.202	0.102
C(2,y)	0.248	-0.110	-0.160	-0.145
C(3,y)	-0.008	0.024	0.028	0.015
C(4,y)	-0.125	-0.030	0.062	0.160
C(5,y)	-0.379	-0.010	-0.115	0.183
C(1,z)	0.003	0.287	0.003	0.167
C(2,z)	-0.086	-0.334	-0.164	0.090
C(3,z)	0.067	0.323	0.128	-0.022
C(4,z)	0.027	0.078	0.026	-0.049
C(5,z)	0.161	0.072	0.123	-0.070

Selected EHMO values for mono-substituted CBD models. Various rotations of the t-butyl methyl hydrogen atoms are studied.

Model No.	Rotation t-butyl methyl hydrogen	LEMO ev	HOMO ev	ΔE n- π* ev
LXII	50°	-12.585	-10.834	1.751
LXIII	70°	-12.579	-10.834	1.745
LXIV	80°	-12.564	-10.833	1.731
	TEE = (ev)	-1072.58	-1072.225	-1071.62

Reduced overlap population values from EHMO Calculations for the crystal structure model, LVI.

Bond	Reduced overlap population
O(1) - C(1)	0.777
C(1) - C(4)	0.809
C(1) - C(2)	0.751
C(4) - C(5)	0.733
C(5) - C(6)	0.757
C(5) - C(7)	0.752
C(5) - C(8)	0.754
C(4) - C(3)	0.691